Effects of perfusate solution composition on the relationship between cardiac conduction velocity and gap junction coupling

Michael William Entz II

Dissertation submitted to the faculty of the Virginia Polytechnic Institute and State University in partial fulfillment of the requirements for the degree of

Doctor of Philosophy
In
Biomedical Engineering

Steven Poelzing
Rob Gourdie
William Huckle
Yong Woo Lee
James Smyth

November 28th, 2017
Roanoke, VA

Keywords: Cardiac, Ephaptic coupling, Gap junctional coupling, Perfusate solution

Effects of perfusate solution composition on the relationship between cardiac conduction velocity and gap junction coupling

Michael William Entz II

ABSTRACT

Reproducibility of results in biomedical research is an area of concern that should be paramount for all researchers. Importantly, this issue has been examined for experiments concerning cardiac electrophysiology. Specifically, multiple labs have found differences in results when comparing cardiac conduction velocity (CV) between healthy mice and mice that were heterozygous null for the gap junction (GJ) forming protein, Connexin 43. While the results of the comparison study showed differing extracellular ionic concentrations of the perfusates, specifically sodium, potassium, and calcium ($[Na^+]_o$, $[K^+]_o$, and $[Ca^{2+}]_o$), there was a lack of understanding why certain combinations of the aforementioned ions led to specific CV changes. However, more research from our lab indicates that these changes can predict modifications to a secondary form of cardiac coupling known as ephaptic coupling (EpC). Therefore the work in this dissertation was twofold, 1) to examine the effects of modulating EpC through perfusate ionic concentrations while also modulating GJC and 2) to investigate the effects of modulating all three of the main ions contributed with cardiac conduction (Na^+, K^+, Ca^{2+}) and the interplay between them.

Firstly I studied the effects of physiologic changes to EpC determinants ($[Na^+]_o$ and $[K^+]_o$) on CV during various states of GJ inhibition using the non-specific GJ uncoupler carbenoxolone (CBX). Multiple pacing rates were used to further modify EpC, as an increased pacing rate leads to a decrease in sodium channel availability through modification of the resting membrane potential. Firstly, with no to low (0 and 15 μM CBX) GJ inhibition, physiologic changes in $[Na^+]_o$ and $[K^+]_o$ did not affect CV, however increasing pacing rate decreased CV as expected. When CBX was

increased to 30 μM, a combination of decreasing $[Na^+]_o$ and increasing $[K^+]_o$ significantly decreased cardiac CV, specifically when pacing rate was increased.

Next, the combinatory effects of cations associated with EpC (Na^+, K^+, and Ca^{2+}) were tested in to examine how cardiac CV reacts to changes in perfusate solution and how this may explain differences in experimental outcomes between laboratories. Briefly, experiments were run where $[K^+]_o$ was varied throughout an experiment and the values for $[Na^+]_o$ and $[Ca^{2+}]_o$ were at one of two specific values during an experiment. 30 μM CBX was added to half of the experiments to see the changes in the CV-$[K^+]_o$ relationship with GJ inhibition. With unaltered GJ coupling, elevated $[Na^+]_o$ maintains CV during hyperkalemia. Interestingly, both $[Na^+]_o$ and $[Ca^{2+}]_o$ must be increased to maintain normal CV during hyperkalemia with reduced GJ coupling. These data suggest that optimized fluids can sustain normal conduction under pathophysiologic conditions like hyperkalemia and GJ uncoupling.

Effects of perfusate solution composition on the relationship between cardiac conduction velocity and gap junction coupling

Michael William Entz II

GENERAL AUDIENCE ABSTRACT

The use of fluid replacement therapy was first used during the outbreak of Blue Cholera in the 1830s. However, after the development of basic fluids for intravenous fluid therapy, there have been very few changes in the fluid recipes. This same principle can be applied to cardiac research, where blood substitute perfusates are used during experimentation. However, there have been disagreements in experimental outcomes between various labs running matching studies which only varied in choice of perfusate solution. Therefore, one of the goals of this dissertation was to explore how changing ionic concentrations in cardiac perfusate solutions affected cardiac electrophysiological parameters. To fully appreciate changes in cardiac conduction, we also had to investigate changes to gap junctional coupling (GJC), which is the canonical determinant of cardiac conduction. Gap junctions are low resistance pathways which allow direct cell-to-cell coupling, which leads to synchronized cardiac conduction and contraction. However, there have been recent studies that have found a secondary form of cardiac coupling, known as ephaptic coupling (EpC), which is controlled through extracellular ionic concentrations, especially sodium, potassium, and calcium ($[Na^+]_o$, $[K^+]_o$, and $[Ca^{2+}]_o$ respectively) and extracellular nano-domains known as the perinexus. We first investigate making small physiologic changes to $[Na^+]_o$ and $[K^+]_o$, while also inhibiting GJs to find the relationship between EpC and GJC. The results indicated that these EpC modulators could indeed modulate conduction, but only after GJs were sufficiently inhibited. However, results from this study disagreed with historical work indicating that $[K^+]_o$ had a biphasic relationship with CV. Therefore, we then examined the effects of $[Na^+]_o$ and $[Ca^{2+}]_o$ on the CV-$[K^+]_o$ relationship. Interestingly, it was found that inclusion of $[Na^+]_o$ and $[Ca^{2+}]_o$ had varying effects, depending on the level of GJ in the hearts. Specifically, hyperkalemia (high levels of potassium)

is associated with decreases cardiac CV. With a full complement of GJs it was found that increased $[Na^+]_o$ was able to maintain cardiac CV at control levels. However, with inhibited GJ coupling, both increased $[Na^+]_o$ and $[Ca^{2+}]_o$ were needed to maintain conduction. This indicated that increasing EpC during GJ inhibition could be a possible safety mechanism for cardiac CV. The data in this dissertation aim to provide information to the importance of perfusate composition when regarding scientific data.

ACKNOWLEDGEMENTS

I would first and foremost like to thank my advisor, Dr. Steven Poelzing. Through our almost seven years spent working together, Steve has always known how to bring the best out in myself and those around me. He has worked tirelessly to help me see my potential, even when that seemed like a nearly impossible task. I am truly grateful for not only learning from Steve's scientific and management styles, but also for the lifelong friend I gained in the process.

Next I would like to thank my entire dissertation committee for the guidance and support that they have shown me throughout my years at Virginia Tech. Dr. Rob Gourdie, Dr. William Huckle, Dr. Yong Woo Lee, and Dr. James Smyth have been instrumental in molding me into researcher that I am today. They have each helped to not only hone my experimental techniques, but also helped me to control my emotions when my work is questioned.

I would next like to thank all past and present members of the Poelzing laboratory. First I would like to thank Dr. Greg Hoeker, who was always around to help make me laugh and spent countless hours helping to mentor me during my studies. I would also like to thank Ryan King, who showed me that the laboratory will be left in good hands after I depart. Finally I would like to acknowledge the rest of my previous lab mates including Dr. Sai Veeraraghavan, Dr. Anders Peter Larsen, Katie Sciuto, Mike Heidinger, Dr. Sharon George, Dr. Amara Greer-Short, and Tristan Raisch, as they have all been great sources of scientific conversation and ideas over the years.

I would next like to thank my family who has supported me in my long journey through multiple undergraduate degrees and finally my graduate career. I know that I haven't always been easy to deal with, but they were always there for me to keep me sane and motivated, keeping my eye on the finish line.

Finally I would like to thank my wife, Melanie. She is honestly the number one reason I made it to the end of my graduate journey. She, along with our dogs, helped to decrease my stress while also taking care of me when things got too busy. She is the best friend I could ask for and supplied the support that helped guide me to where I am today.

TABLE OF CONTENTS

LIST OF FIGURES

LIST OF TABLES

LIST OF ABBREVIATIONS AND ACRONYMS

Φ_i	Intracellular potential
Φ_o	Extracellular potential
$[Ca^{2+}]_o$	Extracellular calcium ion concentration
$[K^+]_o$	Extracellular potassium ion concentration
$[Na^+]_o$	Extracellular sodium ion concentration
ABS	Acrylonitrile Butadiene Styrene
APD	Action potential duration
AR	Anisotropic Ratio
BDM	2,3-Butanedione 2-monoxime
CBX	Carbenoxolone
CV	Conduction Velocity
CV_L	Longitudinal conduction velocity
CV_T	Transverse conduction velocity
Cx43	Connexin43
dV/dt_{max}	Maximum rate of rise of the action potential
ECG	Electrocardiogram
EpC	Ephaptic Coupling
GJ	Gap Junction
GJC	Gap Junctional Coupling
HZ	Heterozygous
I_{Na}	Sodium Current
LS	Lab Standard
LV	Left Ventricle
LVDP	Left Ventricle Developed Pressure
$Na_v1.5$	Cardiac isoform of the voltage gated sodium ion channel

PLA	Poly(Lactic Acid)
PMMA	Poly(Methyl Methcrylate)
RMP	Resting membrane potential
RT	Rise Time
TEM	Transmission Electron Microscopy
V_m	Transmembrane potential
W_P	Perinexal Width
WT	Wild type

CHAPTER – 1

“Differences found may be due to experimental setup”

Why perfusate composition matters.

INTRODUCTION

Cardiovascular disease in the United States is an epidemic that is the cause of death for over 800,000 people annually [1, 2]. These deaths are often due to arrhythmias which result from aberrations in the electrical activity of the heart [3, 4]. The most deadly of these are ventricular arrhythmias, which can result from abnormal cardiac cell-to-cell coupling [5, 6].

Normal cardiac conduction is necessary for uninterrupted cardiac function. In order for a heart to contract regularly, two forms of cardiac electrical coupling occur; gap junctional coupling (GJC) [7] and ephaptic coupling (EpC) [8]. The aim of this dissertation is to first study the interplay between GJC and EpC, followed by investigating the effects of simultaneous changes to multiple ionic concentrations on cardiac conduction, under normal and impaired GJC. While GJC has long been considered the canonical mechanism in cardiac cell-to-cell coupling [9], EpC has been gaining acceptance in the field [10-12]. The prevailing thought that conduction was dominated by a single mechanism has recently been amended by evidence unveiling the cooperative relationship between the two pathways [13, 14]. For example, studies of 50% connexon 43 (Cx43) knockout mice revealed that modest ephaptic uncoupling was necessary to unmask conduction deficits, demonstrating a correlation between GJC and EpC. Therefore, the first aim of this dissertation is to elucidate the relationship between varying levels of GJC and EpC.

Many cardiac events and diseases, such as ischemia [15-18], Brugada syndrome (BrS) [19, 20], Long QT syndrome (LQTS) [21-23], catecholaminergic polymorphic ventricular

tachycardia [24, 25], Anderson-Tawil syndrome [26-28], and Timothy syndrome [29, 30] have been shown to modulate ionic channel conductance in cardiomyocytes. Importantly, some of the aforementioned maladies, such as ischemia, also induce changes to Cx43 localization [31-35], suggesting that ischemic regions could be affected by a combination of conduction changes. Many of these diseases lead to arrhythmogenic substrates that could now possibly be explained by a combination of the GJC and EpC. One predominant form of therapy for many of these diseases is the implantation of a cardioverter defibrillator [36-38]. While these devices are used to decrease death rates in patients [39], all surgery carries an inherent risk [40]. However, with the study of EpC, it has been shown that change in extracellular ionic concentration can help to improve cardiac conduction velocity (CV) [13]. Therefore, the second aim of this dissertation is to determine how modifying extracellular ionic concentration levels of specific cations can serve as a possible therapy for patients with cardiovascular disease.

HYPOTHESIS

The central hypothesis for the dissertation was that the extracellular ionic concentrations of sodium, calcium, and potassium can be modulated in conjunction with pharmacological GJC inhibition to demonstrate the efficacy of modifying the theoretical determinants of EpC as a therapeutic measure for cardiac disease.

SPECIFIC AIMS

Aim 1: *To determine the effects of extracellular sodium ($[Na^+]_o$) and extracellular potassium ($[K^+]_o$) on pharmacological gap junctional mediated conduction slowing in*

guinea pig whole hearts. The working hypothesis for this study is that GJC masks the effects of the CV-EpC relationship. GJC will be modified in Langendorff-perfused guinea pig ventricles using the nonspecific gap junction inhibitor carbenoxolone (CBX). Values of $[Na^+]_o$ and $[K^+]_o$ will be varied at each value of CBX to test changes in EpC. Western blotting of Cx43 and phosphorylated Cx43 will be used to validate that ionic concentration levels are not modifying GJC.

Aim 2: *To determine the effects of extracellular calcium ($[Ca^{2+}]_o$) and $[Na^+]_o$ on the CV – $[K^+]_o$ relationship.* The working hypothesis for this study is that $[Ca2^+]_o$ and $[Na^+]_o$ will modify the CV-$[K^+]_o$ relationship in whole hearts through ephaptic coupling and that these modifications will be modified when GJC is compromised. Transmission electron microscopy will be used to validate the decrease in perinexal width that has previously been found with increased $[Ca^{2+}]_o$ in mice. The following hypotheses will be tested:

(1) Increasing $[Ca^{2+}]_o$ will reduce perinexal width and reduce CV sensitivity to $[K^+]_o$ through ephaptic coupling. $[K^+]_o$ will be varied from 4.56 to 10 mM in separate solutions containing 1.25 and 2.0 mM $[Ca^{2+}]_o$.

(2) Increasing $[Na^+]_o$ will modify the CV-$[K^+]_o$ relationship. $[K^+]_o$ will be varied from 4.56 to 10 mM in separate solutions containing 1.25 and 2.0 mM $[Ca^{2+}]_o$ while also increasing $[Na^+]_o$ from 145.5 to 155.5 mM.

(3) CV slowing due to inhibiting GJC with CBX will be partially reversed due to increased $[Ca^{2+}]_o$ and $[Na^+]_o$, by increasing theoretical determinants of ephaptic coupling. $[K^+]_o$ will be varied from 4.56 to 10 mM in separate solutions containing 1.25 or 2.0 mM $[Ca^{2+}]_o$ and 145.5 or 155.5 mM $[Na^+]_o$ with the inclusion of 30 µM CBX.

CARDIAC CONDUCTION OVERVIEW

Normal cardiac conduction allows for sequential activation of cardiomyocytes, leading to cardiac contraction, which is essential for circulation of oxygenated blood and nutrients throughout the body [41]. Cardiac conduction begins with the depolarization and firing of specialized pacemaker cells in the sinoatrial node. Conduction then moves through the atrium, atrioventricular node, His-Purkinje system, and finally to the ventricles, allowing for a pattern of electrical excitation that optimizes cardiac contraction and blood flow. The conduction of electrical current that coordinates contraction passes from cell-to-cell by a combination of GJC and EpC.

The cardiac action potential (AP), which is a manifestation of cardiac membrane potential changes resulting after cardiac conduction, demonstrates the balance of ionic currents needed for normal cell-to-cell activation to occur [42, 43]. Ventricular cardiomyocytes rest at a negative membrane potential until charge from an upstream cell raises the transmembrane potential, progressing the cell into the first of five phases of the AP, known as phase 0. This allows for voltage gated Na^+ channels to open, followed by a surge of Na^+ ions entering the cell. After rapid depolarization due to Na^+ influx, the cell enters phase 1, which indicates the start of repolarization. Phase 1 includes the inactivation of Na^+ channels and the activation of fast transient voltage gated K^+ channels, I_{to}. These potassium channels are not expressed in guinea pig ventricles [44], so will not be a factor in these experiments. Phase 2 is the plateau phase of the action potential, where excitation-contraction coupling takes place. This occurs through the opening of L-type Ca^{2+} channels, allowing an inward flow of Ca^{2+} ions. At the same time, K^+ ions are moved out of the cell, keeping the membrane

potential relatively stable. These K^+ channels include I_{Kr}, I_{Ks}, and I_{KATP}, which begin to dominate potential changes when L-type Ca^{2+} channels begin to close in phase 3, causing a large repolarizing current. Finally phase 4, which is the resting membrane potential (RMP), is maintained by a combination of Na^+-K^+ and Na^+-Ca^{2+} pumps, Na^+/K^+-ATPase and NCX, as well as the inwardly rectifying K^+ channel, I_{K1} [45-47].

While these channels and exchangers are essential for regulating cellular excitability, there are other mechanisms regulating cardiac excitation since cells other than pacemaker cells must first receive a depolarizing stimulus from an upstream cell.

Gap junctional coupling

GJC has historically been considered the main determining factor in cardiac cell-to-cell conduction [48]. GJs are comprised of two hemichannels known as connexons, each comprised of 6 connexins [49]. GJs are formed when two connexon hemichannels attach to one another, with each hemichannel contributed from a pair of cells that are next to one another. The main ventricular isoform of connexins for GJ formation is Cx43 [50, 51]. GJs aggregate into groups known as GJ plaques in the intercalated disc, typically at the shortest axis of cells [52, 53].

GJC works through the direct passage of ions and metabolites from one cell to another through GJs. Modification of cardiac conduction properties through GJs can be accomplished via multiple mechanisms. For example, cardiac CV can be decreased though pharmacologically blocking GJs [54, 55]. Also, disease states can alter conduction through lateralization of GJs, such as seen in ischemia [56, 57]. Cardiac disease can also lead to alteration of phosphorylation in connexins, which can cause

modified patterns of GJ assembly, conductance, or internalization [58, 59]. While there is no argument whether GJC is important for cardiac conduction, ionic composition of perfusate solutions has recently made a resurgence as a modulating factor in cardiac conduction [13, 14, 60].

Perfusate Solutions

The origins of resuscitation fluid therapy can be traced back to the outbreak of Blue Cholera in England in the 1830s [61-64]. In an elegant review by Awad et al., the historical background of one of the most prevalent resuscitation fluids, 0.9% saline, is chronicled. The authors are able to distinctly show the steps taken to find a suitable solution for human use, while also questioning this choice as there seems to be no scientific basis for the use of a pure NaCl solution. While the use of these resuscitation solutions has found common use within the clinic, another aspect in fluid development included those made for animal models in laboratory research known as perfusate solutions. These solutions are used as blood substitutes in *ex vivo* perfusion based experiments. This chapter aims to elucidate the historical composition of a common perfusate solution in animal models: Tyrode's solution. Also, this chapter will analyze the need for experimentalist to take greater care when choosing a perfusate solution, especially when modifications are made to that solution.

Sydney Ringer

Modern perfusate solutions can be highly attributed to the work of Sydney Ringer in the early 1880s. In 1882 Dr. Ringer first reported that a solution of 0.75% normal saline mixed with one ten-thousandth part potassium chloride could be used as a perfusate in

detached heart experiments [65]. With the knowledge of present day it is clear to see this solution is not adequate for maintaining cardiac activity due to the omission of calcium, which is important in excitation-contraction coupling in cardiomyocytes [66]. However, without that distinct knowledge, Ringer wrote another manuscript in 1883 that revealed this discovery [67]. Interestingly, Ringer soon realized that his experiments could not be repeated. This was due to the fact that water used in experiments in his published study was not distilled, but rather supplied from the New River Water Company, which contained calcium, magnesium, sodium, potassium, carbonic acid, chlorine, and silicates. Therefore, Ringer set out to once again determine a solution capable of sustaining exposed heart preparations. With the knowledge of the water composition in hand, Ringer began testing specific components of the water with his previous saline solution. After experimentation, he noted that contraction could be obtained using a solution containing sodium chloride, potassium chloride, and calcium chloride. He further went on to describe the need to include sodium bicarbonate in the solution to help neutralize the effects of acidosis on contraction. These findings formed the basis for Ringer's solution, which was used in a pure or modified state as the perfusate solution of choice for the next 30 years [68-71].

Maurice Vejux Tyrode

Many derivations of Ringer's solution were made in the late 1800s and early 1900s [72]. However, this chapter will specifically examine the creation and modification of Tyrode's solution, as it is the basis for many electrophysiological studies, including all of the early work in our laboratory [60, 73, 74]. Maurice Vejux Tyrode was a pharmacologist who taught at Harvard Medical School in the early 1900s. While much of Tyrode's career

included research in the areas of pharmacology and gastric affections [75-78], he would leave an impact on cardiac electrophysiology experimentation that he likely never considered.

In a 1910 study, Tyrode tested the effects of purgative salts on intestinal contractions and content passage [72]. In doing so, Tyrode determined that the current nutritive mediums did not work as well as he would have liked. These previously formulated perfusates included those created by Ringer, Locke, Hedon, and Adler. After eliminating the previous solutions, Tyrode experimented until he found a perfusate composition that allowed for greater time of preservation of the intestines. In this moment Tyrode's solution, which in modified states is still used currently [79], was born. While Tyrode's solution was originally derived for use in the intestines, it was quickly modified and used in other physiological systems. However, there is likely no one currently using the original Tyrode's solution for *ex vivo* cardiac preparations, as modifications were made to the solution as early as 1913 [80]. However, the use of the phrase, "*modified Tyrode's*" has become ever present in research literature [81, 82], with the actual modifications varying between experimentalist. Therefore, the question has to be asked, is there a better way to denote changes in perfusate solution?

When is modified a poor description for a solution?

With many experimentalists in the present day using modified versions of historical perfusion solutions, the question that has to be asked is when is modified the incorrect word to be used in research. This brings to mind Theseus's paradox which questions whether an object is still the same object if all of the components are replaced one by

one. The issue with Tyrode's solution is when to stop calling it modified Tyrode's and when to admit that it is an entirely new composition. Does this happen when altering one component? Two? Changing the buffering agent in the solution? To tackle this question, I attempted to trace the lineage from the original Tyrode's solution to the perfusate used in our laboratory, which has been denoted as *modified Tyrode's* solution. The underlying problem is that most experimentalists just say that a modified solution of some sort is being used, with the modifications varying significantly between different manuscripts.

A simple comparison of the Poelzing modified Tyrode's solution [83] compared to the original [72] finds a substantial number of changes (Table 1.1). The only constituent between the two components that is exactly the same is the concentration of glucose. Other than that, all ionic concentrations are modified as well as the buffering component – sodium phosphate and sodium bicarbonate changed to HEPES. Therefore the question is how did the base Tyrode's solution get altered so much, yet still get credited as *modified Tyrode's*, and to what purpose?

In order to elucidate the answer to both questions, the transformation of Tyrode's solution from 1910 to the present was investigated. Importantly for this work, the first cardiac investigation involving Tyrode's solution was conducted by Constance Leetham in 1913. Leetham found that ventricular strip preparations could not reliably be perfused with blood due to the small bore size of the cannula, but a *modified Tyrode's* solution, the first use of the term found, would allow for spontaneous contractions in the strip [80]. In order for the preparation to remain viable, KCl had to be increased from 2.7 to 5.4 mM and $NaHCO_3$ decreased from 12 to 6 mM; however the author did not share the

reason for the modifications. Interestingly, the solution was unable to maintain spontaneous contraction in whole hearts, because the solution caused fibrillation during perfusion. While this solution is still far from what is used in the Poelzing laboratory today, it is an important manuscript as it established the use of *modified Tyrode's* solution for cardiac preparations.

The Leetham manuscript was a logical first step in the search for modifications to Tyrode's solution due to the study being one of the first to look at the use of Tyrode's solution in whole hearts. It is difficult to trace the modifications of Tyrode's solution forward from this point because researchers were more likely to simply state they used *modified Tyrode's* rather than rigorously citing which previously *modified Tyrode's* solution they used as a starting solution. Therefore, it seemed more logical to investigate the lineage of Poelzing's current *modified Tyrode's*. The first publication containing the "modified Tyrode's" solution used in the Poelzing laboratory was published in 2012 [84]. This solution, which is detailed in Table 1.1, has been used in a multitude of experiments up to the present [60, 73, 85, 86]. But who did Poelzing train with, and where did he get this *ex vivo* perfusate?

Throughout his graduate career, Poelzing used modified Tyrode's solution while training in the laboratory of David S. Rosenbaum (Table 1.1) [87-89]. Interestingly, the Rosenbaum perfusate does not match the Poelzing laboratory perfusate. The two largest changes are that the majority of the Rosenbaum manuscripts use a bicarbonate buffer instead of HEPES and $MgSO_4$ instead of $MgCl_2$ as used in the Poelzing buffers. While some of these differences could be due to the difference in preparation, guinea pig and canine wedges in the Rosenbaum group versus mouse and guinea pig whole

heart preparations in the Poelzing group, there may be a better answer. Therefore, it is probable that there were more influences that led Poelzing to a his current lab standard perfusate composition.

The next logical place to explore was in the Deschenês lab, where Poelzing worked as a post-doctoral research scientist. During this tenure, instead of working in wedge preparations or whole hearts, Poelzing worked in HEK293 human embryonic kidney cells [90]. When comparing the Deschenês perfusate with the Poelzing laboratory standard, it can be seen that the solutions are indeed closer to one another than the Rosenbaum solution was. Importantly, the Poelzing/Deschenes solution used a HEPES based buffer instead of bicarbonate. Also, this solution was starting to mimic both the Poelzing as well as the Leetham solutions closely (Table 1.1). This perfusate also matches that which was used by Deschenês at the end of her post-doctoral career in the Tomaselli laboratory [91]. However, tracing through Deschenês' history, it was found that Deschenes also used other solutions while working both with Drs. Tomaselli and Chahine (Table 1.1) [90, 92-94]. While these additional solutions will not be explored, the iterations of perfusate compositions illustrate the high variability in experimental practice, which could be the cause of some experimental variability particularly in whole-heart preparations.

It should be noted that there is a single manuscript to emerge from the Rosenbaum laboratory that cites a nearly identical solution to the one eventually adopted by Poelzing for his laboratory standard composition, and that can be found in a manuscript by Kjølbye et al. [95]. This iteration shows only a difference in HEPES when compared to Poelzing's lab standard (Table 1.1). However, it was difficult to trace the origins of the

Kjølbye composition. It is possible that due to the shared background in mentors, Poelzing used a combination of this solution and the Deschenês/Poelzing solution when he founded his own laboratory group. However, the direct lineage concerning all changes leading to the Poelzing perfusate is unlikely to ever be fully uncovered. In communications with Dr. Poelzing, other principal investigators, and post-doctoral fellows, it appears that scientists often allow small perturbations in laboratory solutions as long as the solutions do not produce significantly different findings from those previously published by the laboratory.

Further investigating Poelzing's academic lineage offered no further indication for the basis of his laboratory standard perfusate solution. For example, Dr. Rosenbaum, Poelzing's PhD advisor, trained in the laboratory of Dr. Guy Salama, a pioneer of optical mapping. Interestingly, early works by Dr. Salama's group also revealed a variety of perfusate compositions used in Langendorff perfused whole-heart preparations [96-99]. Still, there is one distinct change in the Poelzing solution that has no relationship to his scientific lineage with respect to *ex vivo* heart preparations and cannot be traced to the original Tyrode solution. That is the use of a HEPES buffer instead of bicarbonate. Therefore, with direct leads coming up dry, the next focus was to find when and why the buffering solution was changed.

In 1972, Foreman and Mongar were conducting isolated cell studies with the inclusion of alkaline earth metals [100]. HEPES was substituted into the solution because bicarbonate precipitates out of a solution significantly with high levels of alkaline earth metals like calcium and magnesium, which are prominent physiologic divalent cations. To reduce precipitated formation in studies with barium, another alkali earth metal,

Poelzing switched to HEPES as a buffer. Importantly, buffering agents differ from laboratory to laboratory, and a preference for buffer is a basis for the changes found between the original Tyrode solution and the solution used in the Poelzing laboratory.

Why are ions so important?

Some may wonder what the importance was to take such a circuitous route in retracing the history of a single laboratory's perfusate solution. This exercise was completed for multiple reasons. The first is the importance of questioning the use of the word *modified* when talking about perfusion solutions. While this seems to be unimportant, it can clearly be seen that some aspects of the Poelzing laboratory perfusion solution share with Tyrode's solution (Table 1.1), one would be hard pressed to look at the two and say they are highly similar. While this is merely a problem of nomenclature, it can become an issue when a manuscript only describes the solution used by name, with no formulation listed causing confusion through the use of the word modified. Sadly, this is common practice from many laboratories. This leads to the most important issue concerning solution composition in cardiac research; the exact formulation could be a reason for differences in experimental results [101].

While the investigation into the start of the Poelzing laboratory perfusate solution may have taken a tortuous path coming to what could be considered an underwhelming conclusion, the interest lies not in the specific solution, but in the ramifications in the choice of solution. This idea can be summarized in the review by George et al. [101], where the authors demonstrate that perfusate solution can modify experimental results. Specifically it is shown when comparing hearts with and without a 50% heterozygous

reduction in Cx43 that perfusate solution could be linked with whether a significant change in conduction would be found. While there are numerous constituents that make up normal blood plasma [102], the remainder of this narrative will focus on three of the ions highly studied in literature; sodium, potassium, and calcium. These ions have been identified to affect cardiac conduction, because of the essentiality to the cardiac action potential [43].

Sodium

Sodium current has been considered important to cardiac conduction since the inception of the field of cardiac electrophysiology, with some of the earliest findings explored by Hodgkin and Huxley [103, 104]. This is due to the fact that Na^+ ions have been shown to be the dominant driving force behind the sudden depolarization in cardiac myocytes, leading to a cardiac action potential [43]. Therefore, even while GJC was considered the predominant form of cell-to-cell coupling, Na^+ handling is important due to the role in cardiac cell excitability and cell depolarization.

Na^+ has also been widely studied due to the extensive changes to sodium current (I_{Na}) in many cardiac diseases [103, 104]. While changes to I_{Na} are not an exact correlate for $[Na^+]_o$, modifying $[Na^+]_o$ will change the driving force of Na^+ channels, leading to a change in I_{Na}. Physiologic changes in I_{Na} have been primarily attributed to two mechanisms; through genetic mutations of Na^+ channels subunits or by changing the conductance of the channel through direct modification of the channel. Genetic mutations to SCN5A, the α-subunit of the voltage gated sodium channel ($Na_v1.5$), account for the main marker in diseases such as BrS [105]. BrS is associated

approximately ≤30% of the time with a mutation to SCN5A that decreases I_{Na}. Arrhythmias are thought to occur in BrS via phase 2 reentry due to a loss of transmural dispersion of repolarization. Therefore, it can easily be seen that Na^+ plays an important role in normal cardiac conduction, however research has also shown the importance of K^+ in modulating this relationship.

Potassium

As was seen with Na^+, K^+ initial studies can be traced back to Hodgkin and Huxley [103]. This is one of the first manuscripts to establish the principle that K^+ current was delayed in electrical propagation until after Na^+ current caused an initial cellular depolarization. It was later found that a fivefold increase in $[K^+]_o$ from 2.7 mM raised the resting membrane potential (RMP) from -92 to -54 mV [106]. The changes in RMP were accompanied by a decrease in rate of rise for APs. However, the change in rate of rise was found to not be modified by $[K^+]_o$, but by RMP as the APs returned to normal after clamping the cells back to an more negative RMP.

Modifications to RMP were studied further in depth in 1970 by Dominguez and Fozzard who discussed the possibilities of $[K^+]_o$ modifying Na^+ channel availability through modification of RMP. Briefly, as $[K^+]_o$ was increased in the study from 2.7 to 7.0 mM, the investigators demonstrated that conduction speed increased up to 5.4 mM and then decreased. However, the authors hypothesized that the change in RMP at higher levels of $[K^+]_o$ would inactivate Na^+ channels.

The previous study opened an entirely new field in K^+ related conduction known as supernormal conduction [107-110]. The phenomenon was actually discovered in 1964,

but did not garner further attention until the 1980s [111, 112]. These studies showed that cardiac CV has a biphasic relationship with $[K^+]_o$. Specifically, supernormal conduction is when cardiac CV increases due to raised $[K^+]_o$, which has a peak at roughly 8.0 mM $[K^+]_o$ [107, 108] by a mechanism of decreasing the upstream current necessary to depolarize a down-stream membrane to the activation potential of voltage gated sodium channels. However, once $[K^+]_o$ is increased beyond this point, additional $[K^+]_o$ leads to a decrease in CV, due to loss of Na^+ channel availability [113]. Mechanistically the decrease in CV was assumed to occur due to Na^+ channel inactivation as the RMP increased to membrane potentials where sodium channels could more frequently flicker into an activated and inactivated conformation. Support for the hypothesis that conduction slows due to loss of sodium current was supported by studies that used the Na^+ channel blocker TTX [108]. With increasing concentrations, TTX was able to mirror the effects found by increasing $[K^+]_o$. The authors concluded that these studies demonstrated that K^+ was indeed modifying Na^+ availability in a regime of supernormal conduction to obtain the characteristic biphasic relationship.

Calcium

Ca^{2+} is important in a ways too numerous to name even as it relates to cardiac function, including contraction and conduction. A process known as excitation-contraction coupling is what causes electrical activity in cells to translate into cardiac contraction [66]. Briefly, depolarization of the cell membrane causes Ca^{2+} ions to flow into the cell. This leads to Ca^{2+} ions binding to specialized proteins on the sarcoplasmic reticulum known as ryanodine receptors. These receptors then release Ca^{2+} from the sarcoplasmic reticulum into the cytosol, increasing intracellular Ca^{2+} levels in order for

cell contraction to occur. While Ca^{2+} is important for cardiac cell contraction, $[Ca^{2+}]_o$ has also been shown to modulate cardiac conduction.

It is important to note that changes to Ca^{2+} concentrations, both intracellular and extracellular, have been shown to modulate I_{Na}, Cx43, and extracellular cardiac interstitial volume. Increasing $[Ca^{2+}]_i$ has been demonstrated to cause a depolarizing shift in steady state inactivation of Na^+ channels [114, 115]. The changes in GJC due to Ca^{2+} have been controversial over the years; however studies have shown that increasing Ca^{2+} substantially decreased GJ conductance [116, 117]. Interestingly recent studies have shown an increase in CV due to increased $[Ca^{2+}]_o$ [118], indicating that Ca^{2+} mediated GJC modulation may not be the only mechanism at work.

Increased levels of $[Ca^{2+}]_o$ have also been shown to decrease interstitial volume in cells [13]. Interestingly, modeling studies have gone on to show that $[Ca^{2+}]_i$ becomes important in cardiac conduction specifically when significant conduction delays occurred at GJs as a result of GJ uncoupling [119].

As many of these studies demonstrated, ionic concentrations have normally been studied one at a time, while interactions due to altering multiple ions could have unexpected and significant impacts on cardiac conduction.

Ephaptic Coupling

While the previous information provides insight into how Na^+, K^+, and Ca^{2+} modulate cardiac conduction individually, it is rare and unlikely that only a single ionic concentration is modulated during health and disease. EpC is a theory that could be the mechanistic reasoning behind many of the conduction alterations seen due to

modification of ionic concentrations that were previously described. Briefly, EpC is a form of cell-to-cell coupling which relies on extracellular electric fields generated between apposing membranes in a process that is distinctly different from GJC [120, 121]. EpC has been proposed to occur in other parts of the body for some time such as the brain [122-124], with recent resurgence in cardiac studies [10, 13, 60, 83, 125, 126]. There were originally two determinants hypothesized to control EpC through the use of models; close apposition of cells and a dense localization of Na^+ channels at the site of apposition. Both of these determinants were discovered to be present in cardiac ventricular myocardium in a nano-domain that was termed the perinexus, which is located at the edge of GJs [83, 126, 127]. The general mechanism of EpC is that upstream cellular depolarization raises the transmembrane potential (Equation 1.1), which is the difference in the extracellular and intracellular electric potentials, causing voltage gated sodium channels to open at the cleft of the first cell. The withdrawal of Na^+ from the extracellular space will decrease the extracellular potential in the perinexus, which will raise the transmembrane potential for the second cell. Voltage gated sodium channels will then open on the second cell, allowing a depolarizing Na^+ current to flood into the second cell. This passage from cell-to-cell will continue, constituting electrical conduction through a tissue. While this form of conduction is not considered the main determinant of cardiac conduction, there has been research that hints conduction can continue with little to no GJs present, which could be from EpC [128].

$$\boldsymbol{Eq.1.1} \quad V_m = \Phi_o - \Phi_i$$

Some of the initial ideas in cardiac EpC originated due to studies that modulated bulk interstitial volume while also pharmacologically decreasing GJC. These studies showed that conduction failure occurred in hearts with increased interstitial volume with GJ uncoupling, but not in hearts with only one of the changes [86]. This led to studies that identified the perinexus as a possible cardiac ephapse since it is situated adjacent to GJs in the intercalated disc, and highly expresses the voltage gated sodium channel, $Na_v1.5$ [126, 127, 129]. In combination with these findings, as well as with mathematical models [125, 130], it was proposed that the perinexus was an important factor in EpC [14, 131]. At this point, $Na_v1.5$ and the perinexus were both hypothesized to be key factors in EpC, though the relationship was found to be more complicated than originally thought. For example, it was found that perinexal width (W_p) could be narrowed by increasing $[Ca^{2+}]_o$, leading to enhanced EpC [13]. Also, $[K^+]_o$ has also been shown to be a modulator of EpC, as increasing $[K^+]_o$ increases the RMP, which can lead to modification of Na^+ channel availability. Therefore, the main modulators of EpC so far have been identified as $[Na^+]_o$, $[K^+]_o$, $[Ca^{2+}]_o$, and W_p. Even though modulators for EpC were identified, the effects that these modulators had on one another still needed to be explored.

One study in heterozygous mice null for Cx43 showed that modification to $[Na^+]_o$ and $[K^+]_o$ had differing effects on CV, depending on $[Ca^{2+}]_o$ as well as if the mouse expressed the full complement or 50% of Cx43 [13]. The study demonstrated that changes in CV due to $[Na^+]_o$ and $[K^+]_o$ could be masked through an increase in $[Ca^{2+}]_o$. However, some of the CV changes were seen again in the mice with a 50% reduction in Cx43. Interestingly, it was also found that modifications to $[Na^+]_o$ had opposite effects on

CV depending on the amount of $[Ca^{2+}]_o$ present. Specifically, it was shown that increasing $[Ca^{2+}]_o$ in mice, and therefore decreasing W_p, with normal levels of $[Na^+]_o$ leads to increased CV values. However, when these same mice were then perfused with a hyponatremic solutions, CV decreased as $[Ca^{2+}]_o$ increased [118]. All of these findings lead to the conclusion that $[Na^+]_o$, $[K^+]_o$, $[Ca^{2+}]_o$, W_p, and GJC are important modulators of EpC. Therefore, if simply altering ionic composition can conceal a 50% loss of gap junction proteins, it stands to reason that targeting EpC may be an effective future therapeutic target to treat cardiac conduction diseases.

CONCLUSIONS

Reproducibility in scientific experimental outcomes is a cornerstone of the positive and negative control to experimental design. With the findings that perfusate solution composition can modify experimental outcomes, it is important for experimentalists to know and understand what perfusates are being used in their laboratories. However, the heart is a complex organ and *ex vivo* experimental setups are also complex. There is then a question of whether biomedical irreproducibility is a major barrier to scientific progress or an essential component of scientific advances. Should everyone use identical experimental protocols at the risk that we blind ourselves to possible alternative phenotypes? Or should we employ such a wide variety of experimental approaches at the risk that we cannot reproduce each other's data and cause additional confusion in the field? One could conceive that biomedical irreproducibility is important. With respect to cardiac electrophysiology, if diverse starting conditions in perfusate composition produce similar results, there should be higher confidence that the results are likely to occur in human physiologic and pathophysiologic conditions. However, if

these differing starting conditions produce opposite results, as was the case between Morley et al. [132] and Eloff et al. [133], then care should be taken to discover how experimental differences affect outcomes. One important experimental difference often overlooked is the use of *modified* solutions, and I argue that the term “modified” is a poor word choice that increases confusion when discussing cardiac perfusates. Instead, solutions should be described by ionic composition choices that were driven by scientific evidence, rather than citing a solution from over 100 years ago that share little to no resemblance to current solutions.

REFERNCES

1. England, H., P.S. Weinberg, and N.A. Estes, 3rd, *The automated external defibrillator: clinical benefits and legal liability.* JAMA, 2006. **295**(6): p. 687-90.
2. Mozaffarian, D., et al., *Heart Disease and Stroke Statistics-2016 Update: A Report From the American Heart Association.* Circulation, 2016. **133**(4): p. e38-360.
3. Koyak, Z., et al., *Sudden cardiac death in adult congenital heart disease.* Circulation, 2012. **126**(16): p. 1944-54.
4. Mehra, R., *Global public health problem of sudden cardiac death.* J Electrocardiol, 2007. **40**(6 Suppl): p. S118-22.
5. Haissaguerre, M., et al., *Ventricular arrhythmias and the His-Purkinje system.* Nat Rev Cardiol, 2016. **13**(3): p. 155-66.
6. Janse, M.J. and A.L. Wit, *Electrophysiological mechanisms of ventricular arrhythmias resulting from myocardial ischemia and infarction.* Physiol Rev, 1989. **69**(4): p. 1049-169.
7. Nielsen, M.S., et al., *Gap junctions.* Compr Physiol, 2012. **2**(3): p. 1981-2035.
8. Veeraraghavan, R., S. Poelzing, and R.G. Gourdie, *Intercellular electrical communication in the heart: a new, active role for the intercalated disk.* Cell Commun Adhes, 2014. **21**(3): p. 161-7.
9. Kucera, J.P., S. Rohr, and Y. Rudy, *Localization of sodium channels in intercalated disks modulates cardiac conduction.* Circ Res, 2002. **91**(12): p. 1176-82.
10. Wei, N., Y. Mori, and E.G. Tolkacheva, *The dual effect of ephaptic coupling on cardiac conduction with heterogeneous expression of connexin 43.* J Theor Biol, 2016. **397**: p. 103-14.
11. Copene, E.D. and J.P. Keener, *Ephaptic coupling of cardiac cells through the junctional electric potential.* J Math Biol, 2008. **57**(2): p. 265-84.

12. Mori, Y., G.I. Fishman, and C.S. Peskin, *Ephaptic conduction in a cardiac strand model with 3D electrodiffusion.* Proc Natl Acad Sci U S A, 2008. **105**(17): p. 6463-8.

13. George, S.A., et al., *Extracellular sodium and potassium levels modulate cardiac conduction in mice heterozygous null for the Connexin43 gene.* Pflugers Arch, 2015.

14. Veeraraghavan, R., R.G. Gourdie, and S. Poelzing, *Mechanisms of cardiac conduction: a history of revisions.* Am J Physiol Heart Circ Physiol, 2014. **306**(5): p. H619-27.

15. Di Diego, J.M. and C. Antzelevitch, *Acute myocardial ischemia: cellular mechanisms underlying ST segment elevation.* J Electrocardiol, 2014. **47**(4): p. 486-90.

16. Nattel, S., et al., *Arrhythmogenic ion-channel remodeling in the heart: heart failure, myocardial infarction, and atrial fibrillation.* Physiol Rev, 2007. **87**(2): p. 425-56.

17. Carmeliet, E., *Cardiac ionic currents and acute ischemia: from channels to arrhythmias.* Physiol Rev, 1999. **79**(3): p. 917-1017.

18. Kleber, A.G., *Resting membrane potential, extracellular potassium activity, and intracellular sodium activity during acute global ischemia in isolated perfused guinea pig hearts.* Circ Res, 1983. **52**(4): p. 442-50.

19. Hedley, P.L., et al., *The genetic basis of Brugada syndrome: a mutation update.* Hum Mutat, 2009. **30**(9): p. 1256-66.

20. Antzelevitch, C., *Ion channels and ventricular arrhythmias: cellular and ionic mechanisms underlying the Brugada syndrome.* Curr Opin Cardiol, 1999. **14**(3): p. 274-9.

21. Ackerman, M.J., *The long QT syndrome: ion channel diseases of the heart.* Mayo Clin Proc, 1998. **73**(3): p. 250-69.

22. Vincent, G.M., et al., *The inherited long QT syndrome: from ion channel to bedside.* Cardiol Rev, 1999. **7**(1): p. 44-55.

23. Modell, S.M. and M.H. Lehmann, *The long QT syndrome family of cardiac ion channelopathies: a HuGE review.* Genet Med, 2006. **8**(3): p. 143-55.

24. Kujala, K., et al., *Cell model of catecholaminergic polymorphic ventricular tachycardia reveals early and delayed afterdepolarizations.* PLoS One, 2012. **7**(9): p. e44660.

25. Hwang, H.S., et al., *Inhibition of cardiac Ca2+ release channels (RyR2) determines efficacy of class I antiarrhythmic drugs in catecholaminergic polymorphic ventricular tachycardia.* Circ Arrhythm Electrophysiol, 2011. **4**(2): p. 128-35.

26. Sung, R.J., et al., *Electrophysiological mechanisms of ventricular arrhythmias in relation to Andersen-Tawil syndrome under conditions of reduced IK1: a simulation study.* Am J Physiol Heart Circ Physiol, 2006. **291**(6): p. H2597-605.

27. Sandhiya, S. and S.A. Dkhar, *Potassium channels in health, disease & development of channel modulators.* Indian J Med Res, 2009. **129**(3): p. 223-32.

28. Plaster, N.M., et al., *Mutations in Kir2.1 cause the developmental and episodic electrical phenotypes of Andersen's syndrome.* Cell, 2001. **105**(4): p. 511-9.

29. Yarotskyy, V., et al., *The Timothy syndrome mutation of cardiac CaV1.2 (L-type) channels: multiple altered gating mechanisms and pharmacological restoration of inactivation.* J Physiol, 2009. **587**(3): p. 551-65.

30. Navedo, M.F., et al., *Increased coupled gating of L-type Ca2+ channels during hypertension and Timothy syndrome.* Circ Res, 2010. **106**(4): p. 748-56.

31. Kieken, F., et al., *Structural and molecular mechanisms of gap junction remodeling in epicardial border zone myocytes following myocardial infarction.* Circ Res, 2009. **104**(9): p. 1103-12.

32. Macia, E., et al., *Characterization of gap junction remodeling in epicardial border zone of healing canine infarcts and electrophysiological effects of partial reversal by rotigaptide.* Circ Arrhythm Electrophysiol, 2011. **4**(3): p. 344-51.

33. Yu, Z.B. and J.J. Sheng, *[Remodeling of cardiac gap junctions and arrhythmias].* Sheng Li Xue Bao, 2011. **63**(6): p. 586-92.

34. Chkourko, H.S., et al., *Remodeling of mechanical junctions and of microtubule-associated proteins accompany cardiac connexin43 lateralization.* Heart Rhythm, 2012. **9**(7): p. 1133-1140 e6.

35. Kremers, M.S., et al., *The National ICD Registry Report: version 2.1 including leads and pediatrics for years 2010 and 2011.* Heart Rhythm, 2013. **10**(4): p. e59-65.

36. Miller, J.D., O. Yousuf, and R.D. Berger, *The implantable cardioverter-defibrillator: An update.* Trends Cardiovasc Med, 2015. **25**(7): p. 606-11.

37. Sanghera, R., et al., *Development of the subcutaneous implantable cardioverter-defibrillator for reducing sudden cardiac death.* Ann N Y Acad Sci, 2014. **1329**: p. 1-17.

38. Manian, U. and L.J. Gula, *Arrhythmia Management in the Elderly-Implanted Cardioverter Defibrillators and Prevention of Sudden Death.* Can J Cardiol, 2016. **32**(9): p. 1117-23.

39. Olshansky, B. and R.M. Sullivan, *Sudden death risk in syncope: the role of the implantable cardioverter defibrillator.* Prog Cardiovasc Dis, 2013. **55**(4): p. 443-53.

40. Persson, R., et al., *Adverse events following implantable cardioverter defibrillator implantation: a systematic review.* J Interv Card Electrophysiol, 2014. **40**(2): p. 191-205.

41. Fozzard, H.A., *Heart: excitation-contraction coupling.* Annu Rev Physiol, 1977. **39**: p. 201-20.

42. Grunnet, M., *Repolarization of the cardiac action potential. Does an increase in repolarization capacity constitute a new anti-arrhythmic principle?* Acta Physiol (Oxf), 2010. **198 Suppl 676**: p. 1-48.

43. Nerbonne, J.M. and R.S. Kass, *Molecular physiology of cardiac repolarization.* Physiol Rev, 2005. **85**(4): p. 1205-53.

44. Gussak, I., et al., *Rapid ventricular repolarization in rodents: electrocardiographic manifestations, molecular mechanisms, and clinical insights.* J Electrocardiol, 2000. **33**(2): p. 159-70.

45. Shattock, M.J., et al., *Na+/Ca2+ exchange and Na+/K+-ATPase in the heart.* J Physiol, 2015. **593**(6): p. 1361-82.

46. Shih, H.T., *Anatomy of the action potential in the heart.* Tex Heart Inst J, 1994. **21**(1): p. 30-41.

47. Surawicz, B., *Role of potassium channels in cycle length dependent regulation of action potential duration in mammalian cardiac Purkinje and ventricular muscle fibres.* Cardiovasc Res, 1992. **26**(11): p. 1021-9.

48. Rohr, S., *Role of gap junctions in the propagation of the cardiac action potential.* Cardiovasc Res, 2004. **62**(2): p. 309-22.

49. van Veen, A.A., H.V. van Rijen, and T. Opthof, *Cardiac gap junction channels: modulation of expression and channel properties.* Cardiovasc Res, 2001. **51**(2): p. 217-29.

50. Severs, N.J., et al., *Remodelling of gap junctions and connexin expression in diseased myocardium.* Cardiovasc Res, 2008. **80**(1): p. 9-19.

51. Lampe, P.D. and A.F. Lau, *The effects of connexin phosphorylation on gap junctional communication.* Int J Biochem Cell Biol, 2004. **36**(7): p. 1171-86.

52. Larsen, W.J., *Biological implications of gap junction structure, distribution and composition: a review.* Tissue Cell, 1983. **15**(5): p. 645-71.

53. Hoyt, R.H., M.L. Cohen, and J.E. Saffitz, *Distribution and three-dimensional structure of intercellular junctions in canine myocardium.* Circ Res, 1989. **64**(3): p. 563-74.

54. de Groot, J.R., et al., *Conduction slowing by the gap junctional uncoupler carbenoxolone.* Cardiovasc Res, 2003. **60**(2): p. 288-97.

55. Dhillon, P.S., et al., *Relationship between gap-junctional conductance and conduction velocity in mammalian myocardium.* Circ Arrhythm Electrophysiol, 2013. **6**(6): p. 1208-14.

56. Akar, F.G., et al., *Dynamic changes in conduction velocity and gap junction properties during development of pacing-induced heart failure.* Am J Physiol Heart Circ Physiol, 2007. **293**(2): p. H1223-30.

57. Seidel, T., A. Salameh, and S. Dhein, *A simulation study of cellular hypertrophy and connexin lateralization in cardiac tissue.* Biophys J, 2010. **99**(9): p. 2821-30.

58. Hesketh, G.G., J.E. Van Eyk, and G.F. Tomaselli, *Mechanisms of gap junction traffic in health and disease.* J Cardiovasc Pharmacol, 2009. **54**(4): p. 263-72.

59. Dhein, S., *Gap junction channels in the cardiovascular system: pharmacological and physiological modulation.* Trends Pharmacol Sci, 1998. **19**(6): p. 229-41.

60. Entz, M., 2nd, et al., *Heart Rate and Extracellular Sodium and Potassium Modulation of Gap Junction Mediated Conduction in Guinea Pigs.* Front Physiol, 2016. **7**: p. 16.

61. Howard-Jones, N., *Cholera therapy in the nineteenth century.* J Hist Med Allied Sci, 1972. **27**(4): p. 373-95.

62. Masson, A.H., *Latta--pioneer in saline infusion.* Br J Anaesth, 1971. **43**(7): p. 681-6.

63. MacGillivray, N., *Dr Latta of Leith: pioneer in the treatment of cholera by intravenous saline infusion.* J R Coll Physicians Edinb, 2006. **36**(1): p. 80-5.

64. Barsoum, N. and C. Kleeman, *Now and then, the history of parenteral fluid administration.* Am J Nephrol, 2002. **22**(2-3): p. 284-9.

65. Ringer, S., *Concerning the Influence exerted by each of the Constituents of the Blood on the Contraction of the Ventricle.* J Physiol, 1882. **3**(5-6): p. 380-93.

66. Louch, W.E., et al., *No rest for the weary: diastolic calcium homeostasis in the normal and failing myocardium.* Physiology (Bethesda), 2012. **27**(5): p. 308-23.

67. Ringer, S., *A further Contribution regarding the influence of the different Constituents of the Blood on the Contraction of the Heart.* J Physiol, 1883. **4**(1): p. 29-42 3.

68. Lucas, K., *On the gradation of activity in a skeletal muscle-fibre.* Journal of Physiology-London, 1905. **33**(2): p. 125-137.

69. Brodie, T.G., *The perfusion of surviving organs.* Journal of Physiology-London, 1903. **29**(3): p. 266-275.

70. Dixon, W.E., *The innervation of the frog's stomach.* Journal of Physiology-London, 1902. **28**(1/2): p. 57-75.

71. Cullis, W.C., *On secretion in the frog's kidney.* Journal of Physiology-London, 1906. **34**(3): p. 250-266.

72. Tyrode, M.V., *The mode of action of some purgative salts.* Archives Internationales De Pharmacodynamie Et De Therapie, 1910. **20**: p. 205-223.

73. Hoeker, G.S., et al., *Electrophysiologic effects of the IK1 inhibitor PA-6 are modulated by extracellular potassium in isolated guinea pig hearts.* Physiol Rep, 2017. **5**(1).

74. Veeraraghavan, R., et al., *Potassium channel activators differentially modulate the effect of sodium channel blockade on cardiac conduction.* Acta Physiol (Oxf), 2013. **207**(2): p. 280-9.

75. Vejux-Tyrode, M., *The Composition of Zygadenus Venenosus and the Pharmacological Action of its Active Principle.* J Med Res, 1904. **11**(2): p. 399-402.

76. Vejux-Tyrode, M., *On the Active Principle of Jamaica Dogwood.* J Med Res, 1902. **7**(4): p. 405-7.

77. Vejux-Tyrode, M., *Composition of zygadenus frumentii and zygadenus venenosus.* J Med Res, 1901. **6**(2): p. 359.

78. Vejux-Tyrode, M. and L. Nelson, *Mercurial Diuresis.* J Med Res, 1903. **10**(1): p. 132-4.

79. Veeraraghavan, R., et al., *Potassium channels in the Cx43 gap junction perinexus modulate ephaptic coupling: an experimental and modeling study.* Pflugers Arch, 2016. **468**(10): p. 1651-61.

80. Leetham, C., *Action of certain drugs on isolated strips of ventricle.* J Physiol, 1913. **46**(2): p. 151-8.

81. Zhong, J.H., et al., *Effects of hypokalemia on transmural dispersion of ventricular repolarization in left ventricular myocardium.* Asian Pac J Trop Med, 2013. **6**(6): p. 485-8.

82. Cheng, C.Y. and B. Boettcher, *The effect of steroids on the in vitro migration of washed human spermatozoa in modified Tyrode's solution or in fasting human blood serum.* Fertil Steril, 1979. **32**(5): p. 566-70.

83. Veeraraghavan, R., et al., *Sodium channels in the Cx43 gap junction perinexus may constitute a cardiac ephapse: an experimental and modeling study.* Pflugers Arch, 2015.

84. Larsen, A.P., et al., *The voltage-sensitive dye di-4-ANEPPS slows conduction velocity in isolated guinea pig hearts.* Heart Rhythm, 2012. **9**(9): p. 1493-500.

85. Greer-Short, A. and S. Poelzing, *Temporal response of ectopic activity in guinea pig ventricular myocardium in response to isoproterenol and acetylcholine.* Front Physiol, 2015. **6**: p. 278.

86. Veeraraghavan, R., M.E. Salama, and S. Poelzing, *Interstitial volume modulates the conduction velocity-gap junction relationship.* Am J Physiol Heart Circ Physiol, 2012. **302**(1): p. H278-86.

87. Poelzing, S., et al., *Heterogeneous connexin43 expression produces electrophysiological heterogeneities across ventricular wall.* Am J Physiol Heart Circ Physiol, 2004. **286**(5): p. H2001-9.

88. Poelzing, S. and D.S. Rosenbaum, *Altered connexin43 expression produces arrhythmia substrate in heart failure.* Am J Physiol Heart Circ Physiol, 2004. **287**(4): p. H1762-70.

89. Poelzing, S., B.J. Roth, and D.S. Rosenbaum, *Optical measurements reveal nature of intercellular coupling across ventricular wall.* Am J Physiol Heart Circ Physiol, 2005. **289**(4): p. H1428-35.

90. Poelzing, S., et al., *SCN5A polymorphism restores trafficking of a Brugada syndrome mutation on a separate gene.* Circulation, 2006. **114**(5): p. 368-76.

91. Deschenes, I., et al., *Regulation of Kv4.3 current by KChIP2 splice variants: a component of native cardiac I(to)?* Circulation, 2002. **106**(4): p. 423-9.

92. Deschenes, D., et al., *Biophysical characteristics of a new mutation on the KCNQ1 potassium channel (L251P) causing long QT syndrome.* Can J Physiol Pharmacol, 2003. **81**(2): p. 129-34.

93. Deschenes, I., et al., *Electrophysiological study of chimeric sodium channels from heart and skeletal muscle.* J Membr Biol, 1998. **164**(1): p. 25-34.

94. Deschenes, I., E. Trottier, and M. Chahine, *Implication of the C-terminal region of the alpha-subunit of voltage-gated sodium channels in fast inactivation.* J Membr Biol, 2001. **183**(2): p. 103-14.

95. Kjolbye, A.L., et al., *Maintenance of intercellular coupling by the antiarrhythmic peptide rotigaptide suppresses arrhythmogenic discordant alternans.* Am J Physiol Heart Circ Physiol, 2008. **294**(1): p. H41-9.

96. Choi, B.R., et al., *Low osmolarity transforms ventricular fibrillation from complex to highly organized, with a dominant high-frequency source.* Heart Rhythm, 2006. **3**(10): p. 1210-20.

97. Choi, B.R., W. Jang, and G. Salama, *Spatially discordant voltage alternans cause wavebreaks in ventricular fibrillation.* Heart Rhythm, 2007. **4**(8): p. 1057-68.

98. Choi, B.R., T. Liu, and G. Salama, *Calcium transients modulate action potential repolarizations in ventricular fibrillation.* Conf Proc IEEE Eng Med Biol Soc, 2006. **1**: p. 2264-7.

99. Choi, B.R., T. Liu, and G. Salama, *Adaptation of cardiac action potential durations to stimulation history with random diastolic intervals.* J Cardiovasc Electrophysiol, 2004. **15**(10): p. 1188-97.

100. Foreman, J.C. and J.L. Mongar, *The role of the alkaline earth ions in anaphylactic histamine secretion.* J Physiol, 1972. **224**(3): p. 753-69.

101. George, S.A. and S. Poelzing, *Cardiac conduction in isolated hearts of genetically modified mice--Connexin43 and salts.* Prog Biophys Mol Biol, 2016. **120**(1-3): p. 189-98.

102. Li, S.Y., et al., *Seasonal variations in serum sodium levels and other biochemical parameters among peritoneal dialysis patients.* Nephrol Dial Transplant, 2008. **23**(2): p. 687-92.

103. Hodgkin, A.L. and A.F. Huxley, *Propagation of electrical signals along giant nerve fibers.* Proc R Soc Lond B Biol Sci, 1952. **140**(899): p. 177-83.

104. Hodgkin, A.L. and A.F. Huxley, *A quantitative description of membrane current and its application to conduction and excitation in nerve.* J Physiol, 1952. **117**(4): p. 500-44.

105. Corrado, D., et al., *Relationship Between Arrhythmogenic Right Ventricular Cardiomyopathy and Brugada Syndrome: New Insights From Molecular Biology and Clinical Implications.* Circ Arrhythm Electrophysiol, 2016. **9**(4): p. e003631.

106. Weidmann, S., *The effect of the cardiac membrane potential on the rapid availability of the sodium-carrying system.* J Physiol, 1955. **127**(1): p. 213-24.

107. Kagiyama, Y., J.L. Hill, and L.S. Gettes, *Interaction of acidosis and increased extracellular potassium on action potential characteristics and conduction in guinea pig ventricular muscle.* Circ Res, 1982. **51**(5): p. 614-23.

108. Buchanan, J.W., Jr., T. Saito, and L.S. Gettes, *The effects of antiarrhythmic drugs, stimulation frequency, and potassium-induced resting membrane potential changes on conduction velocity and dV/dtmax in guinea pig myocardium.* Circ Res, 1985. **56**(5): p. 696-703.

109. Shaw, R.M. and Y. Rudy, *Electrophysiologic effects of acute myocardial ischemia. A mechanistic investigation of action potential conduction and conduction failure.* Circ Res, 1997. **80**(1): p. 124-38.

110. Nygren, A. and W.R. Giles, *Mathematical simulation of slowing of cardiac conduction velocity by elevated extracellular.* Ann Biomed Eng, 2000. **28**(8): p. 951-7.

111. Mendez, C., D. Erlij, and G.K. Moe, *Indirect Action of Epinephrine on Intraventricular Conduction Time.* Circ Res, 1964. **14**: p. 318-26.

112. Han, J., P. Garciadejalon, and G.K. Moe, *Adrenergic Effects on Ventricular Vulnerability.* Circ Res, 1964. **14**: p. 516-24.

113. Dominguez, G. and H.A. Fozzard, *Influence of extracellular K+ concentration on cable properties and excitability of sheep cardiac Purkinje fibers.* Circ Res, 1970. **26**(5): p. 565-74.

114. Van Petegem, F., P.A. Lobo, and C.A. Ahern, *Seeing the forest through the trees: towards a unified view on physiological calcium regulation of voltage-gated sodium channels.* Biophys J, 2012. **103**(11): p. 2243-51.

115. Pitt, G.S. and S.Y. Lee, *Current view on regulation of voltage-gated sodium channels by calcium and auxiliary proteins.* Protein Sci, 2016. **25**(9): p. 1573-84.

116. Rose, B., I. Simpson, and W.R. Loewenstein, *Calcium ion produces graded changes in permeability of membrane channels in cell junction.* Nature, 1977. **267**(5612): p. 625-7.

117. Noma, A. and N. Tsuboi, *Dependence of junctional conductance on proton, calcium and magnesium ions in cardiac paired cells of guinea-pig.* J Physiol, 1987. **382**: p. 193-211.

118. George, S.A., et al., *Extracellular sodium dependence of the conduction velocity-calcium relationship: evidence of ephaptic self-attenuation.* Am J Physiol Heart Circ Physiol, 2016. **310**(9): p. H1129-39.

119. Shaw, R.M. and Y. Rudy, *Ionic mechanisms of propagation in cardiac tissue. Roles of the sodium and L-type calcium currents during reduced excitability and decreased gap junction coupling.* Circ Res, 1997. **81**(5): p. 727-41.

120. Sperelakis, N. and K. McConnell, *Electric field interactions between closely abutting excitable cells.* IEEE Eng Med Biol Mag, 2002. **21**(1): p. 77-89.

121. Sperelakis, N. and J.E. Mann, Jr., *Evaluation of electric field changes in the cleft between excitable cells.* J Theor Biol, 1977. **64**(1): p. 71-96.

122. Anastassiou, C.A., et al., *Ephaptic coupling of cortical neurons.* Nat Neurosci, 2011. **14**(2): p. 217-23.

123. Bokil, H., et al., *Ephaptic interactions in the mammalian olfactory system.* J Neurosci, 2001. **21**(20): p. RC173.

124. Reutskiy, S., E. Rossoni, and B. Tirozzi, *Conduction in bundles of demyelinated nerve fibers: computer simulation.* Biol Cybern, 2003. **89**(6): p. 439-48.

125. Lin, J. and J.P. Keener, *Ephaptic coupling in cardiac myocytes.* IEEE Trans Biomed Eng, 2013. **60**(2): p. 576-82.

126. Rhett, J.M., et al., *The perinexus: sign-post on the path to a new model of cardiac conduction?* Trends Cardiovasc Med, 2013. **23**(6): p. 222-8.

127. Rhett, J.M., et al., *Cx43 associates with Na(v)1.5 in the cardiomyocyte perinexus.* J Membr Biol, 2012. **245**(7): p. 411-22.

128. Beauchamp, P., et al., *Electrical coupling and propagation in engineered ventricular myocardium with heterogeneous expression of connexin43.* Circ Res, 2012. **110**(11): p. 1445-53.

129. Palatinus, J.A., J.M. Rhett, and R.G. Gourdie, *The connexin43 carboxyl terminus and cardiac gap junction organization.* Biochim Biophys Acta, 2012. **1818**(8): p. 1831-43.

130. Lin, J. and J.P. Keener, *Modeling electrical activity of myocardial cells incorporating the effects of ephaptic coupling.* Proc Natl Acad Sci U S A, 2010. **107**(49): p. 20935-40.

131. Veeraraghavan, R., S. Poelzing, and R.G. Gourdie, *Old cogs, new tricks: a scaffolding role for connexin43 and a junctional role for sodium channels?* FEBS Lett, 2014. **588**(8): p. 1244-8.

132. Morley, G.E., et al., *Characterization of conduction in the ventricles of normal and heterozygous Cx43 knockout mice using optical mapping.* J Cardiovasc Electrophysiol, 1999. **10**(10): p. 1361-75.

133. Eloff, B.C., et al., *High resolution optical mapping reveals conduction slowing in connexin43 deficient mice.* Cardiovasc Res, 2001. **51**(4): p. 681-90.

TABLE

	NaCl	KCl	$CaCl_2$	$MgCl_2$	NaH_2PO_4	$NaHCO_3$	Glucose	$MgSO_4$	NaOH	HEPES
Tyrode	137	2.7	1.8	1	0.4	12	5.5			
Leetham	137	5.4	1.8	1	0.4	6	5.5			
Deschenes/Chahine	150	5	1	2			10			10
Deschenes/Tomaselli	150	2	2	1			10			10
Poelzing/Rosenbaum	129	4	1.8			25	5.5	0.5		
Poelzing/Deschenes	140	5	2	1			10			10
Kjolbye/Rosenbaum	140	4.5	1.25	0.7			5.5			5
Poelzing	140	4.5	1.25	0.7			5.5		5.5	10

Table 1.1 – Perfusate solution compositions (mM)

CHAPTER – 2

Design and validation of a tissue bath 3D printed with PLA for optically mapping suspended whole heart preparations.

FOREWORD

While the main direction of this dissertation is to investigate the effects of perfusate ionic composition on cardiac electrophysiology, there are a multitude of other parameters to consider during an optical mapping experiment. One such component consists of the experimental equipment, such as the bath used for whole heart procedures. A task that was placed in my care was to design and 3D print an optical mapping bath that would alleviate the cost of having a bath designed and manufactured by an outside company. Therefore, this chapter of the dissertation focuses on standardizing the equipment used for experiments and testing the efficacy of the use of 3D printed optical mapping equipment.

INTRODUCTION

Recently, 3D printing has become a popular development platform within the biomedical engineering community. The implementations in the field are varied, including tissue engineering applications and experimental equipment manufacturing [1-4]. Specifically for the field of cardiac electrophysiology, 3D printing is becoming more common for manufacturing equipment used in optical mapping experiments [5, 6]. However, a previous publication mostly describes the process for designing optical mapping baths using 3D printers, such as the Objet 24 (Stratasys, Eden Praire, MN), that are higher quality than a typical desktop hobby printer (11). Therefore, the purpose of this manuscript is to describe the design and validation of a whole heart bath and stabilizers for use in optical mapping experiments where the heart is suspended vertically, printed using a hobby grade desktop printer.

Extrusion deposition 3D printing is an additive manufacturing process in which objects are first modeled using design software and then constructed from the drawings [7]. The printed objects are created through layers of material, usually poly-lactic acid (PLA) or acrylonitrile-butadiene-styrene (ABS), placed one on top of the other until the final design is complete [8]. PLA was chosen as the printing material for multiple reasons. First, ABS based systems require ventilation since the material can toxic when heated past melting temperature [9]. This adds to the indirect cost of 3D printing. The second reason for choosing PLA is that it mimics the optical properties of plexiglass (PMMA), which will presumably reduce an experimental confounder when comparing data obtained with new 3D printed baths to historical data using a PMMA perfusion bath [10-12]. As of 2017 the price of commercially available 3D printers has decreased enough

to be feasible for laboratory use, with desktop printers costing as little as $1,299 (MakerBot, New York City, NY) and pre-manufactured kits costing less, such as the Mendel90 at $1,100 (RepRap), which can alternatively be fully 3D printed itself to further reduce the cost. With the use of 3D printers on the rise, scientists and engineers have the opportunity to manufacture experimental equipment in house.

One of the benefits of 3D printing is that it makes it theoretically possible to design a part in the morning and use it in the afternoon or the next day. Contrast this with traditional manufacturing methods requiring the plans for the part to be sent to the manufacturer, where it is entered in a queue with other customer requests, reviewed by the engineers who know the tolerances and specifications of their manufacturing equipment, sent back to the customer for edits, approval, or requested design changes, before repeating the pre-production cycle. Just the pre-production cycle can take days to months. The rapid turnaround between design and product made with 3D printing reduces the design and testing cycle. In traditional manufacturing, the design process must often terminate at a product solution that is functional but not optimized when the cost of the design process exceeds pre-determined costs and deadlines. Finally, a rapid prototyping product solution in the same space as the final application creates opportunities such as customizing equipment to the specifications of individual users. The net result is that an individually customized part can be rapidly prototyped, manufactured, and implemented for significantly lower production costs than traditional laboratory equipment manufacturing processes.

As mentioned above, cardiac electrophysiologists have already begun adopting 3D printing equipment for optical mapping [5, 6]. Despite all of the advantages of 3D

printing over conventional manufacturing described above, 3D printing is associated with its own design limitations and considerations. For example, 3D printers can jam during a print, disrupting the print process and introducing inhomogeneities resulting in part failure. Furthermore, the product can distort by other means during the printing, setting, or finishing processes, and these changes may significantly alter implementation of common manufacturing solutions that require higher spatial precision such as the use of O-rings and fasteners like screws and bolts.

In this manuscript, we detail the process of constructing an organ bath, base plate, and cannula holder for conducting suspended whole heart optical mapping experiments from inception to final design using a hobby grade desktop 3D printer. Beginning with a user with no prior 3D printing experience, we detail the steps and choices made over the course of a year to manufacture a custom designed and easily adapted laboratory solution at a price significantly less than a bath that was designed and manufactured at a machine shop that cost $2,500 to fabricate in 2012. Finally, we demonstrate that the material and finishing of 3D printed baths did not alter optical mapping results compared to experiments conducted in the traditionally manufactured bath.

MATERIALS AND METHODS

This study abides by and follows all guidelines set forth by the Institutional Animal Care and Use Committee at Virginia Polytechnic Institute and State University and NIH *Guide for the Care and Usage of Laboratory Animals*.

Design

3D models were designed using SolidWorks (Dassault Systemes). Once each of the 3D models were constructed (bath, base plate, and cannula holder), they were converted to a stereolithography file (STL), which describes the surface geometry of the designed object.

Printing

The STL files were exported to Makerbot Desktop software, which spliced the design in order to prepare the part for printing. Splicing is a procedure in which the layer by layer print design is created, including designing any fill patterns for the internal volume of the part. The software was also used to connect the design computer to the printer to transfer the design and initiate the process. The parts were printed using a Fifth Generation Makerbot Replicator desktop 3D printer (Makerbot). All prints were made using PLA filament (Makerbot), printed at a resolution of 10-40 μm. The choice of print resolutions will be discussed in the results section.

Post Processing

After printing, the bath was made water tight using an acetone dip procedure. While it has previously been stated that acetone smoothing works only on ABS [7], we found that an acetone dipping procedure was effective on our PLA printed baths. This was accomplished by dipping the entire bath in acetone for 4 seconds. This process was repeated a second time after the bath had dried from the first dipping process. The bath was then left to dry overnight at room temperature. A microscope slide (Ted Pella, Inc.

75 x 50 x 1 mm, 26005) was used as the bath window when the bath was dry and attached using adhesive (Aleene's, Glass & Bead). Adhesive was added to one side of the glass slide, which was then placed on the interior surface of the bath containing the viewing hole. Two c-clamps were used to hold the glass slide onto the bath overnight to allow the adhesive to cure.

Langendorff Perfusion

Male retired breeder Hartley albino guinea pigs (Hilltop, Scottdale, PA) were anesthetized using isofluorane. The heart was excised for retrograde perfusion in a Langendorff perfusion system and atria were resected to prevent competitive ventricular stimulation. An artificial blood like solution (140 NaCl, 4.56 KCl, 1.25 $CaCl_2$, 5.5 Dextrose, 0.7 $MgCl_2$, 10 HEPES, and 7.5 BDM in mmol/L) was perfused at constant flow and pressure maintained between 40 and 55 mm Hg. Approximately 5.5 mL of NaOH was added per L of solution in order to reach a pH of 7.4. The temperature of the perfusate was held at 37.0 °C. A unipolar AgCl wire was used to pace each heart on the anterior left ventricular epicardium at 1.5 times pacing threshold. Each pulse was 5 ms in duration at a basic cycle length of 300 ms for all recordings.

Electrocradiography

AgCl electrodes were used to record a volume conducted bath electrocardiogram (ECG) at 1 kHz. The electrode wires were placed on either side of the ventricles, with the ground placed at the rear of the bath.

Optical Mapping

Optical mapping was used to assess cardiac conduction velocity (CV) as previously described [13]. Briefly, the voltage sensitive dye, di-4-ANEPPS (7.5 μM), was used to measure optical action potentials. Cardiac electro-mechanical coupling was reduced using 2,3-butanedione monoxime (BDM, 7.5μM), which decreased motion during imaging. The heart was gently pressed against the glass to create a flat imaging plane and to further reduce motion.

Dye was excited using a 510 ± 5 nm filter (Brightline Fluorescence Filter) and a halogen light source (MHAB-150 W, Moritex Corporation). An emission filter of 610 nm (610FG01-50(T257), Andover Corporation) was used in conjunction with a MiCam Ultima CMOS L-camera (SciMedia Ltd.) at 1 kHz to capture the emitted light.

CV was calculated as previously described [14]. Optical signals were binned 2 x 2 before analysis as previously described [15]. Briefly, maximum rate of optical action potential rise at each pixel was calculated to determine activation time. A parabolic surface was fit to activation times to determine vectors for CV at each pixel. Pixels along the fastest and slowest axes of propagation (± 8°) are reported as transverse and longitudinal CV respectively. All hearts were paced with a 300 ms basic cycle of pacing.

Bath Surface Testing

The ability for the bath to be cleaned was tested using the gap junction uncoupler carbenoxolone (30 μM) [16]. Specifically, a clean bath was tested in the optical mapping apparatus using the perfusate previously described. After 30 minutes of perfusion, 30 μM carbenoxolone was added to the perfusate and again analyzed. Consecutive

experiments were run after the bath was cleaned using 150 mL 0.1 M HCl. Multiple (n=3) new baths and cleaned (n=3) baths were analyzed.

Contractility Studies

Left ventricular pressure was recorded in hearts without BDM (140 NaCl, 4.56 KCl, 1.25 $CaCl_2$, 5.5 Dextrose, 0.7 $MgCl_2$, and 10 HEPES in mmol/L). After 30 minutes, 10 µM of blebbistatin, a mechanical uncoupler, was added for 30 minutes.

Left ventricular developed pressure (LVDP) was measured using a size 7 latex balloon (Harvard Apparatus, 733482). The balloon was secured to a metal cannula (Harvard Apparatus, 730184) which connected to a pressure transducer (ADInstruments, MLT844), which recorded at 1 kHz. Following cannulation, the balloon was inserted and secured into the left ventricle for continuous recording for the remainder of the experiment.

Statistical Analysis

Statistical analysis was performed using one way ANOVA and two tailed Student's t-test assuming equal variance. A $p \leq 0.05$ was considered significant. All data shown is reported as mean ± standard error.

RESULTS AND DISCUSSION

The purpose of the project was to create an affordable and customizable 3D printed bath for optically mapping a suspended retrogradely perfused whole heart preparation in the Langendorff configuration using a hobby grade desktop 3D printer. The design

criteria were; 1. that the bath had to be water proof, 2. stable at temperatures up to 37 °C, and 3. compatible with use of a 0.1 M HCl cleaning solution. Most importantly, the finished product should not alter experimental outcomes when compared with similar experiments performed in a manufactured bath made of Plexiglas, glass, rubber O-rings and affixed with silicon adhesive and bolts (Figure 2.1). These goals were accomplished using a series of design steps including 3D computer aided design, printing, post-processing, and testing. The design was optimized for the suspended whole heart perfusion experiments required in our laboratory for optical mapping studies through a series of rapid prototyping design iterations. Major design milestones during bath development can be seen in Figure 2.2.

Design

Our tissue perfusion system requires that a heart can be suspended from a glass cannula, such that the heart hangs vertically and can be gently pressed against a transparent imaging window. In order to accomplish this, we strove to mimic the design of a previously used manufactured bath design (Figure 2.1). The preliminary design only considered the box, the imaging window and a built in cannula holder (Figure 2.2A). This design included an attached base plate that is necessary for affixing the bath in line with the camera objectives on an optical rail. This initial bath revealed two new design limitations; having an attached cannula holder restricted movement of the heart and the bath was not waterproof immediately after printing. Additionally, the first bath design required attaching glass against the imaging window from the outside with adhesive. Testing revealed further extensive leakage around the glass.

In order to address the issue of fluid leakage around the front pane of glass, the next bath design included an exterior wall of plastic that covered the front of the bath and glass (Figure 2.2B), which also included supports running down the side of the bath. The wings were designed to accommodate a microscope glass slide of dimensions 75 x 50 x 1 mm. The rationale was to create a press fit for the glass between the bath and the added material instead of having to rely on adhesive for the water proofing. During testing, users thought the wings were a hindrance. Holes on the sides of the bath were included to accommodate plungers that could be used to position the heart during experiments, which mimicked the manufactured bath (Figure 2.1). Both the plunger and glass press fit design required O-rings to prevent liquid leakage also shown in Figure 2.1. The most important lesson from this iteration was that the settings chosen for printing the bath exceeded the tolerances needed to provide a robust seal with O-rings for both plunger and the glass slide. Therefore O-rings were excluded in subsequent designs. Further, it became apparent that the support wall of plastic did not produce enough uniform pressure on the glass for an adequate press fit, possibly explaining the failure of the O-rings.

The third design encompassed multiple concurrent design alterations as our understanding of bath design progressed (Figure 2.2C). The design returned to the concept of attaching the glass to the front of the bath with a glass adhesive and a smaller wall of plastic for press fitting, which is highlighted in white. Still, with this design, liquid continued to leak around the glass edge when affixed with a combination of adhesive and press fitting.

Additionally, plunger holes were removed from the design and the discussion of how to position the heart was deferred. This iteration also included holes to accommodate the Tygon L/S 16 tubing (Masterflex, HV-06409-16) needed to recirculate bath fluid for temperature control and effluent management. The dimensions for the tube holders were rapidly prototyped before inclusion in the next bath design in order to resolve leakage issues.

Tube dimensions were determined by designing a block with multiple holes of different sizes using the manufacturer's published outer diameter of Tygon L/S 16 tubing (6mm) and varying the diameter from 6 to 9 mm in steps of 1 mm. Fit snugness was determined empirically based on the ease of inserting the tubing and perceived difficulty of accidentally pulling the tubing out. For reference, we chose an inner diameter of 7 mm, which is 1mm larger than the outer diameter of Tygon L/S 16 tubing.

As can be seen in Figure 2.2D, the number of simultaneous design changes continued to accelerate in a feed forward process of design and testing. For this final design of what we consider our "base" bath model, the glass was moved to the inside of the chamber. Moving the glass to the inside of the bath allowed for the application of a silicone bead on the outside of the glass, reducing water leakage around the imaging window. The curing process of the adhesive on the glass was also aided by using c-clamps to hold the glass in place during drying. Since the dimensions of the microscope glass required an inner surface with similar dimensions, we once again increased the volume of the bath, but noted that we could move all the tube holders inside to reduce inner bath volume, and thus the volume of fluid requiring temperature control.

Finally this version of the bath was removed from the bottom holding plate, such that bath and base plate could be printed separately. The advantages of this choice were multifold. First, reducing the print time of a part reduces the number of incomplete prints due to printer jams and delamination as discussed below. Furthermore, we are able to print one common bath holder, and use less material for printing individual baths for each experimentalist. Thus, baths can be changed efficiently, without the need to unscrew the base plate from the experimental apparatus each time an experimentalist uses a different bath. Finally, the locations of the tube holders in the bath were changed after considerations for the bath temperature (Figure 2.3C). Specifically, the outflow ports for effluent management to prevent overflow and for temperature control by recirculation through an external coiled heat exchanger (Radnotti, 158822) were placed in the top right of the bath. The inflow port from recirculation was placed on the opposite side of the bath. This was to allow a flow of warm perfusate across the bath to reduce temperature gradients in the bath. When operating under experimental conditions, we find the following temperature gradients across a suspended heart from left (inflow) to right (outflow) of 0.1°C, and superior to inferior of 0.5°C, and posterior to anterior of 0.1°C.

Waterproofing

Waterproofing is one challenge for additive 3D printing as the process uses a method that requires stacked layers of PLA. The first attempt to decrease leakage was to reduce the filament diameter with the assumption that a thinner piece of PLA would adhere more robustly to previously printed layers. Additionally, the Makerbot 3D printer permits the specification of how much of the structure behind the surface is filled.

Specifically, a lightly filled structure might have a filling pattern 2mm below the exposed surface as seen in Figure 2.3C.

The issues associated with fixing leakage by changing printing parameters are that each parameter, such as print resolution or fill alters the likelihood of print failure precisely because 3D printed objects are multiple strands of PLA stacked, not a solid block of material such as Plexiglas. As a result, 3D printing causes inhomogeneity in the final print that may not be visible to the human eye, but can permit fluid leakage.

We next chose to seal the bath with a plastic clear gloss spray paint (Krylon Products Group) rated appropriate for use with fish tanks. While applying two coats of this spray paint is able to stop most fluid leakage issues, it was difficult to determine which areas of the bath did not receive a uniform coating since the sealant is clear. Also, we found that a thin floating film developed when we circulated water warmed to 37°C through the bath, presumably due to the spray sealant.

The final method attempted and adopted was post processing with an acetone wash. According to do it yourself YouTube videos and online forums, acetone washing was touted as a robust method for chemically melting the outer surface of a PLA print to make the exposed surfaces one solid piece of PLA, rather than many layers [7]. Briefly, the printed parts were dipped into an acetone bath for 4 seconds, allowed to dry, and dipped a second time. This acetone procedure was effective for preventing fluid leakage in 100% of subsequent prints.

Together, acetone post processing followed by sealing glass to the bath from the inside of the chamber completely eliminated all leakage issues. This process has now been

successfully applied to 8 baths used in our laboratory over the past 2 years. Additionally, the final basic design of the bath does not require screws or O-rings to make a waterproof bath that can be produced with a 3 step process: 3D printing, acetone dipping, and glass application. In all, a complete working bath can be made in less than 48 hours.

Wire Holders

Often during an optical mapping experiment, the experimentalist needs to adjust the position of the heart or a pacing electrode. Therefore, it was important to design holders for ECG electrodes, a temperature probe, and grounding electrode for the pacing wire that were maximally functional, and less likely to be in the way of the user (Figure 2.3). The holder positions were decided based on user feedback from laboratory members. There were two non-obvious issues associated with the design of the holders. The first was the thickness of the holder as thin holders often broke or warped; rendering the entire bath print useless. Holders were originally designed at a thickness of 0.5 mm to keep them as thin as possible to keep the interior of the bath as empty as possible. It was found that these only printed correctly approximately 50% of the time. We empirically determined that 1.2 mm was the minimum holder thickness that would print consistently without breaking during use.

The second issue with these holders was the problem of printing a flat surface above empty air. There are three options to deal with this. The first, which is the option we chose, was to print the holders at a fast printing speed. Since the holders were small, the PLA cooled fast enough in empty air and kept the designed shape with minimal

failures. However, this technique will not work as the mass and size of an object printed above open air increases. Therefore, one could also print with supports under the holders that would later be removed after printing. Alternatively, the holders could be printed at an angle to start so that each layer is only a few PLA strands over open air. This method is the most robust, but still requires some experimentation to determine the minimum necessary slope of the angular print.

Bath Base Plate

As was previously mentioned, we decided to print the bath and baseplate (Figure 2.4) separately in part to independently resolve design issues with each structure. In the end, printing the two components separately revealed new advantages that will be discussed later. The design constraints for the base were the dimensions for the bath, bolt holes to affix the plates in line with the optical equipment, and a trench to catch any liquids that spilled during an experiment. The exterior base of the bath measures 47 by 90 mm, and the section for holding the bath was printed at 48 by 91 mm. The 1 mm expansion was found to be appropriate with the printing tolerances and any changes that occurred as a result of acetone washing. The development of holes for mounting bolts on the base plate will have to be designed on a laboratory to laboratory basis. This is due to varying size of bolts as well as the placement of the holes based on mounting plates in individual systems.

Cannula Holder

As mentioned previously, the affixed cannula holder in Figure 2.2A was removed in subsequent designs (Figure 2.2B-D). While this could have been implemented with a

system based on bolts to mount the holder to the bath, we opted for a more simplistic approach as can be seen in Figure 2.5. We found that a simple holder could be built that would fit the base of our cannula (Radnotti, 140153-30) when the cannula was lowered into the holder (Figure 2.6), which would be held and positioned using a micromanipulator (World Precision Instruments, M3301R). This was accomplished by first cutting an initial opening with inner diameter of 9 mm to accommodate the thickness of our cannula. A fillet of 10 mm radius, with a conic radius of 1 mm was used to match the shape of the cannula and hold it steady during an experiment.

Another innovation for the holder came from the observation that the method for stabilizing the heart against the front glass of the window to reduce motion and slightly flatten the epicardial imaging plane could be incorporated into the holder. Originally, hearts were stabilized against the front viewing window with a plunger that passed through the back wall of the bath through an O-ring (Figure 2.1). However, we noticed that mixing spoons (VWR, 58552-002) used in our laboratory had approximately the same shape as the posterior surface of a guinea pig heart. Therefore, a slot was designed on the cannula holder that would also fit the spoon (Figure 2.5). We found that positioning the heart against the glass exerted pressure on the long flexible handle of the mixing spoon that gently pressed the heart against the viewing window as effectively as the plunger design. Interestingly, the spoon was introduced as a stop-gap method with the thought that we would eventually return our attention to this component with a more sophisticated design, but we found over the course of well over 100 experiments, this holder design did not significantly alter cardiac electrophysiology as discussed later.

The entire printed bath setup can be viewed in Figure 2.5B, which includes placement of all tubing, ECG wiring, cannula, and temperature probe.

Printing Parameters

The Makerbot Desktop (Makerbot, New York City, NY) software allows the user to adjust the height of the print layers, percent fill on thick structures, printing temperature, and the number of shells on a segment. At first the assumption was made that the best bath would be filled in completely with the smallest layer height possible in order to form fine details. We quickly learned that printing at the finest resolution significantly prolonged print times and increased the opportunity for print errors such as print head jamming and delamination. Through trial and error we found that a 6-shell, 30% fill gave the best results when paired with a filament diameter of 30 µm. This means that each surface has a minimum of six 30 µm diameter filaments. When a design structure is thicker than 3.6 mm, the MakerBot printing software generates a pre-determined fill pattern that is only 30% of the inter-surface volume (Figure 2.3C). This allowed for a consistent outer coating on the parts, while not wasting material on the interior. Also we did not find a need to print below the 30 µm filament resolution. Finally, we determined that altering the filament diameter was much less effective at preventing leaks than a post-processing acetone wash.

Printing Issues

Even with optimized printing parameters, there are issues that can occur in the printing process rendering a part unusable. This is especially true for the base plate, as the problems occur more often for large flat surfaces. Specifically, recall that the MakerBot

uses a single print filament, and as a result of significant temperature gradients on these large surfaces, delamination can occur, which is common with PLA. Even after testing print parameters, our base plates delaminate approximately 25% of the time. There are a number of approaches for reducing printing errors for large, flat surfaces. As stated above, the best idea for printing the plates is to have a larger layer height and low infill. Therefore, we tried lowering the number of shells on the plates from 6 to 2. Still, when the print did not delaminate, it sometimes warped and the print "pulled" away from the bottom surface of the printing area. This meant that on some pieces, the bottom of the plate was not flat. We therefore decided to build the bottom of the plate from 4 smaller squares in an inverted pyramid shape until the entire plate merged 9 mm above the base of the plate into the final base plate (Figure 2.4B). Starting with only 4 smaller contact areas reduced the temperature gradients that formed for each layer, significantly reducing the probability that any one of the 4 starting print areas would delaminate or warp. Other printers utilize heated printing plates or heated print volumes. Since the Fifth Generation Makerbot Replicator desktop 3D printer did not have either option, we empirically determined that altering non-essential designs could drastically reduce printing errors, and all designers are encouraged to explore similar strategies for reducing these kinds of errors.

Bath Testing

Experiments were conducted to test whether *ex vivo* guinea pig cardiac electrophysiology is different when a heart is Langendorff perfused in a manufactured bath or the 3D printed bath described above. Two representative action potentials in Figure 2.7C from an optical mapping pixel focused on approximately the same portion

of the left ventricular epicardium of two separate hearts suggests that the bath manufacturing process does not alter action potential morphology. However, our cameras record optical action potentials from 100x100 pixels, and therefore it was important to quantify differences in summary data. Using data only from hearts perfused under control conditions for 15 minutes, summary data reveals that the choice of bath (professional n=5 or 3D printed n=5) did not significantly alter CV along either the slow or fast axis of propagation, which corresponds to the transverse and longitudinal axes respectively (Figure 2.7B). Transverse CV in hearts suspended in the manufactured bath was 22.3 ± 2.28 cm/s while in the 3D printed baths CV was 21.3 ± 2.63 cm/s ($p>0.25$). Longitudinal CV in hearts suspended in the manufactured bath was 53.2 ± 4.70 cm/s while in the 3D printed baths CV was 54.7 ± 4.71 cm/s ($p>0.25$). Likewise, action potential duration (APD_{90}) was not significantly different when hearts were suspended in either bath (Figure 2.7D). Specifically, APD_{90} of hearts in the manufactured bath was 181.95 ± 16.63 ms, and 172.83 ± 9.65 ms in the 3D printed bath ($p>0.25$).

In addition to the bath testing described above, our laboratory has made many additional anecdotal observations over the past 2 years while using 3D printed baths. First, seven different scientists used their own copies of the bath, conducted experiments that included perfusates containing standard laboratory perfusion solutions, carbenoxolone (CBX), digoxin, BDM, blebbistatin, ATXII, mannitol, albumin, PA-6, or flecanaide [13, 15, 17]. Experimental procedures included S1 pacing, S1-S2 arrhythmia induction protocols, ischemia reperfusion experiments, and calcium imaging to name a few. In all of the combinations of protocols and solutions, there are no significant

differences in control values quantified from hearts suspended in the 3D or manufactured baths.

Di-4-ANEPPS is the primary dye used in optical mapping in our laboratory, which was a logical starting point for further bath testing. Representative action potentials were taken from a heart loaded with Di-4-ANEPPS and a heart placed in a bath that previously contained dye, but was cleaned as described later. The figures demonstrate that after a bath has been washed, there is no trace of optical signal during imaging of a heart, indicating that the dye was effectively washed from the bath between experiments (Figure 2.7E).

While leaching of dye could affect optical signals in the short term, there is also the possibility of functional changes when pharmacological agents are used. Therefore, conductional velocity was quantified from hearts in baths that were never used with CBX, baths that previously contained CBX but had been washed, and hearts that actively were under the influence of 30 μM CBX (Figure 2.7F). Regardless of conduction direction, 30 μM CBX significantly decreased CV when compared to either a new bath ($p<0.05$) or a bath that had been washed ($p<0.05$). However, CV in hearts perfused in new or washed baths was not significantly different ($p>0.25$).

The myosin II inhibitor blebbistatin was then tested to quantify changes in left ventricular developed pressure (LVDP) in hearts perfused in a new bath, with 10 μM blebbistatin, and in a bath that had been washed after use with blebbistatin. LVDP, normalized to the mean measurements from new baths, was found to significantly decrease after application of blebbistatin for new and cleaned baths ($p<0.05$) (Figure 2.7G). Importantly

there was no significant difference in LVDP between hearts perfused in new or cleaned baths ($p>0.25$).

Together, these data suggest that chemical leaching of PLA or retention of experimental compounds is not a significant issue with 3D printed baths. Additionally, 3D printed baths can be cleaned similar to a bath manufactured with Plexiglas. Specifically, we have yet to notice any adverse effects of cleaning the 3D printed PLA baths with the laboratories washing procedure. Specifically, baths are rinsed with warm water for 10 minutes, washed for 10 minutes with 0.1 M HCL and rinsed for another 10 minutes with warm distilled water.

Cost Savings

A large benefit of 3D printing equipment for optical mapping is the cost savings, as can be seen in Table 2.1. While a manufactured bath will cost upwards of $2,500, the design from our laboratory will cost roughly $30 per print, not including the price of the printer or labor for designs. While there is a high price of entry, a 3D printer allows the freedom to create other laboratory equipment. Also, there are less expensive options for both printers and 3D design software, which have been shown in this manuscript to be adequate for printing equipment in house. Most universities have a shared bank of printing equipment, allowing individual laboratories the ability to print this equipment without the added printer costs. Also, as demonstrated by this and a manuscript by Sulkin, M.S. et al. [5], designs for laboratory equipment will become increasingly more available and free to download. Finally, the relatively inexpensive cost of printing a bath means that if an experimentalist ever becomes worried about bath contaminants as a

result of repeated usage, the experimentalist can simply print a new bath for their next experiment.

Scaling

One additional benefit of 3D printed bath design is the ability to scale bath size to that of the tissue preparation. One example would be the ability to reduce the bath described above for guinea pigs down to a size that accommodates a mouse heart. Since our bath is based on commercially available cover slip glass for the front imaging window, one need only find a new appropriately sized glass suitable for imaging mouse hearts in a scaled down bath volume that preserved dimensions for structures like tube and electrode holders. This scaling was used to design an optical mapping bath for mice hearts, mimicking the guinea pig bath. The main changes include using size 14 tubing instead of 16, as well as a 1x1 in. glass slide for imaging (Quartz Scientific, Inc., 2120).

CONCLUSIONS

Optical mapping equipment can be made in a manner that allows for customization and that is cost effective enough for printing baths for individual users and even experimental protocols. These designs can also be made in a way that labor intensive manufacturing techniques are unnecessary. Besides a 3D printer, including many of the affordable desktop versions on the market currently, the bath discussed above can be manufactured using only adhesive, glass, acetone, and c-clamps. The STL files for a guinea pig and mouse bath, base plate, and cannula holder can be found in the Table 2.2 along with a detailed list of manufacturing and part numbers for supporting equipment. A 3D printed bath does not observably alter optical mapping results relative

to baths made of Plexiglas, glass, adhesive, sealants, O-rings and/or stainless steel bolts. Printed baths have been shown to withstand over a year of use, including over 50 experiments during that time. These results demonstrate the promise of 3D printing experimental quality laboratory equipment. In short, the versatility of 3D printing increases the possibilities for what an electrophysiologist can try in the laboratory in less time and for less money.

REFERENCES

1. Hockaday, L.A., et al., *Rapid 3D printing of anatomically accurate and mechanically heterogeneous aortic valve hydrogel scaffolds.* Biofabrication, 2012. **4**(3): p. 035005.
2. Rengier, F., et al., *3D printing based on imaging data: review of medical applications.* Int J Comput Assist Radiol Surg, 2010. **5**(4): p. 335-41.
3. Hollister, S.J., *Porous scaffold design for tissue engineering.* Nat Mater, 2005. **4**(7): p. 518-24.
4. Herrmann, K.H., et al., *3D printing of MRI compatible components: why every MRI research group should have a low-budget 3D printer.* Med Eng Phys, 2014. **36**(10): p. 1373-80.
5. Sulkin, M.S., et al., *Three-dimensional printing physiology laboratory technology.* Am J Physiol Heart Circ Physiol, 2013. **305**(11): p. H1569-73.
6. Zhang, C., et al., *Open-source 3D-printable optics equipment.* PLoS One, 2013. **8**(3): p. e59840.
7. Horvath, J.C., *Mastering 3D printing*. Technology in action. 2014, Berkeley, California: Apress. xxiii, 196 pages.
8. Gross, B.C., et al., *Evaluation of 3D printing and its potential impact on biotechnology and the chemical sciences.* Anal Chem, 2014. **86**(7): p. 3240-53.
9. Wojtyla, S., P. Klama, and T. Baran, *Is 3D printing safe? Analysis of the thermal treatment of thermoplastics: ABS, PLA, PET, and nylon.* J Occup Environ Hyg, 2017. **14**(6): p. D80-D85.
10. Domenichelli, I., et al., *Towards a better control of the radical functionalization of poly(lactic acid).* Polymer International, 2015. **64**(5): p. 631-640.
11. Battistutta, R., A. Negro, and G. Zanotti, *Crystal structure and refolding properties of the mutant F99S/M153T/V163A of the Green Fluorescent Protein.* Proteins-Structure Function and Genetics, 2000. **41**(4): p. 429-437.

12. Zidan, H.M. and M. Abu-Elnader, *Structural and optical properties of pure PMMA and metal chloride-doped PMMA films.* Physica B-Condensed Matter, 2005. **355**(1-4): p. 308-317.

13. Entz, M., 2nd, et al., *Heart Rate and Extracellular Sodium and Potassium Modulation of Gap Junction Mediated Conduction in Guinea Pigs.* Front Physiol, 2016. **7**: p. 16.

14. George, S.A., et al., *Extracellular sodium and potassium levels modulate cardiac conduction in mice heterozygous null for the Connexin43 gene.* Pflugers Arch, 2015.

15. Hoeker, G.S., et al., *Electrophysiologic effects of the IK1 inhibitor PA-6 are modulated by extracellular potassium in isolated guinea pig hearts.* Physiol Rep, 2017. **5**(1).

16. Veeraraghavan, R., M.E. Salama, and S. Poelzing, *Interstitial volume modulates the conduction velocity-gap junction relationship.* Am J Physiol Heart Circ Physiol, 2012. **302**(1): p. H278-86.

17. George, S.A., et al., *Extracellular sodium dependence of the conduction velocity-calcium relationship: evidence of ephaptic self-attenuation.* Am J Physiol Heart Circ Physiol, 2016. **310**(9): p. H1129-39.

FIGURES

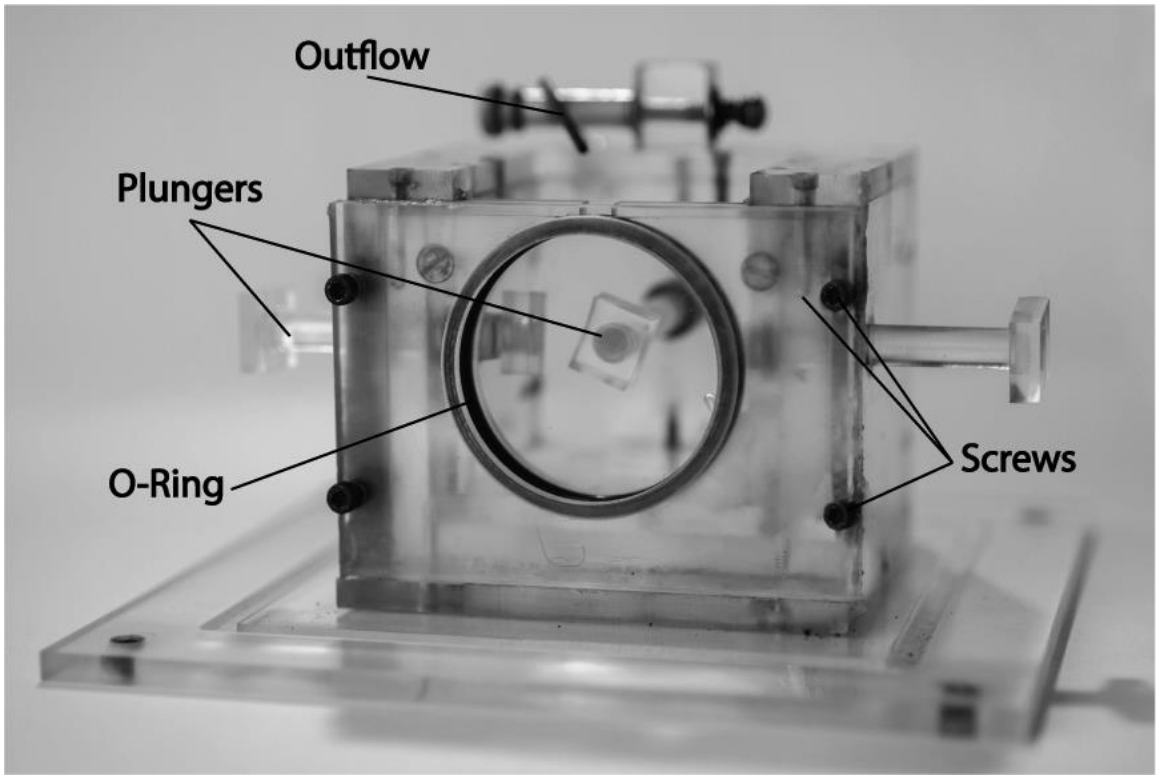

Figure 2.1 – Previously used optical mapping bath that was designed and manufactured in a machine shop. A manufactured optical mapping bath designed for guinea pig whole heart optical mapping experiments. The main components included that were removed for 3D printed baths are plungers for holding the heart in place, a built in outflow on the rear of the bath, O-rings for water sealing, and screws holding the Plexiglas bath together. However, this bath did not include holders for the temperature probe, pacing grounding electrode, or the recirculation tubing which led to crowding the bath space with loose wires and tubing during experiments.

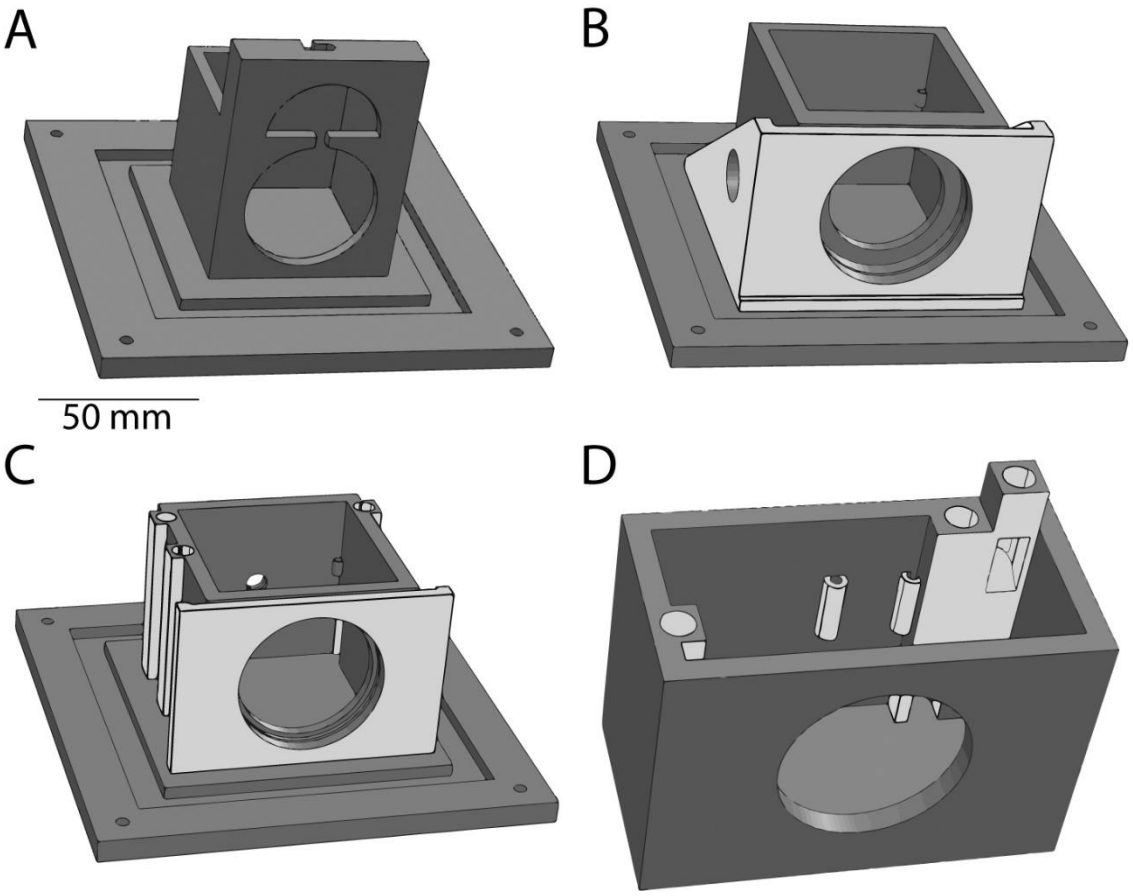

Figure 2.2 – Progression of optical mapping bath during the rapid prototyping process. A step-by-step progression of designing a 3D printed whole heart optical mapping bath. White highlighted areas are the main changes in the bath design when compared to the previous iteration. (A) First design of the 3D printed optical mapping bath which was modeled after a manufactured bath. (B) Second design. In this iteration design steps were taken to press fit the viewing glass between two pieces of the bath. Also, holes for plungers were added to secure the heart for imaging. (C) Third design. The press fit design of the bath was modified, while holes were included for effluent and recirculation control. (D) Final design. The bath was removed from the base plate and all tubing lines were moved to the interior of the bath.

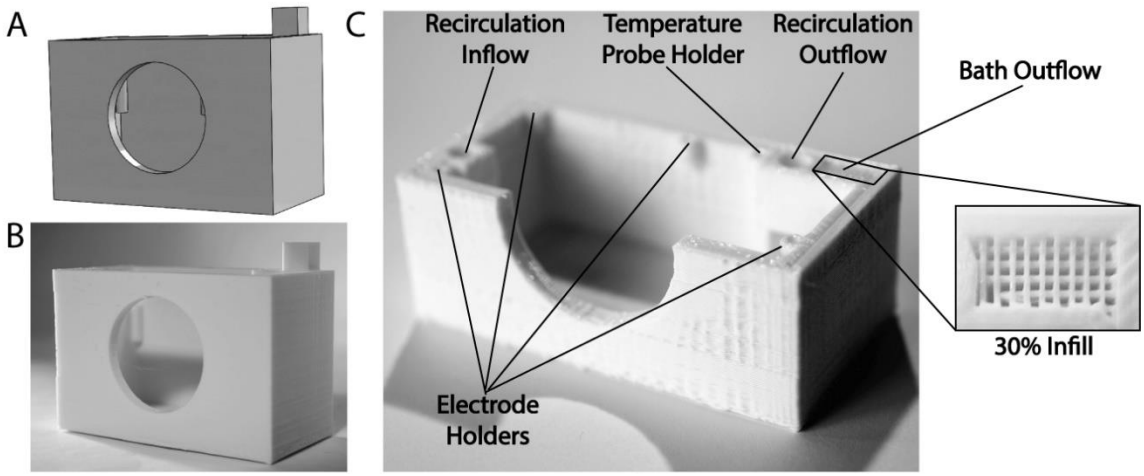

Figure 2.3 – Design features for finalized 3D printed bath. (A) 3D model of the optical mapping bath. (B) 3D printed optical mapping bath. (C) Image of a half printed optical mapping bath. The image shows the location of the ECG holders, pacing electrode ground holder, temperature probe holder, recirculation inflow, recirculation outflow, and bath outflow. The zoomed in region shows an example of 30% infill patterning for a MakerBot 3D printer.

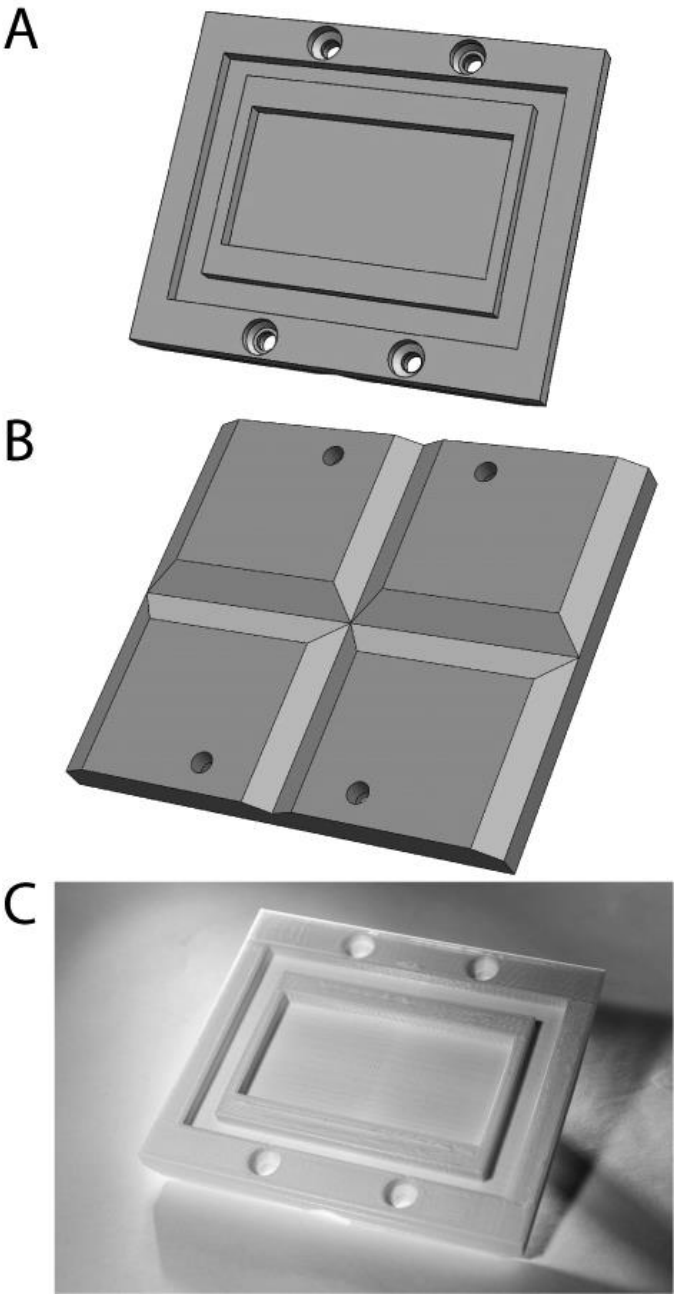

Figure 2.4 – Base plate comparison between 3D models and printed part. (A) 3D model of the optical mapping bath holding plate. (B) 3D model of the back side of the base plate showing the angled edges to reduce printing errors due to decreased surface area. (C) 3D printed optical mapping bath holding plate.

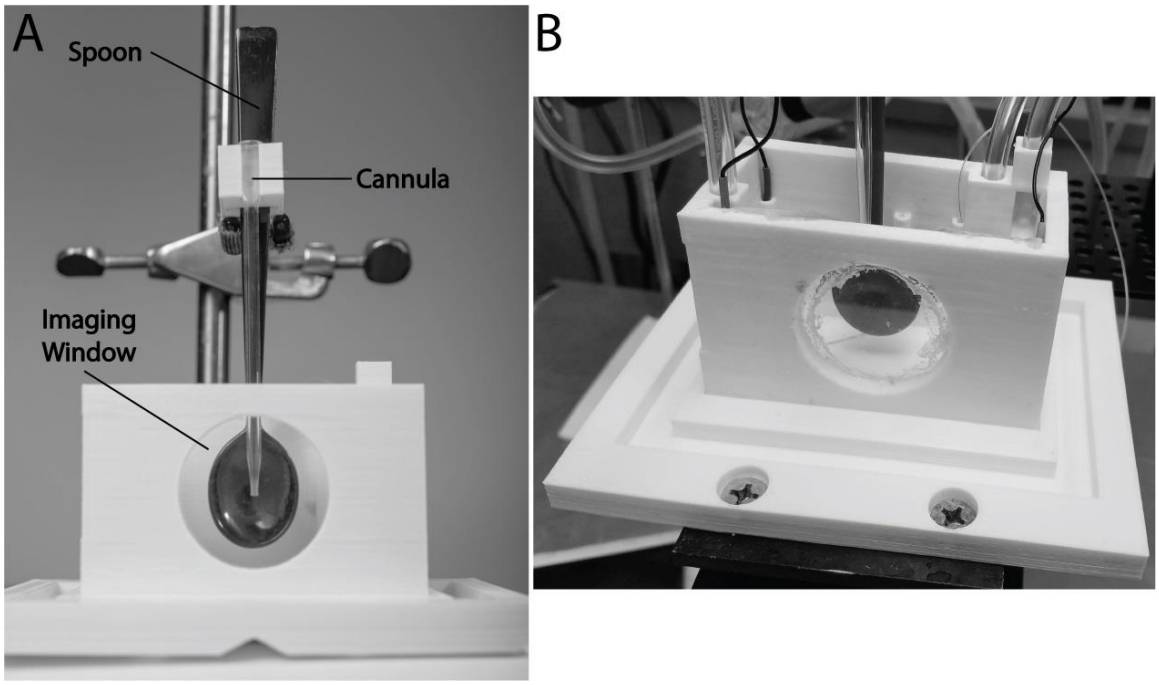

Figure 2.5 – Fully assembled optical mapping apparatus. (A) 3D printed cardiac optical mapping bath including a bath placed in the base plate. A glass cannula and spoon used for light mechanical pressure on the heart are held inside the 3D printed cannula holder, which is held up with a ring stand in the image. (B) 3D printed bath and base plate placed for use in an experimental setup. ECG electrodes, temperature probe, canula, and effluent lines included in setup.

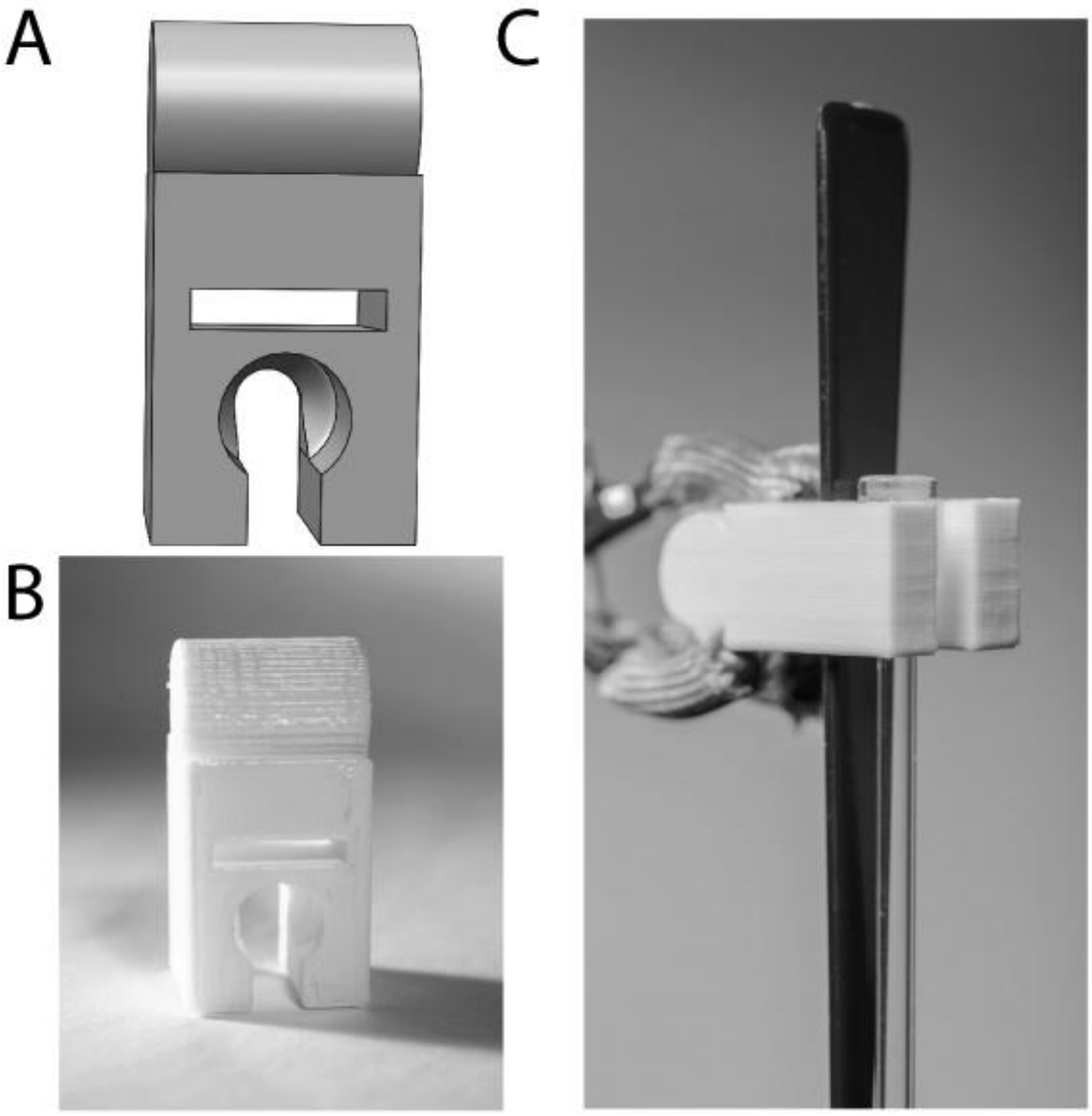

Figure 2.6 – Cannula holder comparison between 3D models and printed part. (A) 3D model of the cannula holder. (B) 3D printed cannula holder. (C) Cannula holder with glass cannula and red spoon used for mechanical pressure on the heart.

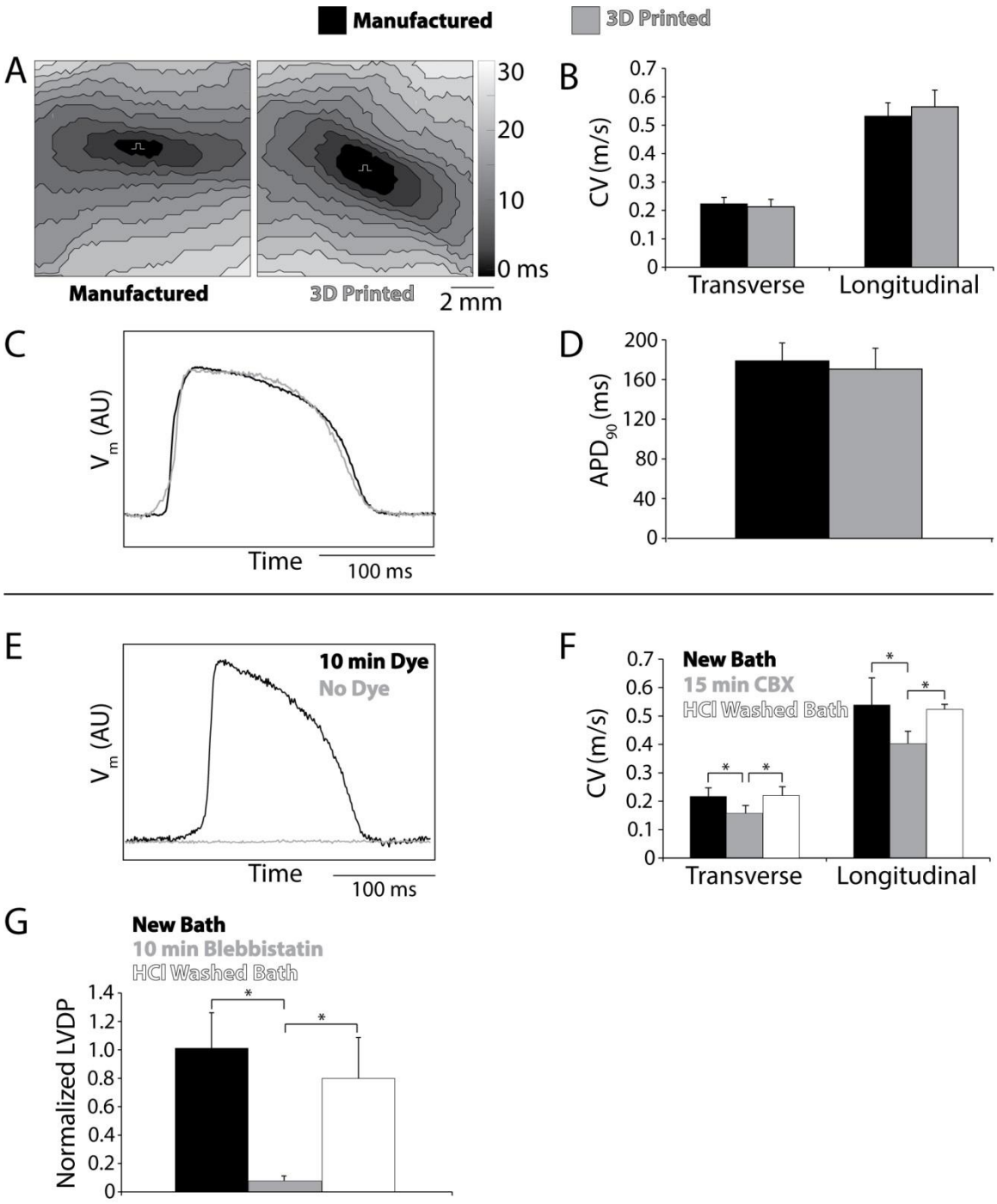

Figure 2.7 – Electrophysiological parameters are unchanged between manufactured and 3D printed baths. (A) Representative isochrones from hearts in a manufactured bath and a 3D printed bath showing no changes in conduction between the two. White symbol (Π) indicates site of pacing. (B) Neither transverse nor

longitudinal conduction velocity measurements were significantly different from hearts suspended in the two baths (n=5). (C) Representative action potentials for manufactured and 3D printed baths. (D) APD_{90} measurements for each bath were not significantly different (n=5). (E) Representative action potentials for a heart loaded with Di-4-ANEPPS versus a heart with no dye added in a bath after HCl cleaning. (F) Transverse and longitudinal conduction velocity was not altered at baseline between baths that had previously contained CBX versus those that had not. Conduction velocity was only slower in hearts perfused with 15 minutes of 30 μM CBX (n=3). (G) Normalized left ventricular developed pressure is unaffected between a new and old bath. However, pressure significantly decreased when the heart was loaded with 10 μM blebbistatin for 10 min compared to new and washed baths (n=3).

Part	Price (2017)
Heart Chamber	$5.30
Chamber Plate	$4.31
Heart Manipulator	$0.23
Adhesive	$0.46
Glass	$0.53-6.50
Acetone	$7.58
Print Head Wear and Tear	$12.00
Total	$30.41-36.38

Table 2.1 – 3D printed optical mapping equipment costs. Cost breakdown for each component of the optical mapping bath, bath holder plate, and cannula holder. Without the cost of a 3D printer, each of these baths costs roughly $30 compared to a manufactured bath, which costed $2,500 in 2012.

	Manufacturer	Item #	Price (2017)
Bath	3D Pinted in Laboratory		
Base Plate	3D Pinted in Laboratory		
Cannula Holder	3D Pinted in Laboratory		
Aortic Cannula, 3mm x 120mm	Radnoti	140153-30	$25.65
Tygon E-Lab Pump Tubing, L/S 16 (50 feet)	Masterflex	EW-06509-16	$68.25
Tygon E-Lab Pump Tubing, L/S 14 (50 feet)	Masterflex	EW-06509-14	$46.75
Micromanipulator	World Precision Instruments	M3301R	$1165.00
Polystyrene Spoons (50/pack)	Spirit Brands	58552-002	$55.68
Platinum Bond Adhesive Glass & Bead	Aleene's		$6.99
Corning® Glass Slides, 75mm x 50mm (144/pack)	Ted Pella, Inc.	26005	$73.25
Quartz Scientific, Inc. 1" x 1" mm Microscope Slide	Quartz Scientific, Inc.	2120	$6.50

Table 2.2 – Deatiled list of all components needed for working optical mapping bath. Manufacturer, part number, and cost breakdown for each of the printed components of a suspended whole heart optical mapping apparatus, including all of the miscelaneous parts that were discussed throughout the manuscript.

CHAPTER – 3

Heart rate and extracellular sodium and potassium modulation of gap junction mediated conduction in guinea pigs

FOREWORD

After the design and fabrication of a 3D printed bath for optical mapping was completed, the next step for this dissertation was to begin the study of perfusate solution composition changes on cardiac conduction velocity. Specifically, previous research from our laboratory indicated that a heterozygous knockout of gap junctions in mice could be masked through perfusate solution composition. Therefore, this study looked at modifying extracellular sodium and potassium concentration, while blocking gap junctions with varying levels of carbenoxolone. Therefore, this chapter of the dissertation is focused on investigating whether ephaptic coupling mechanisms are affected by a change in species as well as an alternate form of gap junctional inhibition.

INTRODUCTION

Normal cardiac conduction is critical for maintaining efficient pumping of the heart, and abnormal conduction can lead to arrhythmias and sudden cardiac death. Cardiac conduction is dependent on propagation of electrical signals from cell-to-cell. Cell membrane depolarization can occur by raising the intracellular potential *via* direct axial current through high resistance gap junctions (gap junctional coupling), or by a decrease in the extracellular potential between closely adjacent cells (ephaptic coupling) [1-5]. The concept of ephaptic coupling (EpC) is an old theory that has received renewed interest recently. While considered controversial in the cardiac field, EpC is more widely accepted in neurology [6-10] and has even been proposed to be important for uterine contraction [11]. An elegant review by Nicholas Sperelakis and Keith McConnell in 2002 summarizes 6 possible mechanisms for EpC [3]. While the majority of the proposed mechanisms reduce EpC to electric field coupling, the alteration of ionic concentrations within restricted extracellular microdomains in parallel with electric field coupling can also play an important role in modulating non-gap junction (GJ) mediated cell-to-cell electrical coupling [5, 12-15].

Recent evidence in guinea pig ventricular myocardium demonstrates that inducing acute interstitial edema can increases intercellular separation within the perinexal intercalated disc microdomain and slow cardiac conduction by mechanisms consistent with mathematical predictions of EpC [12-14]. Further, increasing perinexal width hypersensitizes myocardial conduction to pharmacologic GJ uncoupling [2] and sodium channel inhibition [16]. This hypersensitivity is also consistent with computational predictions of EpC. Importantly, the corollary statement is that narrowing intercellular

separation within the perinexus should decrease conduction sensitivity to GJ uncoupling and sodium channel inhibition.

In mice, we previously demonstrated that the relationships between cardiac conduction and GJs, perinexal width, and extracellular concentrations of sodium ($[Na^+]_o$) and potassium ($[K^+]_o$) are complex [17]. Since it has also been shown that a change in $[K^+]_o$ from 5 to 8mM increased CV in guinea pig hearts [18, 19], one should expect a similar increase in mice. However, in mouse hearts with the native compliment of Cx43 (wild type), and wide perinexi (>15nm), cardiac conduction was reduced when $[K^+]_o$ was raised from 4.6 to 6.1mM and concurrently $[Na^+]_o$ was decreased from 155 to 147mM. More intriguing was the finding that the wild type hearts were insensitive to the same changes in $[K^+]_o$ and $[Na^+]_o$ when perinexal width was reduced. However, when Cx43 was reduced by 50%, hearts with narrow perinexi perfused with a solution containing the higher $[K^+]_o$ and lower $[Na^+]_o$ had slower conduction relative to the solution with lower $[K^+]_o$ and higher $[Na^+]_o$. Therefore, the width of the perinexus has important effects on modulating cardiac conduction sensitivity to alterations in $[K^+]_o$ and $[Na^+]_o$, and these effects are unmasked by GJ uncoupling.

Importantly, the relationship between conduction and perinexal width does not appear to be species dependent as similar findings were observed in guinea pig [16]. However, it remains unknown whether small extracellular changes in $[K^+]_o$ and $[Na^+]_o$ can alter conduction sensitivity to pharmacologic GJ coupling in guinea pig.

The purpose of this study was twofold. First, we wanted to determine if the observed response of cardiac conduction to $[K^+]_o$ and $[Na^+]_o$ is similar in normal guinea pig hearts

as was observed in Cx43 wild type mouse hearts with narrow perinexi. Second, we sought to demonstrate that pharmacologically uncoupling GJs with a non-specific GJ uncoupler like carbenoxolone (CBX) would unmask conduction sensitivity to $[K^+]_o$ and $[Na^+]_o$ in hearts with narrow perinexi.

MATERIALS AND METHODS

This study abides by and follows all guidelines set forth by the Institutional Animal Care and Use Committee at Virginia Polytechnic Institute and State University and NIH *Guide for the Care and Usage of Laboratory Animals*.

Langendorff perfusion

Male retired breeder Hartley albino guinea pigs (Hilltop, Scottdale, PA, N=28, 800-1200g, 12-19 months old) were anesthetized using sodium pentobarbital [Nembutal, 30mg/kg IP]. The heart was extracted, retrogradely perfused in a Langendorff perfusion apparatus and the atria excised to reduce competitive stimulation. The hearts were perfused with constant flow to maintain pressure between 40 and 55mmHg. Tyrode solutions were altered as described in Table 3.1. The laboratory's historical Tyrode composition in Table 3.1 is presented as a point of reference for the modified solutions used in these experiments.

Since "normal" plasma ion concentrations are species specific [20], we calculated a percentage change of $[K^+]_o$ and $[Na^+]_o$ from the lowest values used in our previous mouse study [17]. Thus, $[K^+]_o$ was changed by 52% (4.56 to 6.95mM) and $[Na^+]_o$ by

5.4% (145.5 to 153.3mM) from historic guinea pig Tyrode solutions [2]. By this method, we designed Solutions A and B as noted in Table 3.1.

Solutions were perfused at 37°C, pH 7.4. In each experiment, historic Tyrode's solution without the gap junction uncoupler CBX was perfused for 30 minutes at the beginning of the experiment, and then Solutions A and B were perfused for 10 minutes in a random order without CBX. This was followed by CBX (15 and 30μM) in Solution A or B.

All conduction measurements were taken 10 minutes after the new perfusate reached the heart to control for the amount of time each heart was exposed to the solution, and because we previously demonstrated CBX slowed conduction to near steady-state values within 10 minutes [16]. Hearts were paced from the anterior left ventricular (LV) epicardium with a unipolar AgCl wire at basic cycle lengths (BCL) of 300 and 160ms with a 5ms pulse at 1.5 times pacing threshold [21]. A baseline BCL of 300ms was chosen to mimic physiological resting guinea pig heart rate, while 160ms BCL has been shown to decrease CV [22-24].

Transmission electron microscopy

Left ventricular tissue from each intervention reported (3 hearts per intervention, 3 samples per heart) was sectioned into 1 mm^3 cubes. The sections were fixed in 2.5% glutaraldehyde at 4°C overnight and then transferred to PBS at 4°C. The tissue was processed as previously described [17]. Images were collected using a transmission electron microscope (JEOL JEM1400) at 150,000X magnification. Measurements were obtained using ImageJ (NIH) from 15 perinexi per sample. Total number of perinexi measured was 135.

Electrocardiography

A volume conducted bath electrocardiogram (ECG) was obtained using AgCl electrodes. An anode was placed near the right ventricle, a cathode near the left ventricle, and a common ground at the back of the bath. The ECG was recorded at 1kHz.

Optical mapping

The voltage sensitive dye di-4-ANEPPS (15μM) was perfused for 10 minutes before the start of the experimental protocol. Cardiac motion was reduced with 2,3-butanedione monoxime (BDM, 7.5μM). Hearts were further stabilized by applying light pressure on the posterior surface of the heart.

The dye was excited with a halogen light source (MHAB-150 W, Moritex Corporation) with an excitation filter of 510nm (Brightline Fluorescence Filter). An emission filter of 610 nm (610FG01-50(T257), Andover Corporation) was used before the emitted light was recorded using a MiCam Ultima CMOS L-camera, sampling at a rate of 1 kHz. Images were captured on a 100x100 array with an interpixel resolution of 0.1 mm.

CV was calculated as previously described [17] using an algorithm by Bayly et al. [25]. Briefly, maximum rate of optical action potential rise at each pixel was calculated to determine activation time. A parabolic surface was fit to activation times to determine vectors for CV at each pixel. CV was quantified in two directions, longitudinal and transverse (CV_L and CV_T, respectively), with anisotropic ratio (AR) calculated as CV_L/CV_T. Conduction in each direction was calculated from a group of vectors that were

within 5 pixels and with an angle of ±8 degrees from direction of longitudinal (fastest) or transverse (slowest) propagation. The first vectors immediately adjacent to the site of pacing were excluded to reduce pacing artifacts in the CV analysis. CV was only quantified up to 32 pixels from the site of pacing in the longitudinal direction and 16 pixels in the transverse direction to reduce the contribution of conduction breakthrough. Longitudinal CV was only quantified if there were at least 10 vectors meeting the criteria above and transverse CV was quantified if at least 50 vectors met the criteria above.

Rise time (RT) was calculated by the time difference from 20% to 80% of the peak fluorescent action potential amplitude during depolarization. RT was calculated both in the longitudinal (RT_L) and transverse (RT_T) directions. Action potential duration (APD) was calculated as the difference between the activation time and 85% repolarization from peak action potential amplitude.

Western blotting

Hearts (n=3), perfused with the respective solutions for 30 minutes, were snap frozen. Tissue was homogenized in a RIPA lysis buffer (50mM Tris pH 7.4, 150mM NaCl, 1mM EDTA, 1% Triton X-100, 1% sodium deoxycholate, 2mM NaF, 200 µM Na3VO4) supplemented with HALT Protease and Phosphatase Inhibitor Cocktail (ThermoScientific). Following sonication and clarification by centrifugation, the BioRad DC protein assay was employed to determine protein concentrations and normalize prior to analysis. SDS-PAGE electrophoresis was performed as previously described using 4-20% NuPage Bis-Tris or 3-8% Tris-Acetate gels (Life Technologies) which were then transferred using the Trans-Blot Turbo system (BioRad) to low-fluorescence PVDF

membrane and blocked with 5% BSA in TNT buffer (0.1% Tween 20, 150mM NaCl, 50mM Tris pH 8.0) for one hour at room temperature. Membranes were then incubated with rabbit anti-phospho-Cx43^{Ser368} (1:1000 in 5% BSA TNT, #3511 Cell Signaling Technology) overnight at 4°C. Following several washes in TNT, secondary detection was performed using goat anti-rabbit HRP antibody (1:5000, abcam) for 1 hour at room temperature. Bound antibody was detected post washing using Clarity Western ECL Substrate (BioRad) and imaged using the BioRad Chemidoc MP system. Membranes were then stripped with Re-Blot Plus Strong (Millipore) according to manufacturer's instructions. To detect total Cx43, stripped membranes were blocked for 1 hour at room temperature in 5% milk in TNT buffer, and subsequently incubated overnight at 4°C with primary antibodies against Cx43 (1:4000, C6219 rabbit, Sigma Aldrich), and alpha-tubulin (1:4000, T6199 mouse, Sigma-Aldrich) diluted in 5% milk TNT. Membranes were then washed and incubated with the fluorescently distinct secondary antibodies goat anti-mouse AlexaFluor555 and goat anti-rabbit AlexaFlour647 (both 1:1000 in milk TNT, Life Technologies) for 1 hour at room temperature. Following several washes in TNT, membranes were fixed in methanol, dried, and imaged using the Biorad Chemidoc MP System. Protein expression was quantified by densitometry using ImageLab software (BioRad), Cx43 expression levels were normalized to alpha-tubulin, and Cx43 phosphorylate Serine 368 (Cx43-p368S) to total Cx43.

Statistics analysis

Statistical analysis was performed using a two tailed Student's t test for both paired and unpaired data. A $p \leq 0.025$ after Bonferrroni correction was considered significant. All values are reported as mean ± standard error unless otherwise noted.

RESULTS

Conduction Velocity – Control Conditions (0μM Carbenoxolone)

Cardiac conduction was quantified from guinea pig ventricles to determine whether increasing $[K^+]_o$ and decreasing $[Na^+]_o$ produced similar effects in *ex vivo* guinea pig as it did in mice hearts [17]. Representative epicardial isochrones in Figure 3.1A demonstrate the effect of solution composition on the spatial extent of activation at both 300 and 160 ms BCL. These maps suggest that cardiac conduction under control conditions was similar when hearts were perfused with Solution A or B. Further, representative isochrones maps suggest that decreasing BCL slows CV_L and CV_T, consistent with sodium channel restitution kinetics [26]. Representative action potential upstrokes in Figure 3.1B from equally spaced sites demonstrate slower CV_T than CV_L as evidenced by increased temporal separation between action potential upstrokes in the transverse direction.

Decreasing BCL significantly reduced CV_L for both Solutions A and B (Figure 3.1C). Interestingly, decreasing BCL to 160 ms with Solution A did not slow CV_T, although there was a slowing trend ($p=0.03$). On the other hand, changing BCL with Solution B caused a significant decrease in CV_T. For all experiments, solution composition did not significantly change CV_L or CV_T under control conditions (Figure 3.1D). These data suggest that solution composition does not significantly modulate conduction dependence on pacing rate with normal GJ coupling, because both solutions changed CV similarly under all conditions.

Conduction Velocity - 15μM Carbenoxolone

We previously demonstrated that GJ inhibition with 15μM CBX does not significantly alter CV [2]. For Solution A + 15 μM CBX, decreasing BCL to 160ms significantly decreased CV_L but did not significantly slow CV_T (Figure 3.2A). Under these conditions the relationship did not trend toward significance (p=0.70) in contrast to control.

Similar to control, Solution B still decreased CV_L and CV_T at a BCL of 160 relative to 300ms (Figure 3.2A). Importantly, comparing CV_L and CV_T for Solutions A and B did not reveal conduction differences when hearts were perfused with 15μM CBX at either pacing rate (Figure 3.2B), and this is similar to findings under control conditions. These data suggest that solution composition does not significantly modulate conduction dependence on pacing rate when a GJ uncoupler does not measurably slow conduction.

Conduction Velocity - 30μM Carbenoxolone

Next, we increased CBX to 30μM since it has been previously demonstrated that CBX between 20-100μM can slow cardiac conduction [27]. For Solution A + 30μM CBX, decreasing BCL from 300 to 160ms did not significantly slow CV_L but it did slow CV_T (Figure 3.3A).

Similar to control and 15μM CBX, CV_L and CV_T significantly decreased when BCL was decreased to 160ms in heart perfused with Solution B + 30μM CBX (Figure 3.3A). Thus, Solution B was always associated with rapid pacing induced CV slowing in both the

longitudinal and transverse direction for all degrees of GJ coupling, whereas Solution A was not.

In contrast to control and 15μM CBX, comparing conduction for Solutions A and B now revealed CV_L and CV_T differences when heart were perfused with 30μM CBX (Figure 3.3B, †). These data demonstrate that significant GJ uncoupling can exacerbate CV dependent differences on $[K^+]_o$ and $[Na^+]_o$ when pacing rate is increased.

Perinexal Width

The perinexus is an extracellular microdomain adjacent to GJ plaques, and these microdomains, rich in the cardiac isoform of the voltage gated sodium channel, have been proposed as the structural unit of a cardiac ephapse [16, 17, 28]. Using transmission electron microscopy, the perinexus was quantified from hearts perfused with Solution A, Solution A + CBX 30μM, and Solution B + CBX 30μM (Figure 3.4A). The yellow shaded region in the images represents the first 100nm of the perinexus adjacent to a GJ. The widths of the perinexi were measured in 5 nm increments for the first 15 nm and then in 15nm intervals up to150 nm away from the GJ (Figure 3.4B). Perinexal width was significantly larger with Solution A when compared to tissue perfused with CBX (Solution A or B). With CBX, there were no significant differences in perinexal width between Solutions A and B as summarized in Figure 3.4C. The data also demonstrates that the perinexus from 60 to 105nm from the GJ edge is reduced by CBX independent of solution composition. Therefore, the difference in CV observed between Solutions A and B at 30μM CBX is not likely related to solution induced perinexal differences.

Cx43 Expression

Many studies have demonstrated that CV is dependent on ionic perfusate composition [19, 29, 30]. We sought to determine whether the reported changes in perfusate composition can also alter Cx43 expression. Expression levels of total and Cx43-p368S were measured using alpha-tublin as a protein loading control in hearts perfused for 30 minutes with Solution A or B. Figure 3.5A and B demonstrate that solution composition did not alter total Cx43 expression. Dephosphorylation at serine 368 leads to a cascade which internalizes Cx43 in cardiac cells [31], and Cx43-p368S protein levels are often quantified as a correlate of non-functional Cx43 GJs [32, 33]. Importantly, Cx43-p368S expression levels were not different in preparations perfused with Solution A or B (Figure 3.5C and D). In a separate set of experiments, Cx43-p368S was compared to total Cx43 in hearts perfused with Solutions A or B, and freshly explanted hearts, revealing that perfusion did not alter the ratio of phosphorylated Cx43 (Figure 3.8). These data suggest that solution associated conduction changes were not predominantly due to Cx43 expression changes.

Action potential duration

APD during perfusion of Solution B was shorter than perfusion with Solution A for all CBX concentrations and BCLs (Figure 3.6, †). As expected, APD significantly shortened with both solutions when BCL was reduced from 300 to 160ms (Figure 3.6, *). Since APD shortened approximately equally with Solutions A and B, and the magnitude of APD shortening was similar, these data suggest that APD restitution kinetics may not explain the changes in CV reported above. In fact, one might expect that Solution A,

which produced the longer APD, would exhibit greater CV slowing at a 160ms BCL, and this was not the case.

Rise time

Optical rise time (RT) has been previously used as an inverse correlate of cellular excitability [34-36]. Importantly, 15μM CBX did not alter RT relative to control (Figure 3.7). With 30μM CBX, RT increased (Figure 3.7, †). Solution composition (A & B) did not significantly alter RT. Altering pacing rate also did not significantly change RT in either the longitudinal (RT_L) or transverse (RT_T) directions of propagation.

DISCUSSION

The data demonstrate how varying $[K^+]_o$, $[Na^+]_o$, and pacing rate modulates conduction sensitivity to pharmacologic GJ inhibition in guinea pig ventricular preparations. Previous studies have demonstrated that each of these factors can affect CV individually, but that small combined changes in these parameters can lead to relatively significant emergent effects on conduction [16-18, 37]. The present study is consistent with this finding and supports a hypothesis that small differences in artificial blood substitute solutions do not produce significant electrophysiological differences with normal GJ coupling. However, when GJ coupling is reduced, extracellular ionic composition and heart rate have important effects on cardiac conduction.

Effects of $[K^+]_o$ and $[Na^+]_o$

The relationship between CV and $[K^+]_o$ is biphasic. Specifically, in guinea pig, it was demonstrated that CV is maximal around 8mM $[K^+]_o$ [18, 19, 38, 39]. Interestingly,

increasing $[K^+]_o$ from 4.6mM in Solution A to 7.0mM with Solution B, did not alter CV during control conditions or 15μM CBX, which is unexpected based on previous works with $[K^+]_o$ altered in a similar range [18, 19]. One important difference between this and previous studies is that $[Na^+]_o$ is reduced in Solution B relative to A. The results show that CV is relatively insensitive to the changes in $[K^+]_o$ and $[Na^+]_o$ during normal and presumably low GJ uncoupling (15μM CBX), with increased sensitivity at 30μM CBX. These results are consistent with our results obtained in mice with narrow perinexal widths and presumably increased EpC [17].

The finding that increasing $[K^+]_o$ in guinea pig myocardium can slow conduction is consistent with the study of Pandit et al. who found that dominant rotor frequencies are decreased, suggesting slowed conduction, when $[K^+]_o$ is increased from 4 to 7mM [40]. The intriguing finding that increasing $[K^+]_o$ in ventricular myocardium can increase CV under certain conditions and decrease it under others is an important future direction for research since increased $[K^+]_o$ is critically important to our understanding of electrical abnormalities in diseases such as cardiac ischemia [18, 19]. Ischemia is also acutely associated with increased heart rate and collapse of the extracellular space, and on a longer time scale, loss of GJ coupling, [41-43] further highlighting the importance of understanding these diverse modulators of cardiac conduction.

Increases in $[K^+]_o$ and $[Na^+]_o$ have both been associated with changes in ion channel kinetics. During hypokalemia for example, peak current density of the inward rectifier potassium current (I_{K1}) is reduced, the slow component of the delayed rectifier potassium current (I_{Ks}) is increased, and the rapid component delayed rectifier

potassium current (I_{Kr}) is decreased [44, 45]. Additionally, co-transporters such as the Na-K pump can be activated through a combination of $[Na^+]_i$ and $[K^+]_o$ [46, 47]. Therefore, future studies will be required to elucidate additional effects of other channels, pumps, and exchangers on cardiac conduction.

Effects of pacing rate

It is well accepted that CV decreases when pacing rate increases, due to sodium channel inactivation [26, 48]. Here, we demonstrated that reducing BCL decreased CV depending on the solution composition and level of pharmacologic GJ inhibition. Specifically, decreasing BCL in hearts perfused with Solution B with and without CBX decreased CV_L and CV_T. The same effects were not always observed with Solution A. Our previous research suggests that EpC can support normal conduction when GJs are reduced [2, 16, 17]. The finding that Solution A is less sensitive to GJ uncoupling, suggests that Solution A may promote EpC by maintaining sodium channel availability (lower $[K^+]_o$) and increasing sodium driving force ($[Na^+]_o$). Further, even greater sodium channel inactivation by rapid pacing does not significantly slow CV even with GJ uncoupling sufficient to slow CV.

Effects of gap junctional coupling

In the current study, increasing the concentration of CBX appeared to progressively decrease CV. This agrees with previous research which demonstrated that concentrations as high as 13μM CBX did not significantly slow CV, while concentrations between 20 and 100μM CBX can slow CV [2, 16, 27]. According to previous research, the IC50 of GJ inhibition by CBX is between 50 and 100μM [27, 49-51]. The observation

that significant CV slowing secondary to CBX can be modulated by solution composition and cardiac hydration further suggests that the IC50 of conduction slowing with CBX may be dependent on alternative modes of conduction.

It is also possible that ionic differences in solutions altered Cx43 functional expression. However, the lack of a significant total or Cx43-p368S change in Cx43 expression suggests, but does not prove, that reported results are not due to GJ remodeling.

Effects on rise time

Previous studies suggest that I_{Na} correlates with CV and that the maximal rate of action potential upstroke rise (dV/dt_{max}) is a correlate of peak $I_{Na.}$ This is supported by studies which demonstrated that decreasing $I_{Na,max}$ can decrease dV/dt_{max} and CV [52]. Optical RT is an inverse correlate of dV/dt_{max} [34-36]. The theory of cardiac conduction reserve during GJ uncoupling suggests that RT should first decrease during GJ uncoupling without a measurable effect on cardiac conduction [52-54]. We never observed such a relationship. In short, RT either did not change with GJ uncoupling by CBX or it increased, and this is consistent with other similar studies [55, 56]. However, it is important to note that CBX is a pharmacologic GJ uncoupler with off target effects, and this may explain a lack of agreement with theoretical predictions.

Effects on perinexal width

Our group previously demonstrated that changing bulk interstitial volume can modulate CV [2, 16]. We also demonstrated that CV is inversely correlated to perinexal width [16, 17]. In other words, increasing perinexal width can decrease ventricular CV. To our

knowledge, this is the first demonstration that CBX can decrease perinexal width, which from previous work should increase CV. An important difference in this study compared to our previous manuscripts [2, 17] is that changes in perinexal width in this study were caused by pharmacological intervention with CBX, instead of mannitol or calcium concentration. As changes in perinexal width due to CBX have not been previously reported, it is difficult to discuss the mechanism since this effect was not explored in this study. However, the relationship between CBX and perinexal width may be related to a study by Goldberg et al. demonstrating that glycyrrhetinic acid derivatives disrupt gap junction plaques [57], which could alter the structure of the perinexus. Therefore, these results suggest that CBX may promote ephaptic EpC while simultaneously reducing GJ coupling. By this mechanism, modest levels of CBX GJ uncoupling may not alter CV.

Limitations

This study relies entirely upon using pacing protocols as well as pharmacological GJ inhibitors. However, the findings that altering $[Na^+]_o$ and $[K^+]_o$ can modulate cardiac conduction with pharmacologic inhibition is similar to findings in mice heterozygous null for Cx43 [17]. It will be interesting to know in the future whether connexin targeting peptides behave similarly to glycerhetinic acid derivatives.

It is well established that the electromechanical uncoupler BDM can affect cardiac conduction, and may have therefore confounded the results here. While this possibility cannot be excluded, BDM was present for each experiment, and all electrophysiologic comparisons were paired. However, perinexal measurements were analyzed in an unpaired fashion, and BDM may have altered these results. Yet, we previously

demonstrated that BDM does not change perinexal width relative to freshly excised hearts [16].

It has been shown that Cx43 localization can change due to cardiac disease [58-60]. While we provide evidence that perinexal spacing was only changed for samples that included CBX, alteration of Cx43 localization could account for some of the electrophysiological changes that were seen. However, the effects quantified in this study occurred in 10 or less minutes and were independent of perfusion order. Therefore, it may be unlikely that Cx43 cellular expression patterns were significantly altered on this time scale.

The mechanisms that underlie this atypical response to perfusate composition during GJ uncoupling could be due to either altered cellular excitability [61, 62] around the entire myocyte or ephaptic mechanisms as previously suggested [2, 16, 17]. Importantly, the finding that conduction slowing secondary to GJ uncoupling can be exacerbated by relatively small changes in extracellular ions suggests that the mechanism governing the CV-GJ relationship is very sensitive to ionic perturbations within the physiologic range, and this warrants additional investigation.

CONCLUSIONS

We present evidence that altering $[K^+]_o$, $[Na^+]_o$, and heart rate have important effects on GJ mediated conduction slowing. The magnitude of ionic changes, while small, were in accordance with the original hypothesis that the changes in $[K^+]_o$ and $[Na^+]_o$ would not substantially alter CV as previously demonstrated in mice under conditions of normal GJ coupling, but GJ uncoupling can produce solution dependent CV changes. The

implications of this study are that relatively small physiologic changes in extracellular ionic composition do not significantly perturb cardiac electrophysiology under “normal” conditions, but these same changes may have significant effects during cardiac stress as a result of GJ remodeling or increased heart rate.

REFERENCES

1. Veeraraghavan, R., R.G. Gourdie, and S. Poelzing, *Mechanisms of cardiac conduction: a history of revisions.* Am J Physiol Heart Circ Physiol, 2014. **306**(5): p. H619-27.
2. Veeraraghavan, R., M.E. Salama, and S. Poelzing, *Interstitial volume modulates the conduction velocity-gap junction relationship.* Am J Physiol Heart Circ Physiol, 2012. **302**(1): p. H278-86.
3. Sperelakis, N. and K. McConnell, *Electric field interactions between closely abutting excitable cells.* IEEE Eng Med Biol Mag, 2002. **21**(1): p. 77-89.
4. Kucera, J.P., S. Rohr, and Y. Rudy, *Localization of sodium channels in intercalated disks modulates cardiac conduction.* Circ Res, 2002. **91**(12): p. 1176-82.
5. Mori, Y., G.I. Fishman, and C.S. Peskin, *Ephaptic conduction in a cardiac strand model with 3D electrodiffusion.* Proc Natl Acad Sci U S A, 2008. **105**(17): p. 6463-8.
6. Anastassiou, C.A., et al., *Ephaptic coupling of cortical neurons.* Nat Neurosci, 2011. **14**(2): p. 217-23.
7. Bokil, H., et al., *Ephaptic interactions in the mammalian olfactory system.* J Neurosci, 2001. **21**(20): p. RC173.
8. Maina, I., et al., *Discrete impulses in ephaptically coupled nerve fibers.* Chaos, 2015. **25**(4): p. 043118.
9. Su, C.Y., et al., *Non-synaptic inhibition between grouped neurons in an olfactory circuit.* Nature, 2012. **492**(7427): p. 66-71.
10. Van der Goes van Naters, W., *Inhibition among olfactory receptor neurons.* Front Hum Neurosci, 2013. **7**: p. 690.
11. Young, R.C., *Myocytes, myometrium, and uterine contractions.* Ann N Y Acad Sci, 2007. **1101**: p. 72-84.
12. Lin, J. and J.P. Keener, *Ephaptic coupling in cardiac myocytes.* IEEE Trans Biomed Eng, 2013. **60**(2): p. 576-82.

13. Lin, J. and J.P. Keener, *Microdomain effects on transverse cardiac propagation.* Biophys J, 2014. **106**(4): p. 925-31.

14. Lin, J. and J.P. Keener, *Modeling electrical activity of myocardial cells incorporating the effects of ephaptic coupling.* Proc Natl Acad Sci U S A, 2010. **107**(49): p. 20935-40.

15. Hand, P.E. and C.S. Peskin, *Homogenization of an electrophysiological model for a strand of cardiac myocytes with gap-junctional and electric-field coupling.* Bull Math Biol, 2010. **72**(6): p. 1408-24.

16. Veeraraghavan, R., et al., *Sodium channels in the Cx43 gap junction perinexus may constitute a cardiac ephapse: an experimental and modeling study.* Pflugers Arch, 2015.

17. George, S.A., et al., *Extracellular sodium and potassium levels modulate cardiac conduction in mice heterozygous null for the Connexin43 gene.* Pflugers Arch, 2015.

18. Buchanan, J.W., Jr., T. Saito, and L.S. Gettes, *The effects of antiarrhythmic drugs, stimulation frequency, and potassium-induced resting membrane potential changes on conduction velocity and dV/dtmax in guinea pig myocardium.* Circ Res, 1985. **56**(5): p. 696-703.

19. Kagiyama, Y., J.L. Hill, and L.S. Gettes, *Interaction of acidosis and increased extracellular potassium on action potential characteristics and conduction in guinea pig ventricular muscle.* Circ Res, 1982. **51**(5): p. 614-23.

20. UoM, R.A.R., *Reference values for laboratory animals. Normal hematology values.* 2009.

21. Veeraraghavan, R., et al., *Potassium channel activators differentially modulate the effect of sodium channel blockade on cardiac conduction.* Acta Physiol (Oxf), 2013. **207**(2): p. 280-9.

22. Lou, Q., W. Li, and I.R. Efimov, *The role of dynamic instability and wavelength in arrhythmia maintenance as revealed by panoramic imaging with blebbistatin vs. 2,3-butanedione monoxime.* Am J Physiol Heart Circ Physiol, 2012. **302**(1): p. H262-9.

23. Girouard, S.D., et al., *Optical mapping in a new guinea pig model of ventricular tachycardia reveals mechanisms for multiple wavelengths in a single reentrant circuit.* Circulation, 1996. **93**(3): p. 603-13.

24. Akar, F.G., K.R. Laurita, and D.S. Rosenbaum, *Cellular basis for dispersion of repolarization underlying reentrant arrhythmias.* J Electrocardiol, 2000. **33 Suppl**: p. 23-31.

25. Bayly, P.V., et al., *Estimation of conduction velocity vector fields from epicardial mapping data.* IEEE Trans Biomed Eng, 1998. **45**(5): p. 563-71.

26. Allouis, M., et al., *14-3-3 is a regulator of the cardiac voltage-gated sodium channel Nav1.5.* Circ Res, 2006. **98**(12): p. 1538-46.

27. Spray, D.C., Z.C. Ye, and B.R. Ransom, *Functional connexin "hemichannels": a critical appraisal.* Glia, 2006. **54**(7): p. 758-73.

28. Rhett, J.M., et al., *The perinexus: sign-post on the path to a new model of cardiac conduction?* Trends Cardiovasc Med, 2013. **23**(6): p. 222-8.

29. Kishida, H., B. Surawicz, and L.T. Fu, *Effects of K+ and K+-induced polarization on (dV/dt)max, threshold potential, and membrane input resistance in guinea pig and cat ventricular myocardium.* Circ Res, 1979. **44**(6): p. 800-14.

30. Pressler, M.L., V. Elharrar, and J.C. Bailey, *Effects of extracellular calcium ions, verapamil, and lanthanum on active and passive properties of canine cardiac purkinje fibers.* Circ Res, 1982. **51**(5): p. 637-51.

31. Smyth, J.W., et al., *A 14-3-3 mode-1 binding motif initiates gap junction internalization during acute cardiac ischemia.* Traffic, 2014. **15**(6): p. 684-99.

32. Hund, T.J., et al., *Protein kinase Cepsilon mediates salutary effects on electrical coupling induced by ischemic preconditioning.* Heart Rhythm, 2007. **4**(9): p. 1183-93.

33. Palatinus, J.A., J.M. Rhett, and R.G. Gourdie, *Enhanced PKCepsilon mediated phosphorylation of connexin43 at serine 368 by a carboxyl-terminal mimetic peptide is dependent on injury.* Channels (Austin), 2011. **5**(3): p. 236-40.

34. Spach, M.S., et al., *The discontinuous nature of propagation in normal canine cardiac muscle. Evidence for recurrent discontinuities of intracellular resistance that affect the membrane currents.* Circ Res, 1981. **48**(1): p. 39-54.

35. Poelzing, S., et al., *Heterogeneous connexin43 expression produces electrophysiological heterogeneities across ventricular wall.* Am J Physiol Heart Circ Physiol, 2004. **286**(5): p. H2001-9.

36. Poelzing, S. and D.S. Rosenbaum, *Altered connexin43 expression produces arrhythmia substrate in heart failure.* Am J Physiol Heart Circ Physiol, 2004. **287**(4): p. H1762-70.

37. de Groot, J.R., et al., *Conduction slowing by the gap junctional uncoupler carbenoxolone.* Cardiovasc Res, 2003. **60**(2): p. 288-97.

38. Nygren, A. and W.R. Giles, *Mathematical simulation of slowing of cardiac conduction velocity by elevated extracellular.* Ann Biomed Eng, 2000. **28**(8): p. 951-7.

39. Veenstra, R.D., et al., *Effects of hypoxia, hyperkalemia, and metabolic acidosis on canine subendocardial action potential conduction.* Circ Res, 1987. **60**(1): p. 93-101.

40. Pandit, S.V., et al., *Mechanisms underlying the antifibrillatory action of hyperkalemia in Guinea pig hearts.* Biophys J, 2010. **98**(10): p. 2091-101.

41. Severs, N.J., et al., *Gap junction alterations in human cardiac disease.* Cardiovasc Res, 2004. **62**(2): p. 368-77.

42. Kostin, S., et al., *Gap junction remodeling and altered connexin43 expression in the failing human heart.* Mol Cell Biochem, 2003. **242**(1-2): p. 135-44.

43. Janse, M.J. and A.L. Wit, *Electrophysiological mechanisms of ventricular arrhythmias resulting from myocardial ischemia and infarction.* Physiol Rev, 1989. **69**(4): p. 1049-169.

44. Scamps, F. and E. Carmeliet, *Effect of external K+ on the delayed K+ current in single rabbit Purkinje cells.* Pflugers Arch, 1989. **414 Suppl 1**: p. S169-70.

45. Sanguinetti, M.C. and N.K. Jurkiewicz, *Role of external Ca2+ and K+ in gating of cardiac delayed rectifier K+ currents.* Pflugers Arch, 1992. **420**(2): p. 180-6.

46. Gadsby, D.C., *The Na/K pump of cardiac cells.* Annu Rev Biophys Bioeng, 1984. **13**: p. 373-98.

47. Glitsch, H.G., *Electrophysiology of the sodium-potassium-ATPase in cardiac cells.* Physiol Rev, 2001. **81**(4): p. 1791-826.

48. Stein, M., et al., *A 50% reduction of excitability but not of intercellular coupling affects conduction velocity restitution and activation delay in the mouse heart.* PLoS One, 2011. **6**(6): p. e20310.

49. Suadicani, S.O., C.F. Brosnan, and E. Scemes, *P2X7 receptors mediate ATP release and amplification of astrocytic intercellular Ca2+ signaling.* J Neurosci, 2006. **26**(5): p. 1378-85.

50. Bruzzone, R., et al., *Pharmacological properties of homomeric and heteromeric pannexin hemichannels expressed in Xenopus oocytes.* J Neurochem, 2005. **92**(5): p. 1033-43.

51. Ye, Z.C., et al., *Functional hemichannels in astrocytes: a novel mechanism of glutamate release.* J Neurosci, 2003. **23**(9): p. 3588-96.

52. Shaw, R.M. and Y. Rudy, *Ionic mechanisms of propagation in cardiac tissue. Roles of the sodium and L-type calcium currents during reduced excitability and decreased gap junction coupling.* Circ Res, 1997. **81**(5): p. 727-41.

53. Rudy, Y. and W.L. Quan, *A model study of the effects of the discrete cellular structure on electrical propagation in cardiac tissue.* Circ Res, 1987. **61**(6): p. 815-23.

54. Cole, W.C., J.B. Picone, and N. Sperelakis, *Gap junction uncoupling and discontinuous propagation in the heart. A comparison of experimental data with computer simulations.* Biophys J, 1988. **53**(5): p. 809-18.

55. Jalife, J., et al., *Electrical uncoupling and impulse propagation in isolated sheep Purkinje fibers.* Am J Physiol, 1989. **257**(1 Pt 2): p. H179-89.

56. Rohr, S., J.P. Kucera, and A.G. Kleber, *Slow conduction in cardiac tissue, I: effects of a reduction of excitability versus a reduction of electrical coupling on microconduction.* Circ Res, 1998. **83**(8): p. 781-94.

57. Goldberg, G.S., et al., *Evidence that disruption of connexon particle arrangements in gap junction plaques is associated with inhibition of gap junctional communication by a glycyrrhetinic acid derivative.* Exp Cell Res, 1996. **222**(1): p. 48-53.

58. Duffy, H.S., *The molecular mechanisms of gap junction remodeling.* Heart Rhythm, 2012. **9**(8): p. 1331-4.

59. Spragg, D.D., et al., *Abnormal conduction and repolarization in late-activated myocardium of dyssynchronously contracting hearts.* Cardiovasc Res, 2005. **67**(1): p. 77-86.

60. Spragg, D.D. and D.A. Kass, *Pathobiology of left ventricular dyssynchrony and resynchronization.* Prog Cardiovasc Dis, 2006. **49**(1): p. 26-41.

61. Kleber, A.G., C.B. Riegger, and M.J. Janse, *Extracellular K+ and H+ shifts in early ischemia: mechanisms and relation to changes in impulse propagation.* J Mol Cell Cardiol, 1987. **19 Suppl 5**: p. 35-44.

62. Kleber, A.G., C.B. Riegger, and M.J. Janse, *Electrical uncoupling and increase of extracellular resistance after induction of ischemia in isolated, arterially perfused rabbit papillary muscle.* Circ Res, 1987. **61**(2): p. 271-9.

FIGURES

	Historical	Solution A	Solution B
GP Tyrode's solution (mmol/L)			
NaCl	140	147.8	140
NaOH	5.5	5.5	5.5
Total [Na^+]	**145.5**	**153.3**	**145.5**
KCl	4.56	4.56	6.95
Total [K^+]	**4.56**	**4.56**	**6.95**
$CaCl_2$	1.25	1.25	1.25
Dextrose	5.5	5.5	5.5
$MgCl_2$	0.7	0.7	0.7
HEPES	10	10	10
BDM	7.5	7.5	7.5

Table 3.1 – Modified Tyrode solution compositions (mM).

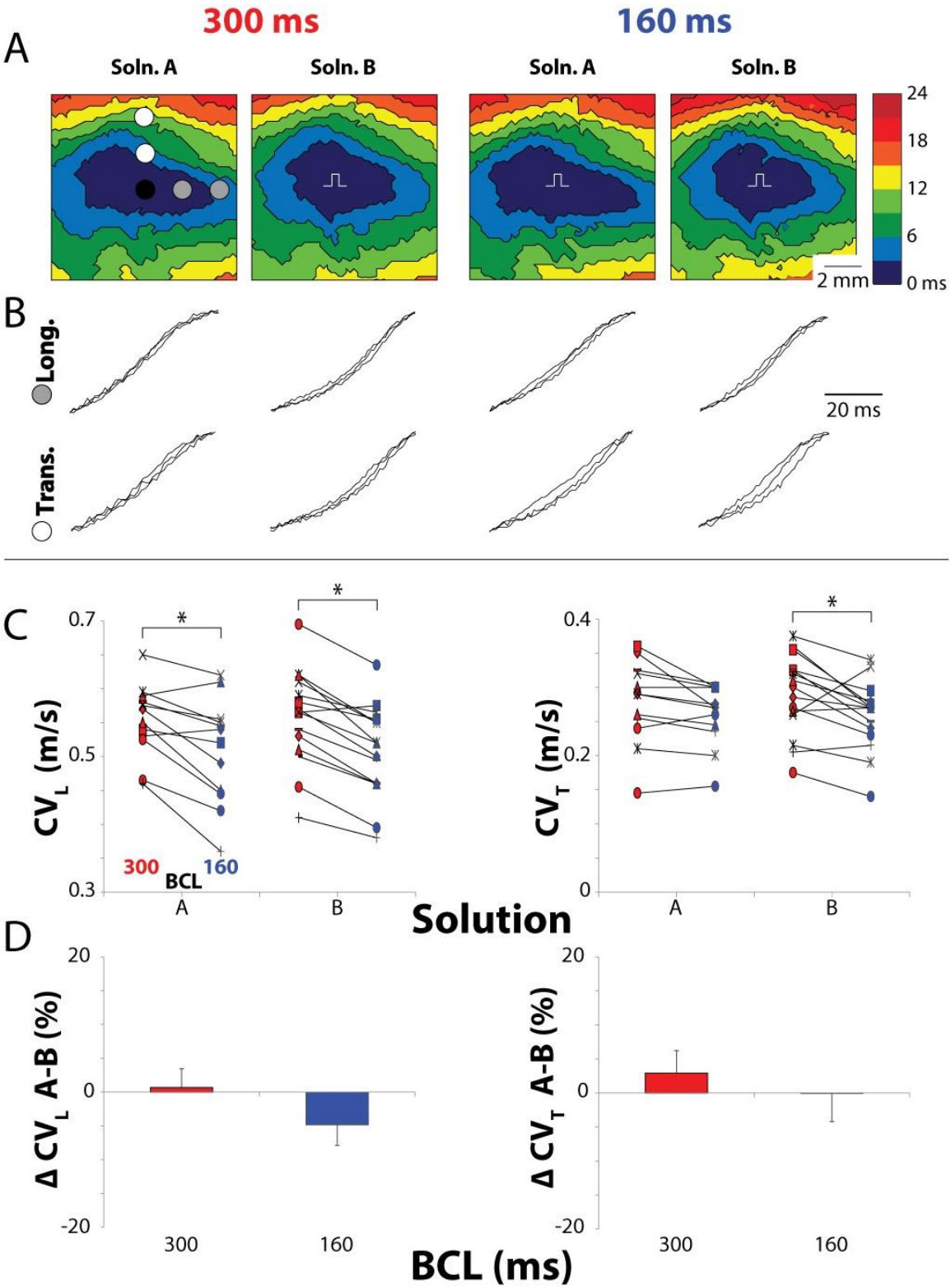

Figure 3.1 – Pacing rate but not solution composition alters CV in hearts with normal GJ coupling. (A) Representative isochrones from hearts perfused without CBX, showing

conduction slowing between pacing rates, but not solutions. **(B)** Uniformly spaced action potential upstrokes from the same hearts as pictured in **(A)**, demonstrating temporal upstroke separation as another indicator of decreased CV. **(C)** Red symbols: 300 ms BCL, Blue symbols: 160 ms BCL. CV measurements for longitudinal and transverse directions. CV decreased due to increased pacing rate for each combination except Solution A in the transverse direction. **(D)** Relative percent changes in CV_L and CV_T between Solutions A and B show no changes in CV due to perfusate. *$p < 0.025$ between pacing rates.

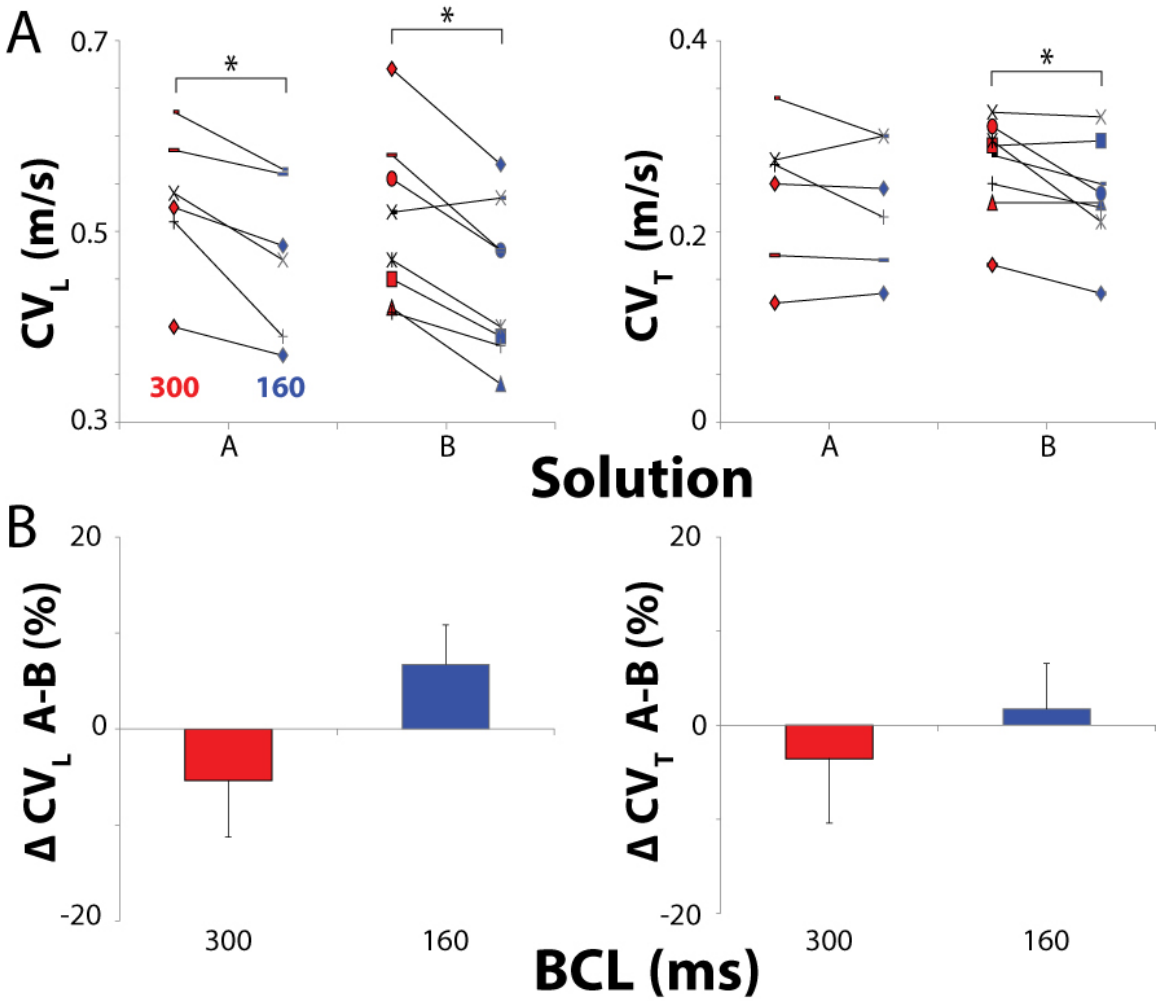

Figure 3.2 – Conduction in hearts perfused with 15µM CBX. **(A)** Red symbols: 300 ms BCL, Blue symbols: 160 ms BCL. Effects of BCL on CV_L and CV_T. **(B)** Percent changes in CV_L and CV_T between Solutions A and B. Solution did not change CV at 15 µM CBX. *$p < 0.025$ between pacing rates.

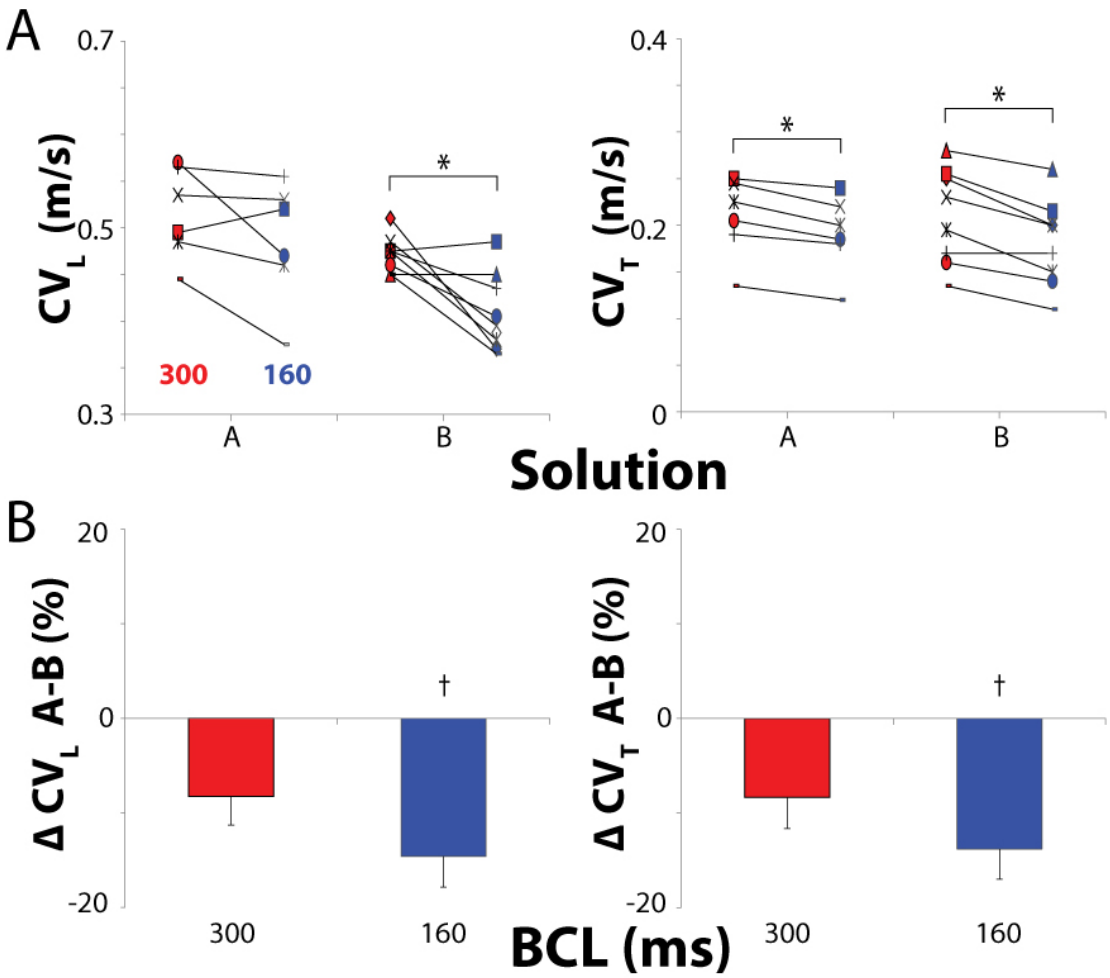

Figure 3.3 – Conduction in hearts perfused with 30μM CBX. (A) Red symbols: 300 ms BCL, Blue symbols: 160 ms BCL. Effects of BCL on CV_L and CV_T. **(B)** Percent changes in CV_L and CV_T between Solutions A and B. Solution B decreases CV_L and CV_T more than Solution A at 160 ms BCL with 30 μM CBX. * $p < 0.025$ between pacing rates. † $p < 0.025$ between Solutions A and B.

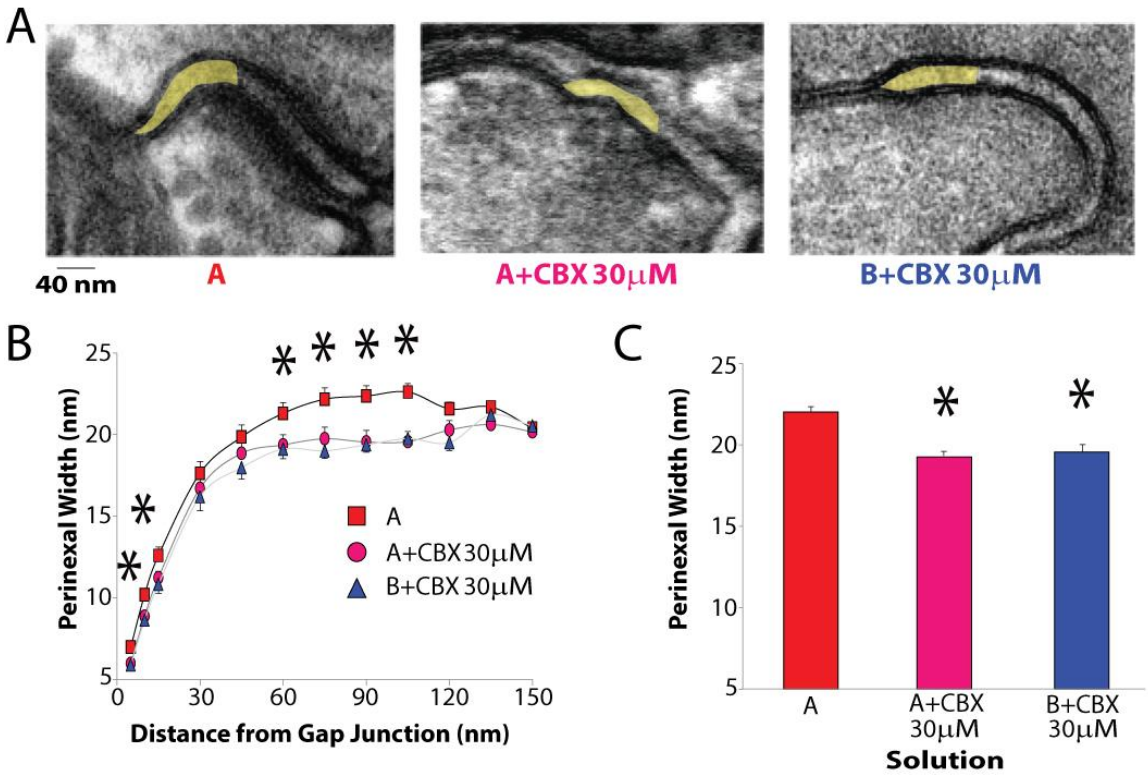

Figure 3.4 – CBX decreases perinexal width. (A) Representative transmission electron microscopy images of the edge of a GJ plaque and the perinexus (highlighted in yellow). (B) Perinexal width as a function of distance from the GJ plaque. CBX decrease the intercellular separation between 60 and 105 nm from the GJ. (C) Summary data between 60-105nm from the GJ plaque. *, p<0.025 from Solution A. * $p < 0.025$ from Solution A.

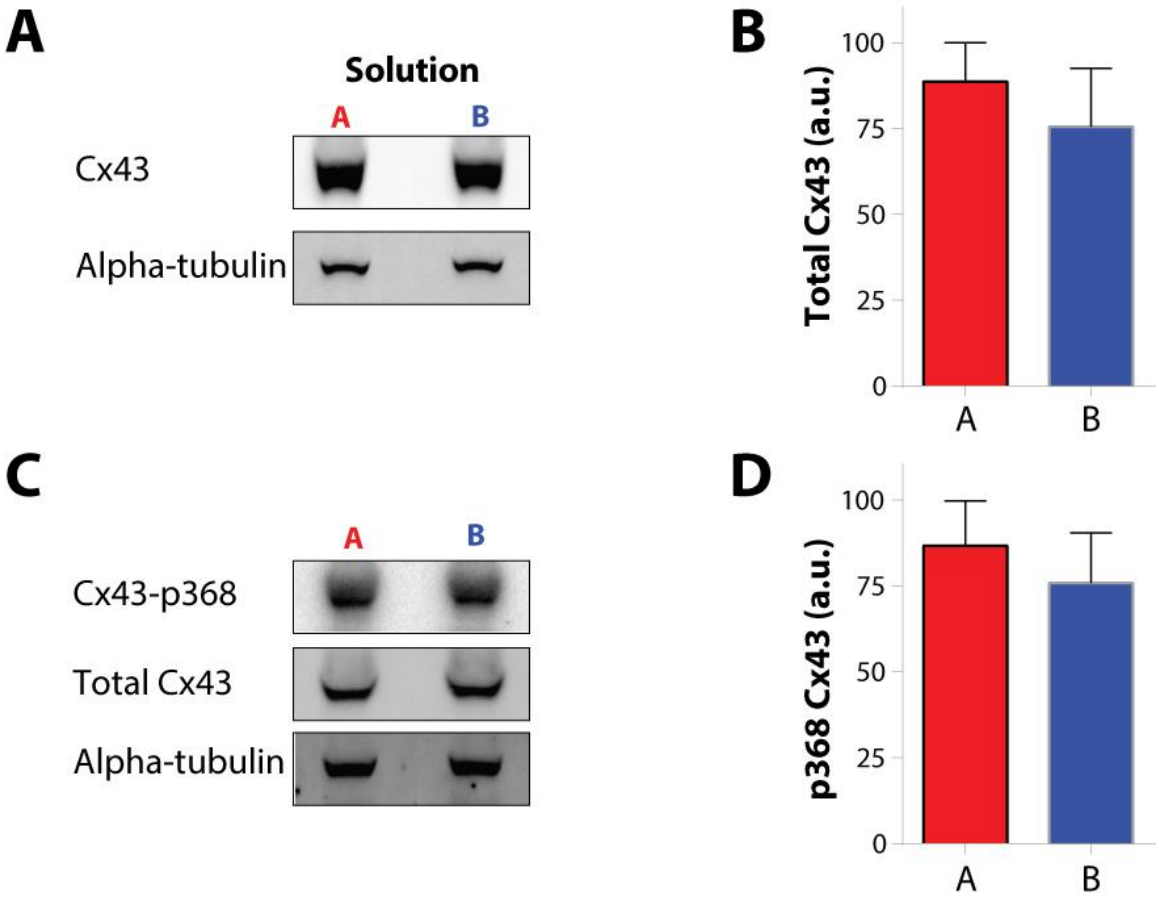

Figure 3.5 – Solution changes do not alter Cx43 expression or p368 phosphorylation. (A) Representative Western imunoblots of Cx43 with alpha-tublin as a loading control. **(B)** Quantification of total Cx43 expression reveals no difference between hearts perfused with Solutions A or B. **(C)** Representative Western immunoblots of Cx43-p368S and total Cx43 with alpha-tublin as a loading control. **(D)** Quantification of Cx43-p368S expression reveals no difference between hearts perfused with Solutions A or B.

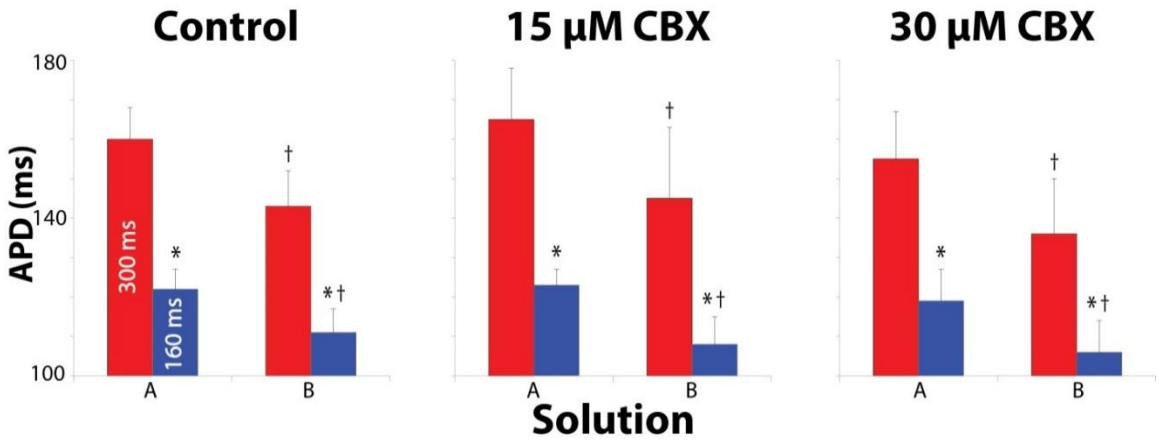

Figure 3.6 – Action potential duration measurements for all solution and pacing rate combinations tested. Reducing BCL always shortened APD for all solutions at every CBX concentrations. * $p < 0.025$ between BCLs. Solution B significantly shortened APD relative to Solution A for all CBX concentrations. † $p < 0.025$.

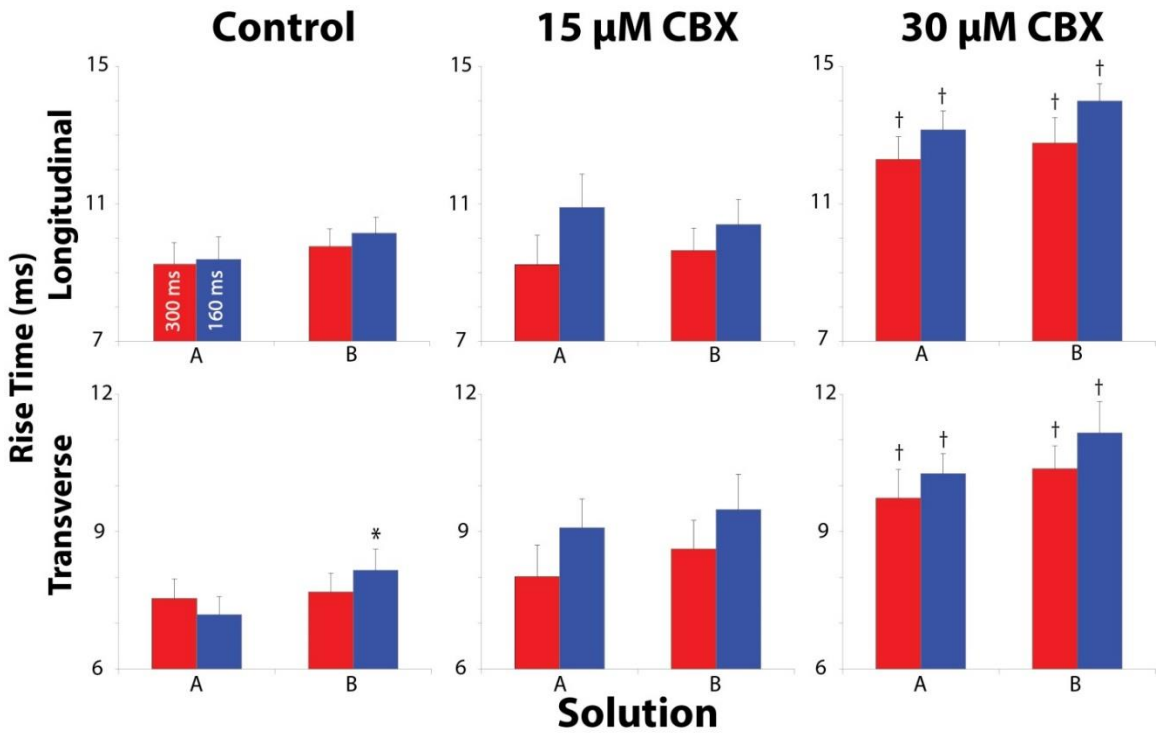

Figure 3.7 – Rise Time measurements in both longitudinal and transverse directions for both Solutions and pacing rates. Pharmacologic uncoupling with CBX progressively increased RT. † $p < 0.025$ relative to control. * $p < 0.025$ between BCLs.

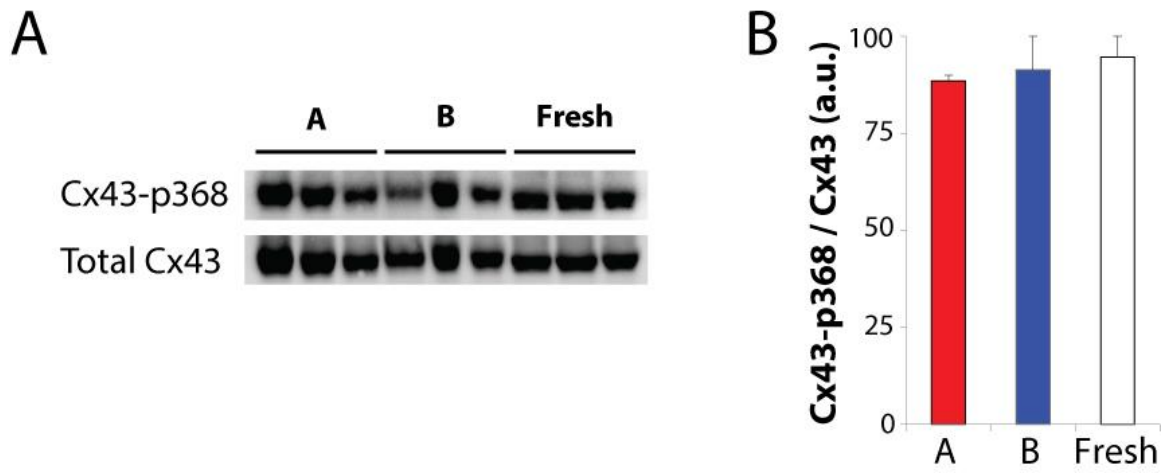

Figure 3.8 – The ratio of p368 to total Cx43 between hearts perfused with Solution A, B, and freshly explanted hearts was not different. (A) Representative western immunoblots of Cx43-p368 and total Cx43 protein expression. (B) Quantification of Cx43-p368 to total Cx43 ratio for hearts perfused with Solution A, B, and freshly explanted hearts.

CHAPTER – 4

Modifications to the CV-$[K^+]_o$ relationship *via* perfusate composition variations

FOREWORD

With the conclusion of the previous chapter, we were able to discover that physiologic changes in perfusate extracellular sodium and potassium were only able to modulate cardiac conduction velocity after sever gap junctional inhibition and also pathophysiological pacing rates. However, another discovery from this study was that changes in extracellular potassium did not match up with previous reports. Specifically, an increase of extracellular potassium to 6.9 mM resulted in no change or a loss in CV, when historic studies indicate this value should increase conduction velocity. Therefore, we wanted to explore the effects of perfusate composition on the conduction velocity – extracellular potassium relationship. This chapter of the dissertation will look at demonstrating how extracellular sodium, extracellular calcium, and gap junctional coupling modify the relationship between cardiac conduction velocity and extracellular potassium.

INTRODUCTION

Normal electrical activity in the heart is achieved through a conducted sequence of ion channels, pumps, and exchangers [1]. One major determinant of cardiac conduction is the inward sodium current (I_{Na}) produced by the cardiac isoform of the voltage gated sodium channel, $Na_{V1.5}$ [2]. The current through sodium channels can be modulated through changes in resting membrane potential (RMP) of cardiomyocytes [3]. One well established physiological mechanism that modulates RMP is by modulating extracellular potassium concentration ($[K^+]_o$) due to the prominent role potassium channels like the inward rectifier potassium channel $K_{ir}2.1$ plays in establishing RMP [4, 5].

The relationship between cardiac conduction velocity (CV) and $[K^+]_o$ has been repeatedly described as biphasic [6-8]. Specifically, in guinea pigs, multiple experimental and computational models demonstrate that CV increases until approximately 8.0 mM $[K^+]_o$ by reducing the potential difference from RMP to Na^+ channel activation [9]. In short, each cell requires less current to reach the activation potential of Na^+ channels, and as a result, they activate more rapidly for the same amount of current entering from upstream myocytes. However, if $[K^+]_o$ is increased beyond this value, CV begins to decrease due to Na^+ channel inactivation kinetics. Specifically, increasing RMP increases Na^+ channel steady-state inactivation, reducing Na^+ channel availability and decreasing CV [10].

Importantly, a recent study from our laboratory found confounding results while working within this $[K^+]_o$ regime [11]. Specifically, as $[K^+]_o$ was increased from 4.56 to 6.9 mM, we found either no change in CV with nominal GJC or a decrease in CV with GJC

inhibition, while the expectation was that CV would increase. One potential reason why our study does not agree with the Gettes' laboratory [6, 7] was that we also modified $[Na^+]_o$, pacing rate (another well-established mechanism for inactivating sodium channels) [12], and GJC in conjunction with variations in $[K^+]_o$.

A decrease in the main ventricular isoform of connexin, Cx43, has historically been associated with a decrease in CV. However, in a review by George et al. it was found that a decrease in CV for heterozygous null Cx43 mice when compared to wild type could be masked by crystalloid perfusate solution composition [13]. Specifically the review looked at differences in perfusate $[Na^+]_o$, $[Ca^{2+}]_o$, and $[K^+]_o$. The 8 studies investigated were retrospectively categorized into three specific groups based on perfusate composition, which correlated with 3 distinct differences in CV between wild-type and Cx43 heterozygous null mice. To further investigate the effects of perfusate composition research from our laboratory have demonstrated that modifications to $[Na^+]_o$ could alter the relationship between CV and $[Ca^{2+}]_o$ [14]. Therefore, these findings lead to the notion that combinatory effects between perfusate ions and GJC can modify CV heterogeneously in different cardiac states.

In other words, our research suggests that perfusate solution composition is an important modulator of cardiac conduction in health and disease. Previously, we altered the three principal cations between two values. However, the combinatory effects of $[Na^+]_o$ and $[Ca^{2+}]_o$, have not been assessed with a well-established range of $[K^+]_o$. Therefore the purpose of this manuscript was to test the hypothesis that $[Na^+]_o$ and $[Ca^{2+}]_o$ alter the biphasic CV-$[K^+]_o$ relationship in cardiac tissue. Secondly, we tested the hypothesis that uncoupling GJs also modulates the CV-$[K^+]_o$, $[Na^+]_o$, and $[Ca^{2+}]_o$

relationship. In short we demonstrate that the CV-$[K^+]_o$ is non-linearly modulated by $[Na^+]_o$, $[Ca^{2+}]_o$ and GJC.

MATERIALS AND METHODS

All studies were designed to adhere to all guidelines set forth by the Institutional Animal Care and Use Committee at Virginia Polytechnic Institute and State University and NIH *Guide for the Care and Usage of Laboratory Animals*.

Langendorff Perfusion

Adult male Hartley albino guinea pigs (Hilltop, Scottdale, PA, N = 42, 800-1200 g, 14-16 months old) were anesthetized using isofluorane (4% in O_2). After loss of peripheral stimuli response, the heart was excised and the atria were removed to inhibit competitive stimulation. The heart was cannulated for retrograde perfusion using our Laboratory Standard (LS) perfusion solution in a 3D printed PLA bath [15]. The LS solution (140 NaCl, 4.56 KCl, 1.25 $CaCl_2$, 5.5 Dextrose, 0.7 $MgCl_2$, 10 HEPES, and 7.5 BDM in mmol/L) was perfused at a constant pressure (40-60 mmHg) and flow. The perfusate was calibrated to a pH of 7.4 using roughly 5.5 mL NaOH per L of LS solution at 37.0 °C. A unipolar AgCl wire was used to pace each heart on the anterior left ventricular epicardium at 1.5 times ventricular pacing threshold. The basic cycle length of pacing was 300 ms, with 5 ms duration pulses.

Using the LS perfusate as a baseline, $[Na^+]_o$, $[Ca^{2+}]_o$, and $[K^+]_o$ were varied in experiments. For each individual experiment, $[Na^+]_o$ and $[Ca^{2+}]_o$ were held constant, while $[K^+]_o$ was varied between four concentrations (4.56, 6.4, 8.0, and 10 mM).

Specifically, $[Na^+]_o$ was changed from 145 to 155 mM and $[Ca^{2+}]_o$ was changed from 1.25 and 2.0 mM.

Gap junctional inhibition was induced by perfusion of the non-specific gap junction uncoupler CBX (30 μM), which has previously been shown to decrease cardiac conduction velocity [16]. For experiments containing CBX, the first measurements were taken after 15 minutes, as time control studies indicated CV reached steady state within that time (data not shown). Measurements were then made at 10 minute time intervals to control the time the heart was exposed to each solution.

Electrocardiography

A volume conducted bath electrocardiogram (ECG) was recorded using AgCl electrodes, collected at 1 kHz. Electrodes were placed on both sides of the ventricles, with the ground placed at the rear of the bath.

Transmission Electron Microscopy

Tissue was sectioned into 1 mm^3 cubes from the anterior LV free wall (4 hearts per intervention, 3 samples per heart). The tissue was fixed overnight in 2.5% glutaraldehyde at 4 °C, which was washed and transferred to PBS at 4 °C. The tissue was processed as previously described [13]. Images were collected at 150,000 X magnification on a transmission electron microscope (JEOL JEM1400). ImageJ (NIH) was used for manual segmentation of the perinexus. For each sample, 15 pernexi were analyzed, starting at the point directly adjacent to gap junctions, measuring up to 150

nm from the GJ plaque. Changes in perinexal width (W_p) were analyzed as the average width for the measurements from 45 to 105 nm from the GJ plaque.

Optical Mapping

Before the start of the experimental protocol, the voltage sensitive dye di-4-ANEPPS (7.5 μM) was perfused in 100 mL LS perfusate. The electro-mechanical uncoupler 2,3-butanedione monoxime (BDM, 7.5 μM) was used to decrease cardiac motion. In order to further stabilize the heart for imaging, light mechanical pressure was placed on the posterior surface of the heart.

Excitation of Di-4-ANEPPS occurred through use of a halogen light source (MHAB-150 W, Moritex Corporation) using an excitation filter of 510 nm (Brightline Fluorescence Filter). Emitted light passed through a filter of 610 nm (610FG01-50(T257), Andover Corporation) before being recorded with a MiCam Ultima CMOS L-camera (Scimedia) at 1 kHz sampling rate. The camera used a 100 x 100 array with a 0.1 mm inter-pixel resolution for image recording.

Cardiac conduction velocity was calculated as previously described [17] using a calculation by Bayly et al. [18]. Activation time for each pixel was determined as the maximum rate of optical action potential rise. CV was quantified in two directions, longitudinal (CV_L) and transverse (CV_T). Conduction vectors in each direction were selected as the vectors within 5 pixels and an angle of ± 8° from the direction of longitudinal (fastest) and transverse (slowest) propagation. Conduction vectors immediately adjacent to the pacing site were excluded to reduce pacing artifacts.

Statistical Analysis

Statistical analysis was performed using one and two-way ANOVA. Two tailed Student's t-tests were used in post hoc analysis. A $p \leq 0.05$ was considered significant. All values are reported as mean ± standard error unless otherwise noted.

RESULTS

Conduction Velocity – 145.5 mM $[Na^+]_o$

Representative epicardial isochrones in Figure 4.1A suggests that increasing $[K^+]_o$ first increases and then decreases cardiac conduction, consistent with previously reported biphasic relationships between CV and $[K^+]_o$. Summary data in Figure 4.1B demonstrates that relative to 4.56 mM $[K^+]_o$, CV is significantly faster in both the transverse and longitudinal directions at 6.4 mM $[K^+]_o$ and slower at 10 mM $[K^+]_o$. Further, changing $[Ca^{2+}]_o$ from 1.25 to 2.0 mM does not change the finding that 6.4 mM $[K^+]_o$ increases CV and 10 mM $[K^+]_o$ decreases CV. In order to further evaluate the relative change caused by modifying $[Ca^{2+}]_o$, CV was normalized to control (4.56 mM $[K^+]_o$) (Figure 4.1C). In summary, the CV-$[K^+]_o$ relationship was unaffected by relatively small changes in $[Ca^{2+}]_o$ with 145.5 mM $[Na^+]_o$.

Conduction Velocity – 155.5 mM $[Na^+]_o$

Previous studies suggested that altering $[Na^+]_o$ modulates the relationship between CV and $[Ca^{2+}]_o$ [14]. Therefore, $[Na^+]_o$ was increased to 155 mM to determine how $[Ca^{2+}]_o$ affects the CV-$[K^+]_o$ relationship. Representative epicardial isochrones for both $[Ca^{2+}]_o$, demonstrating the effects of increasing $[K^+]_o$ on cardiac conduction can be seen in

Figure 4.2A. The maps for both $[Ca^{2+}]_o$ suggest that 155.5 mM $[Na^+]_o$ does not affect the biphasic CV-$[K^+]_o$ relationship. Similar to the findings with 145 mM $[Na^+]_o$, CV_T and CV_L were significantly greater at 6.4 mM $[K^+]_o$ relative to 4.56 mM $[K^+]_o$ with 155 mM $[Na^+]_o$ (Figure 4.2B). In contrast, increasing $[K^+]_o$ to 10 mM did not slow CV relative to 4.56 mM $[K^+]_o$, suggesting that increasing $[Na^+]_o$ alters the CV-$[K^+]_o$ relationship.

Interestingly, increased $[Na^+]_o$ also altered the effects of $[Ca^{2+}]_o$ as a modulator of the CV-$[K^+]_o$ relationship. Specifically, 2.0 mM $[Ca^{2+}]_o$ increased normalized CV_T at 8.0 mM $[K^+]_o$ significantly more relative to 8mM $[K^+]_o$ with 1.25mM $[Ca^{2+}]_o$. Taken together with data obtained with 145 mM $[Na^+]_o$, the relationship between CV and $[K^+]_o$ is not straightforward, and non-linear effects emerge when altering more than one other ion.

Perinexal Width

Previously, we demonstrated in mice that elevating $[Ca^{2+}]_o$ can reduce perinexal width (W_p) [13]. Representative transmission electron microscope images of cardiac tissue perfused with 155.5 mM $[Na^+]_o$ with either 1.25 or 2.0 mM $[Ca^{2+}]_o$ are shown in Figure 4.3A. The perinexus is highlighted in yellow, which represents the 150 nm directly adjacent to a cardiac GJ plaque. Measurements were taken of the first 150 nm of the perinexus, as summarized in Figure 4.3B. The measurements from 45 to 105 nm were averaged together for each heart (n=4) and separated into two groups: 1.25 and 2.0 mM $[Ca^{2+}]_o$. Importantly, increasing $[Ca^{2+}]_o$ to 2.0 mM decreased W_p compared to 1.25 mM $[Ca^{2+}]_o$, consistent with previous reports in murine hearts [13]. The histogram of all W_p measurements in Figure 4.3D demonstrates that increasing $[Ca^{2+}]_o$ not only narrows

mean W_p,, but importantly, decreases the amount of large W_p measurements, suggesting that increasing $[Ca^{2+}]_o$ reduces W_p heterogeneity.

Conduction Velocity – Gap Junction Uncoupling with 145 mM $[Na^+]_o$

It is generally accepted that GJs are a major determinant of cardiac conduction, and GJ remodeling is a hallmark of multiple cardiac diseases. Therefore GJs were inhibited using the nonspecific GJ uncoupler carbenoxolone (CBX) to determine how GJ coupling modulates the relationships between CV and $[Na^+]_o$, $[Ca^{2+}]_o$, and most importantly $[K^+]_o$. Summary data for CV_T and CV_L in hearts perfused with 30 μM CBX and 145 mM $[Na^+]_o$ are shown in Figure 4.4A. Inclusion of CBX was found to decrease CV_T and CV_L regardless of $[Ca^{2+}]_o$. Specifically, CV_T decreased from 21.7 ± 3.1 to 14.1 ± 0.9 cm/s with 1.25 mM $[Ca^{2+}]_o$ and from 21.2 ± 3.1 to 15.2 ± 1.4 cm/s with 2.0 mM $[Ca^{2+}]_o$. Unlike the hearts with a full complement of GJs, the CBX perfused hearts demonstrated only a visually biphasic relationship between CV and $[K^+]_o$. However, only 10 mM $[K^+]_o$ for hearts with 1.25 mM $[Ca^{2+}]_o$ showed a significant decrease in both CV_T and CV_L. In order to evaluate the relative change caused by modulating $[Ca^{2+}]_o$, CV was normalized to control at 4.56 mM $[K^+]_o$ (Figure 4.4C). However, there was no change in CV due to variations in $[K^+]_o$, independent of $[Ca^{2+}]_o$.

Conduction Velocity – Gap Junction Uncoupling with 155 mM $[Na^+]_o$

Next, $[Na^+]_o$ was increased to 155 mM in the presence of GJ uncoupling in order to further explore the relationship between GJC, $[Ca^{2+}]_o$, and $[K^+]_o$. As with 145 mM $[Na^+]_o$, CV_T and CV_L were decreased at 4.56 mM $[K^+]_o$ with the addition of 30 μM CBX and 155 mM $[Na^+]_o$, independent of $[Ca^{2+}]_o$. CV_T decreased from 20.6 ± 3.0 to 18.4 ± 2.7 cm/s

with 1.25 $[Ca^{2+}]_o$ and from 21.1 ± 4.3 to 16.3 ± 1.5 cm/s with 2.0 mM $[Ca^{2+}]_o$. When the biphasic relationship between CV and $[K^+]_o$ was analyzed for 155 mM $[Na^+]_o$ it was found that as with 145 mM $[Na^+]_o$, there was only a visual biphasic relationship (Figure 4.5A). However, the only significant change when compared to 4.56 mM $[K^+]_o$ was a decrease in CV_T at 10 mM $[K^+]_o$ with 1.25 mM $[Ca^{2+}]_o$. Interestingly, when comparing normalized CV values (Figure 4.5B), there were no changes in sensitivity to $[K^+]_o$, which is inconsistent with the findings under the same conditions with no CBX.

Conduction Recovery during Hyperkalemia

Since pathologic hyperkalemia (10mM $[K^+]_o$) produced particularly interesting results during gap junction uncoupling, we analyzed the normalized responses of CV_T at 10 relative to 4.56 mM $[K^+]_o$ (Figure 4.6). Specifically, we compared all solutions to the 145 mM $[Na^+]_o$ and 1.25 mM $[Ca^{2+}]_o$ solution, further grouping solutions based on the inclusion of CBX. Without GJ uncoupling, when hearts were perfused with 10 mM $[K^+]_o$, CV_T was increased compared to the control solution when $[Na^+]_o$ was increased to 155 mM, independent of $[Ca^{2+}]_o$. Importantly, during GJ uncoupling, CV_T was increased compared to the solution with 145 mM $[Na^+]_o$ and 1.25 $[Ca^{2+}]_o$ only when both $[Na^+]_o$ and $[Ca^{2+}]_o$ were elevated to 155 and 2.0 mM respectively. These data suggest that cardiac conduction can be rescued under normal conditions by increasing $[Na^+]_o$ or $[Na^+]_o$ and $[Ca^{2+}]_o$. In contrast, conduction can be rescued during GJ uncoupling only when both $[Na^+]_o$ and $[Ca^{2+}]_o$ are increased. These data suggest that cardiac conduction secondary to the loss of functional GJC is relatively insensitive to perturbations in $[K^+]_o$ when both $[Na^+]_o$ and $[Ca^{2+}]_o$ are elevated within the physiologic range.

DISCUSSION

The purpose of this study was to determine how changes in $[Na^+]_o$ and $[Ca^{2+}]_o$ modulated the CV-$[K^+]_o$ relationship with and without GJ inhibition in guinea pig ventricles. The data in this manuscript demonstrate the complex relationship between ionic components of perfusate solutions. Previous studies have demonstrated how the modifications of one or two of the ions ($[Na^+]_o$, $[Ca^{2+}]_o$, or $[K^+]_o$) can facilitate a change in CV [11, 13, 19, 20]. The present experimental data is consistent with the findings from the aforementioned studies, however we demonstrate that the relationship between ionic concentrations is more complex than originally thought. Interestingly, this is the first report to show that modulating $[Na^+]_o$ and $[Ca^{2+}]_o$ in combination can modify the CV-$[K^+]_o$ relationship. Importantly, when GJ coupling was decreased, the data indicated that the relationship was further modified.

Effects of $[Na^+]_o$ and $[Ca^{2+}]_o$

The CV-$[K^+]_o$ relationship has previously been shown to be biphasic [6-8]. Specifically, CV increases until roughly 8.0 mM $[K^+]_o$, while it decreases past that point. Importantly, we showed that CV did increase up until 8.0 mM $[K^+]_o$, with a decrease at 10 mM $[K^+]_o$, consistent with previous reports. However, one important difference in the current experiments compared to foundational experiments by Kagiyama [6] or Buchanaon [7] were the changes in $[Na^+]_o$ and $[Ca^{2+}]_o$. Specifically, an increase in $[Na^+]_o$ was shown to maintain CV during hyperkalemia in hearts with no GJ inhibition compared to 4.56 mM $[K^+]_o$. Importantly, we found that increases in CV_T due to $[K^+]_o$ could be attenuated due to increasing $[Ca^{2+}]_o$, specifically for hearts perfused with 155 mM $[Na^+]_o$. These results

mimic those found previously in mice in our laboratory [14]. However, the trends were slightly altered between the two studies. Specifically, an increase in $[K^+]_o$ to 6.1 mM in mice was sufficient to decrease CV. However, as previously stated, it has been shown on multiple occasions that 6.1 mM $[K^+]_o$ in guinea pigs leads to an increase in CV. Therefore, the differences in the two studies may be species dependent reactions to $[K^+]_o$.

Effects of Gap Junctional Coupling

Inhibiting GJC with 30 μM CBX was previously shown to decrease cardiac CV [21]. We also demonstrated that decreasing GJ coupling via CBX leads to a modified relationship between CV, pacing rate, $[Na^+]_o$, and $[K^+]_o$ [11]. Specifically, $[Ca^{2+}]_o$ no longer caused a modification in CV sensitivity to changes in $[K^+]_o$, independent of $[Na^+]_o$. One possible explanation for this change is based on the decrease in W_p previously shown due to the use of CBX from our lab [11]. If the perinexus was already decreased in size due to the addition of CBX, it is possible that $[Ca^{2+}]_o$ did not have a further effect on W_p in these experiments.

Effects on Hyperkalemia

Hyperkalemia is associated with many diseases, including ischemia [22] and renal failure [23-25]. Once affected, this can lead to paralysis [26, 27] or sudden cardiac death [28, 29]. The effects of $[K^+]_o$ on cardiac CV has been shown to be biphasic [6-8]. Historic data indicates that CV increases up until 8.0 mM $[K^+]_o$, and decreases at more hyperkalemic values. Specifically, previous research demonstrated that 10 mM $[K^+]_o$ decreases CV when compared to normokalemia. Interestingly, through modification of

$[Na^+]_o$ and $[Ca^{2+}]_o$ we were able to show that CV_T decrease due to $[K^+]_o$ can be attenuated (Figure 4.6). Specifically, there are two regimes of maintaining CV_T which correlate with the level of GJC. With a full complement of GJC, it can be seen that increasing $[Na^+]_o$ or both $[Na^+]_o$ and $[Ca^{2+}]_o$ maintains CV_T during hyperkalemia. This would indicate that increased $[Na^+]_o$ is the main factor underlying CV_T maintenance in healthy hearts. However, when GJC is inhibited via 30 μM CBX, the increase of both $[Na^+]_o$ and $[Ca^{2+}]_o$ are needed to maintain CV_T during hyperkalmia. This would indicate that EpC coupling needs to be increased to maintain CV_T during GJ inhibition.

Effects on Perinexal Width

Our group has extensively studied the effects of both bulk interstitial volume as well as the nano-domain known as the perinexus in relation to CV changes [14, 20]. Specifically, we have shown that both bulk interstitial volume and W_p are inversely correlated with cardiac CV [13, 16]. These results have been corroborated with mathematical models indicating the importance of closely apposed membranes for EpC transmission [30-32]. We previously showed that mouse and guinea pig W_p could be narrowed by an increase in $[Ca^{2+}]_o$ and an increase in perfusate osmolarity respectively [13, 16]. Importantly, this manuscript is the first experimental evidence indicating that small physiologic changes in $[Ca^{2+}]_o$ can modulate W_p in guinea pig ventricles.

W_p has been indicated as an important factor in ephaptic transmission [16, 20]. This study supports that notion, especially during GJ inhibition. Specifically, CV_T is maintained regardless of $[Ca^{2+}]_o$ during normal GJC with increased $[Na^+]_o$. However, during GJ inhibition an increase in $[Ca^{2+}]_o$ and $[Na^+]_o$ are both needed for CV_T

maintenance. This shows the need for increased EpC during GJ loss, indicated by increased $[Ca^{2+}]_o$ leading to a decrease in W_p, which strengthens EpC.

Experimental Perfusates

The most important takeaway from these experiments is the sheer importance of perfusate selection in the laboratory. The level of variation in perfusate compositions used between different laboratories is appreciable [33-39]. These differences include modifications to $[Na^+]_o$, $[Ca^{2+}]_o$, $[K^+]_o$, buffering agents, mechanical uncouplers, and more. The results in this manuscript show that not only do ionic concentrations matter when it comes to experimental results, but the combinatory effects may be even more important than previously thought. Therefore, experimentalists should take care in selecting an appropriate solution based on experimental protocol and outcomes to avoid any further confusion between confounding results.

CONCLUSIONS

Historically, cardiac perfusate solutions are experimental tools that have been passed down in a laboratory's lineage, with large differences between laboratories. However, these seemingly small differences between the perfusate solutions have been mostly ignored, but may have led to confounding experimental results in the past [19]. In this manuscript, we provide evidence that altering $[Na^+]_o$, $[Ca^{2+}]_o$, and GJ coupling lead to modifications in the CV-$[K^+]_o$ relationship, indicating the importance of perfusate solution composition. Interestingly, we were also able to highlight the importance of EpC mechanisms, specifically during GJ inhibition. In conclusion, experimentalists need to

take care when designing perfusates, as modifications to $[Na^+]_o$, $[Ca^{2+}]_o$, and $[K^+]_o$ can lead to confounding results based on the combination of concentrations used.

REFERENCES

1. Nerbonne, J.M. and R.S. Kass, *Molecular physiology of cardiac repolarization.* Physiol Rev, 2005. **85**(4): p. 1205-53.
2. Veerman, C.C., A.A. Wilde, and E.M. Lodder, *The cardiac sodium channel gene SCN5A and its gene product NaV1.5: Role in physiology and pathophysiology.* Gene, 2015. **573**(2): p. 177-87.
3. Chen, C.M., L.S. Gettes, and B.G. Katzung, *Effect of lidocaine and quinidine on steady-state characteristics and recovery kinetics of (dV/dt)max in guinea pig ventricular myocardium.* Circ Res, 1975. **37**(1): p. 20-9.
4. Weidmann, S., *Shortening of the cardiac action potential due to a brief injection of KCl following the onset of activity.* J Physiol, 1956. **132**(1): p. 157-63.
5. Jongsma, H.J. and R. Wilders, *Channelopathies: Kir2.1 mutations jeopardize many cell functions.* Curr Biol, 2001. **11**(18): p. R747-50.
6. Kagiyama, Y., J.L. Hill, and L.S. Gettes, *Interaction of acidosis and increased extracellular potassium on action potential characteristics and conduction in guinea pig ventricular muscle.* Circ Res, 1982. **51**(5): p. 614-23.
7. Buchanan, J.W., Jr., T. Saito, and L.S. Gettes, *The effects of antiarrhythmic drugs, stimulation frequency, and potassium-induced resting membrane potential changes on conduction velocity and dV/dtmax in guinea pig myocardium.* Circ Res, 1985. **56**(5): p. 696-703.
8. Shaw, R.M. and Y. Rudy, *Electrophysiologic effects of acute myocardial ischemia. A mechanistic investigation of action potential conduction and conduction failure.* Circ Res, 1997. **80**(1): p. 124-38.
9. Weidmann, S., *The effect of the cardiac membrane potential on the rapid availability of the sodium-carrying system.* J Physiol, 1955. **127**(1): p. 213-24.

10. Dodge, F.A. and B. Frankenhaeuser, *Sodium currents in the myelinated nerve fibre of Xenopus laevis investigated with the voltage clamp technique.* J Physiol, 1959. **148**: p. 188-200.

11. Entz, M., 2nd, et al., *Heart Rate and Extracellular Sodium and Potassium Modulation of Gap Junction Mediated Conduction in Guinea Pigs.* Front Physiol, 2016. **7**: p. 16.

12. Osadchii, O.E., E. Soltysinska, and S.P. Olesen, *Na+ channel distribution and electrophysiological heterogeneities in guinea pig ventricular wall.* Am J Physiol Heart Circ Physiol, 2011. **300**(3): p. H989-1002.

13. George, S.A., et al., *Extracellular sodium and potassium levels modulate cardiac conduction in mice heterozygous null for the Connexin43 gene.* Pflugers Arch, 2015.

14. George, S.A., et al., *Extracellular sodium dependence of the conduction velocity-calcium relationship: evidence of ephaptic self-attenuation.* Am J Physiol Heart Circ Physiol, 2016. **310**(9): p. H1129-39.

15. Entz, M.W., 2nd, D.R. King, and S. Poelzing, *Design and validation of a tissue bath 3D printed with PLA for optically mapping suspended whole heart preparations.* Am J Physiol Heart Circ Physiol, 2017: p. ajpheart 00150 2017.

16. Veeraraghavan, R., M.E. Salama, and S. Poelzing, *Interstitial volume modulates the conduction velocity-gap junction relationship.* Am J Physiol Heart Circ Physiol, 2012. **302**(1): p. H278-86.

17. Hoeker, G.S., et al., *Electrophysiologic effects of the IK1 inhibitor PA-6 are modulated by extracellular potassium in isolated guinea pig hearts.* Physiol Rep, 2017. **5**(1).

18. Bayly, P.V., et al., *Estimation of conduction velocity vector fields from epicardial mapping data.* IEEE Trans Biomed Eng, 1998. **45**(5): p. 563-71.

19. George, S.A. and S. Poelzing, *Cardiac conduction in isolated hearts of genetically modified mice--Connexin43 and salts.* Prog Biophys Mol Biol, 2016. **120**(1-3): p. 189-98.

20. Veeraraghavan, R., et al., *Sodium channels in the Cx43 gap junction perinexus may constitute a cardiac ephapse: an experimental and modeling study.* Pflugers Arch, 2015.

21. Spray, D.C., Z.C. Ye, and B.R. Ransom, *Functional connexin "hemichannels": a critical appraisal.* Glia, 2006. **54**(7): p. 758-73.

22. Kleber, A.G., *Resting membrane potential, extracellular potassium activity, and intracellular sodium activity during acute global ischemia in isolated perfused guinea pig hearts.* Circ Res, 1983. **52**(4): p. 442-50.

23. Kovesdy, C.P., et al., *Potassium homeostasis in health and disease: A scientific workshop cosponsored by the National Kidney Foundation and the American Society of Hypertension.* J Am Soc Hypertens, 2017.

24. Jain, N., et al., *Predictors of hyperkalemia and death in patients with cardiac and renal disease.* Am J Cardiol, 2012. **109**(10): p. 1510-3.

25. An, J.N., et al., *Severe hyperkalemia requiring hospitalization: predictors of mortality.* Crit Care, 2012. **16**(6): p. R225.

26. Wilson, N.S., et al., *Hyperkalemia-induced paralysis.* Pharmacotherapy, 2009. **29**(10): p. 1270-2.

27. Panichpisal, K., et al., *Acute quadriplegia from hyperkalemia: a case report and literature review.* Neurologist, 2010. **16**(6): p. 390-3.

28. Pun, P.H., *The interplay between CKD, sudden cardiac death, and ventricular arrhythmias.* Adv Chronic Kidney Dis, 2014. **21**(6): p. 480-8.

29. McCullough, P.A., et al., *Acute and chronic cardiovascular effects of hyperkalemia: new insights into prevention and clinical management.* Rev Cardiovasc Med, 2014. **15**(1): p. 11-23.

30. Lin, J. and J.P. Keener, *Ephaptic coupling in cardiac myocytes.* IEEE Trans Biomed Eng, 2013. **60**(2): p. 576-82.

31. Lin, J. and J.P. Keener, *Modeling electrical activity of myocardial cells incorporating the effects of ephaptic coupling.* Proc Natl Acad Sci U S A, 2010. **107**(49): p. 20935-40.

32. Lin, J. and J.P. Keener, *Microdomain effects on transverse cardiac propagation.* Biophys J, 2014. **106**(4): p. 925-31.

33. Veeraraghavan, R., et al., *Potassium channel activators differentially modulate the effect of sodium channel blockade on cardiac conduction.* Acta Physiol (Oxf), 2013. **207**(2): p. 280-9.

34. Deschenes, D., et al., *Biophysical characteristics of a new mutation on the KCNQ1 potassium channel (L251P) causing long QT syndrome.* Can J Physiol Pharmacol, 2003. **81**(2): p. 129-34.

35. Deschenes, I., et al., *Regulation of Kv4.3 current by KChIP2 splice variants: a component of native cardiac I(to)?* Circulation, 2002. **106**(4): p. 423-9.

36. Poelzing, S., et al., *SCN5A polymorphism restores trafficking of a Brugada syndrome mutation on a separate gene.* Circulation, 2006. **114**(5): p. 368-76.

37. Poelzing, S., et al., *Heterogeneous connexin43 expression produces electrophysiological heterogeneities across ventricular wall.* Am J Physiol Heart Circ Physiol, 2004. **286**(5): p. H2001-9.

38. Leetham, C., *Action of certain drugs on isolated strips of ventricle.* J Physiol, 1913. **46**(2): p. 151-8.

39. Tyrode, M.V., *The mode of action of some purgative salts.* Archives Internationales De Pharmacodynamie Et De Therapie, 1910. **20**: p. 205-223.

FIGURES

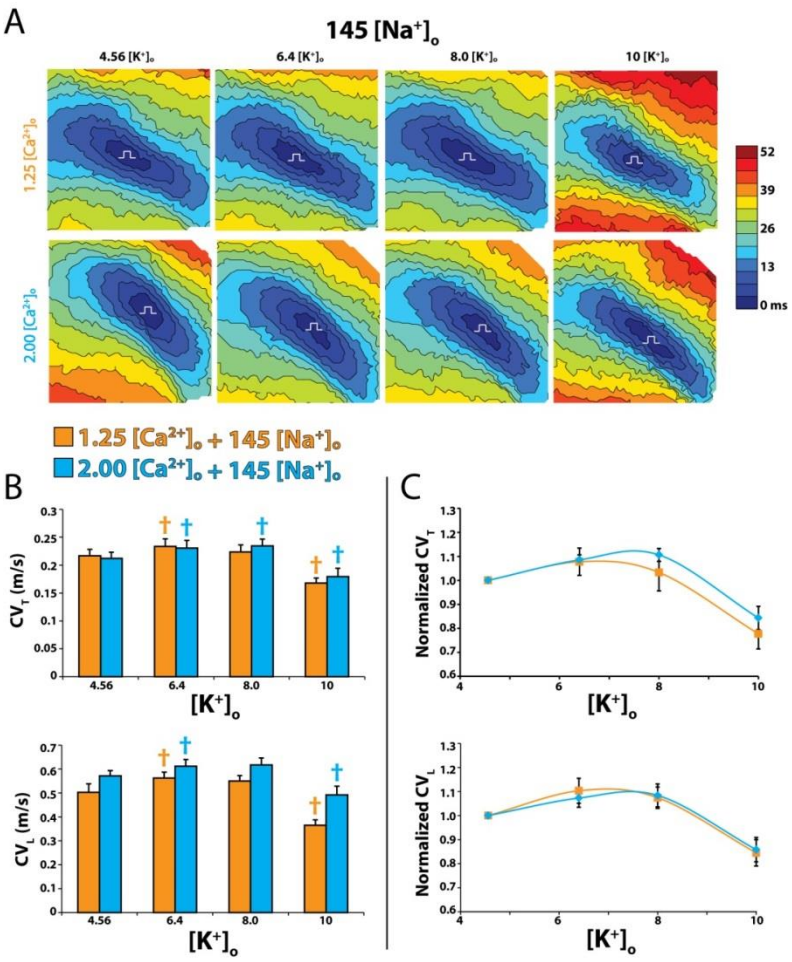

Figure 4.1 – $[Ca^{2+}]_o$ does not modify the CV-$[K^+]_o$ relationship with 145 mM $[Na^+]_o$. A) Representative contour maps of action potential activation times for all four of $[K^+]_o$ at 1.25 and 2.0 mM $[Ca^{2+}]_o$ with 145 mM $[Na^+]_o$. Each color on the maps represents 4 ms of time. The symbol at the center of each map represents the site of pacing stimulus. B) Biphasic nature of CV_T-$[K^+]_o$ (Top) and CV_L-$[K^+]_o$ (Bottom) relationship maintained regardless of $[Ca^{2+}]_o$. C) There were no changes in CV_T (Top) or CV_L (Bottom) sensitivity to $[K^+]_o$ due to $[Ca^{2+}]_o$. † $p<0.05$ vs 4.56 mM $[K^+]_o$.

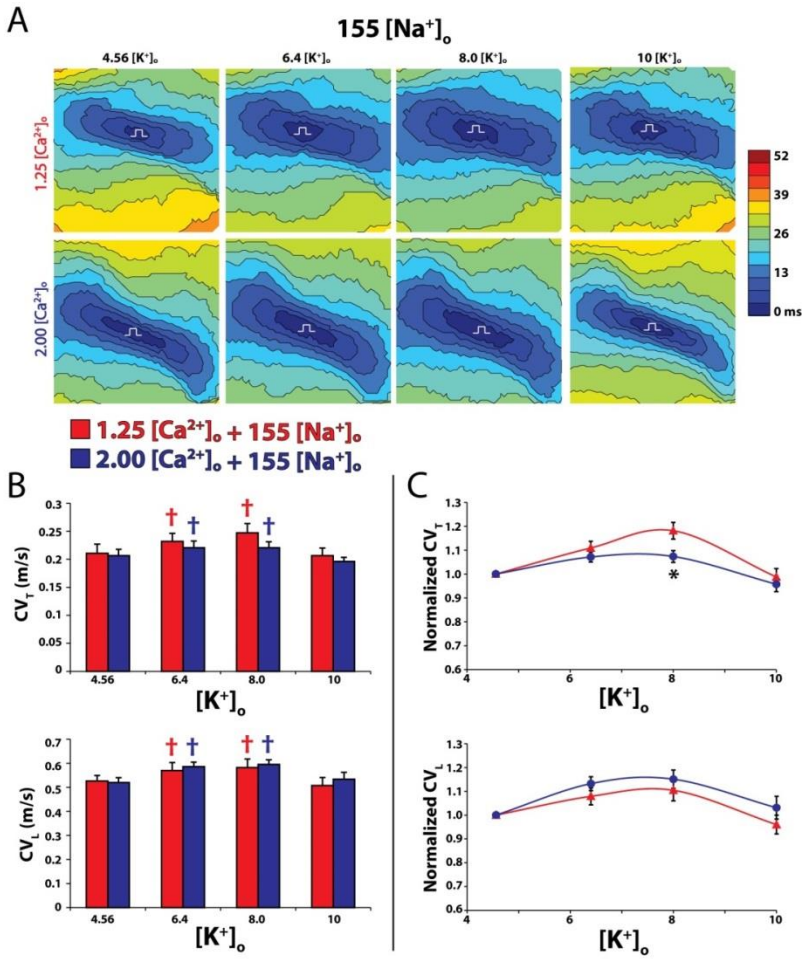

Figure 4.2 – $[Ca^{2+}]_o$ flattens the CV-$[K^+]_o$ relationship with 155 mM $[Na^+]_o$. A) Representative contour maps of action potential activation times for all four of $[K^+]_o$ at 1.25 and 2.0 mM $[Ca^{2+}]_o$ with 155 mM $[Na^+]_o$. Each color on the maps represents 4 ms of time. The symbol at the center of each map represents the site of pacing stimulus. B) Biphasic nature of CV_T-$[K^+]_o$ (Top) and CV_L-$[K^+]_o$ (Bottom) relationship maintained regardless of $[Ca^{2+}]_o$. C) 2.0 mM $[Ca^{2+}]_o$ decreases CV_T sensitivity to $[K^+]_o$ with 155 mM $[Na^+]_o$. However, there were no changes in CV_L sensitivity to $[K^+]_o$ due to $[Ca^{2+}]_o$. † $p<0.05$ vs 4.56 mM $[K^+]_o$. * $p<0.05$ vs 1.25 mM $[Ca^{2+}]_o$.

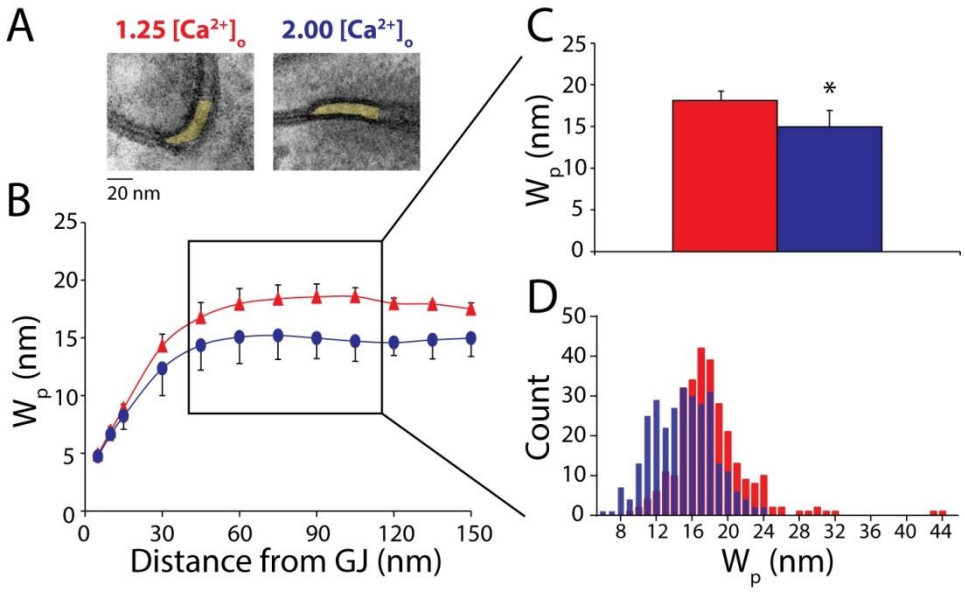

Figure 4.3 – $[Ca^{2+}]_o$ decreases W_p with 155 mM $[Na^+]_o$. A) Representative transmission electron micrographs of perinexi for 1.25 and 2.0 mM $[Ca^{2+}]_o$ with 155 mM $[Na^+]_o$. B) W_p measurements start at 0 nm from the GJ up until 150 nm. C) Combined W_p measurements for 45 to 105 nm from GJ, indicating decreased W_p with 2.0 mM $[Ca^{2+}]_o$. D) Histogram of W_p measurements for both $[Ca^{2+}]_o$, demonstrating not only an increase in narrow measurements for 2.0 mM $[Ca^{2+}]_o$, but also a decrease in wide measurements. *$p<0.05$ vs 1.25 mM $[Ca^{2+}]_o$.

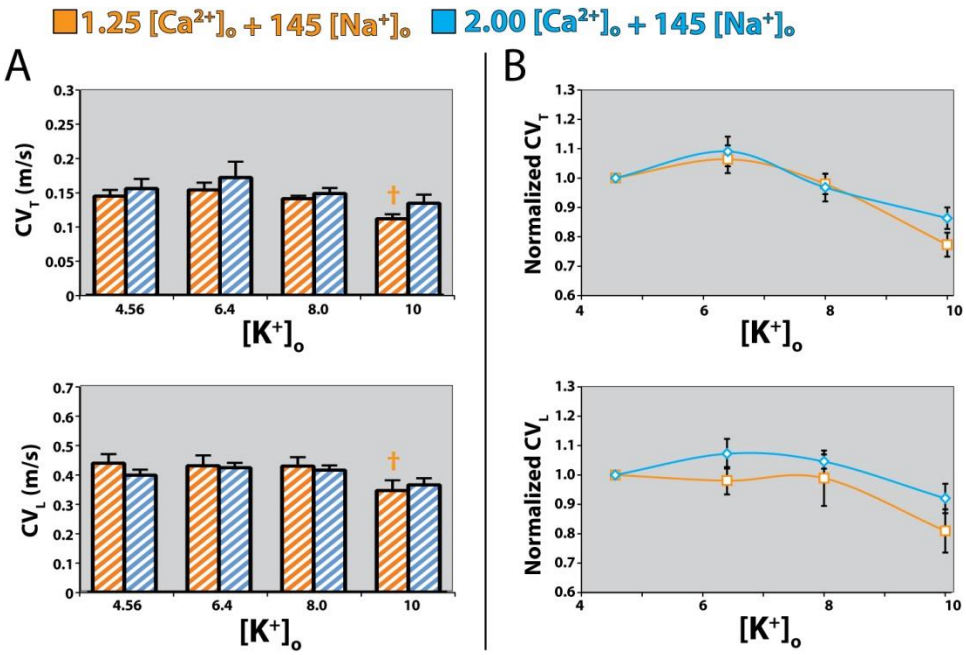

Figure 4.4 – CBX does not alter the relationship between CV, $[Ca^{2+}]_o$, and $[K^+]_o$ with 145 mM $[Na^+]_o$. A) Biphasic relationship between CV and $[K^+]_o$ is visually present after GJ uncoupling with CBX. Specifically, 10 mM $[K^+]_o$ decreases both CV_T and CV_L with 1.25 mM $[Ca^{2+}]_o$. B) Sensitivity to $[Ca^{2+}]_o$ was unaltered in either normalized CV_T or CV_L with CBX. †$p<0.05$ vs 4.56 mM $[K^+]_o$.

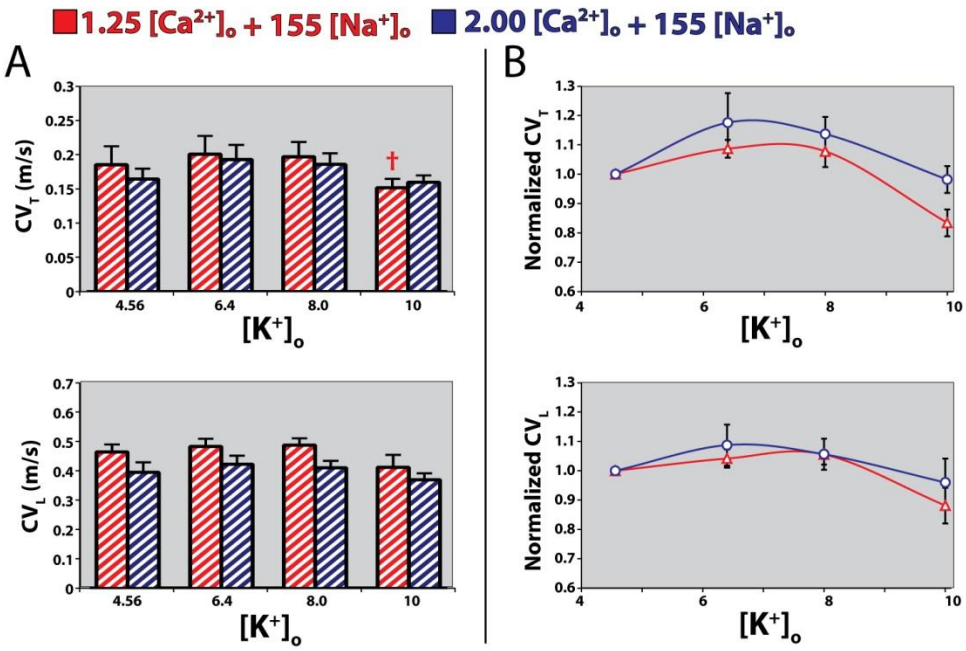

Figure 4.5 – CBX decreases $[Ca^{2+}]_o$ mediated sensitivity of CV due to changes in $[K^+]_o$ with 155 mM $[Na^+]_o$. A) Biphasic relationship between CV and $[K^+]_o$ is visually present after GJ uncoupling with CBX. Specifically, 10 mM $[K^+]_o$ decreases CV_T with 1.25 mM $[Ca^{2+}]_o$. B) Sensitivity to $[Ca^{2+}]_o$ was unaltered in either normalized CV_T or CV_L with CBX. †$p<0.05$ vs 4.56 mM $[K^+]_o$.

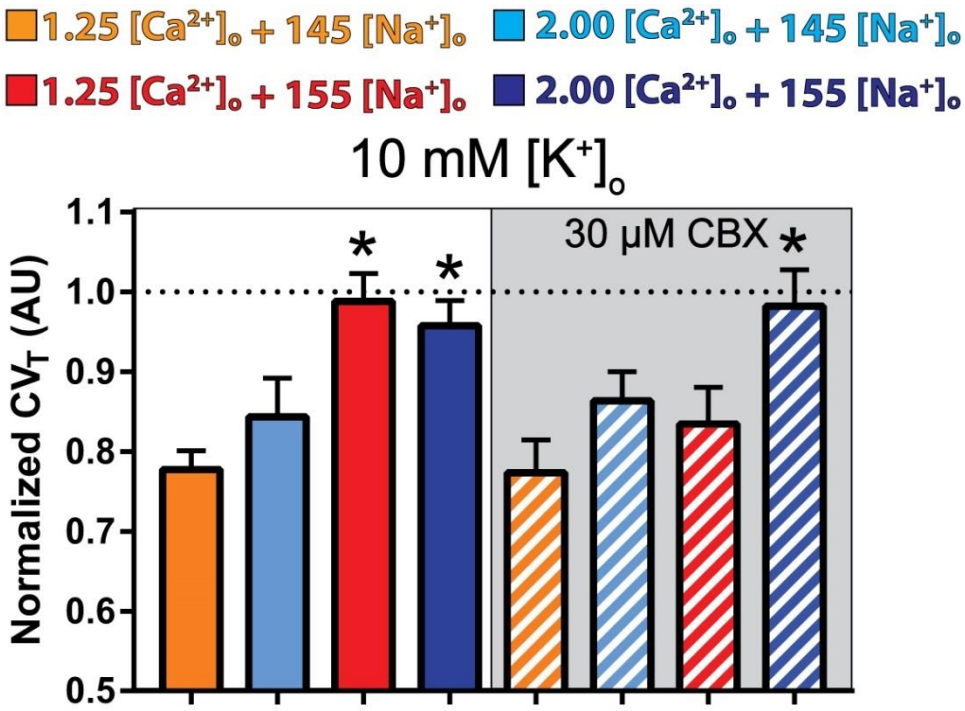

Figure 4.6 – Modified concentrations of $[Na^+]_o$ and $[Ca^{2+}]_o$ can prevent CV decrease due to hyperkalemia. Effects of $[Ca^{2+}]_o$, $[Na^+]_o$, and CBX on normalized CV_T at 10 mM $[K^+]_o$. Without CBX, solutions containing 155 mM $[Na^+]_o$ were able to maintain CV_T during hyperkalemia. However, with 30 µM CBX, both 155 mM $[Na^+]_o$ as well as 2.0 mM $[Ca^{2+}]_o$ were needed to maintain CV_T during hyperkalemia. *$p<0.01$ vs 145 mM $[Na^+]_o$ / 2.0 mM $[Ca^{2+}]_o$.

Chapter 5

Summary and future directions

Whole heart optical mapping has seen dramatic technological advances since the inception of the field. This includes advances in cameras, filters, and electrical processing equipment [1]. However, some protocols that have generally been passed down from mentor to student are the baths used as well as the perfusate composition for experiments. However, recent research has begun to elucidate the nature of perfusate effects on cardiac conduction. Therefore, study into the recipes that are passed from one scientist to the next needed further investigation to understand the implications of solution choice.

Optical Mapping Equipment

The first goal of this dissertation was to create a 3D printed optical mapping bath that was easy to manufacture, long lasting, and had comparable experimental outcomes versus traditional manufactured baths. The study in Chapter 2 aimed at achieving these goals through the use of 3D printing with a hobby grade printer. We were able to show that more affordable 3D printers were capable of producing optical mapping equipment for use in a research laboratory. These claims were verified through the combination of electrophysiological studies as well as through functional contractile experiments. Specifically, CV, APD, and action potential morphology were compared between traditionally manufactured and 3D printed baths. It was found that these electrophysiological parameters remained similar regardless of bath style.

Once the 3D printed baths were found to produce adequate experimental results when compared to traditionally manufactured baths, tests were run to test the effectiveness of removing pharmacological agents from the baths after experiments. Firstly, the retention

of the optically active dye Di-4-ANEPPS was assessed through optically mapping a heart in a bath with no dye, directly following an experiment that included dye. These results indicated that 3D printed baths did not retain any dye between experiments. A similar study was conducted to evaluate changes in CV due to the addition of CBX. It was found that hearts perfused with 30 μM CBX had a decrease in CV, however new baths or baths that had been washed after an experiment with CBX had no change in CV, indicating that CBX was indeed washed out of the baths. Finally, optical mapping experiments often use mechanical uncouplers such as blebbistatin or BDM. Therefore, left ventricular developed pressure (LVDP) was analyzed to test if blebbistatin was trapped inside the 3D printed baths. The data show that hearts with blebbistatin had highly decreased LVDP, but new baths or baths that were washed after the use of blebbistatin had similar LVDP. Therefore, it was found that 3D printed baths resulted in similar electrophysiological findings as traditional manufactured baths, while also not trapping pharmacological agents in the bath between experiments.

Ephaptic coupling – gap junctional coupling relationship

The second goal of this dissertation was to explore the effects of pharmacologically decreasing GJC, while also modulating ephaptic coupling through a combination of $[Na^+]_o$, $[K^+]_o$, and pacing rate. The study described in Chapter 3 was aimed at addressing the interplay between the canonical form of cardiac conduction, GJC, and the alternate form of electrical coupling, EpC. Therefore, the design of the experiments for this study were twofold, 1) to modulate EpC through changes in $[Na^+]_o$, $[K^+]_o$, and pacing rate to test for changes in electrophysiology due to EpC and 2) to uncouple GJs pharmacologically to see if GJC masks changes in EpC. During these studies we also

wanted to investigate if changes in CV were due to structural or functional changes in the heart. Therefore, additional testing took place for total Cx43 levels as well as p368 Cx43 to look for transcriptional changes to the GJs due to perfusate solution, while W_p was also measured to look at changes in cellular spacing. In short, the results of the study were,

1. CV was unaltered between EpC solutions when GJC was nominal
2. With high GJC uncoupling (30 µM CBX)
    a. Decreasing $[Na^+]_o$ and increasing $[K^+]_o$ decreased CV
    b. Only with 160 ms BCL
3. Solution composition did not alter W_p
    a. Unexpectedly, 30 µM CBX decreases W_p independent of solution
4. Neither total Cx43 or p3687 Cx43 expression changed due to solution composition

The data from these experiments mimicked the results from genetically modified mice in our laboratory [2], which indicates that this phenomenon of masking EpC with changes in GJC is apparent across species and GJ inhibition methods. The modification to EpC through perfusate composition has been theorized in multiple manuscripts [3-6]. Specifically, an increase in $[Na^+]_o$ increases the driving force for I_{Na} which should increase EpC [7]. However, increasing $[K^+]_o$ raises RMP, which eventually leads to a decrease I_{Na} due to inactivation of Na^+ channels [8]. Previous studies have demonstrated that CV has a biphasic relationship with $[K^+]_o$ which peaks at roughly 8.0 mM [9, 10]. However, we found that increasing $[K^+]_o$ to 6.9 mM led to either no change

in CV or a decrease. Therefore, these data indicate that modulating EpC could affect the CV-$[K^+]_o$ relationship.

CV-$[K^+]_o$ Relationship

The final goal of this dissertation was to explore the biphasic relationship between CV and $[K^+]_o$. Specifically, we investigated the modification of this relationship through changes in $[Na^+]_o$, $[Ca^{2+}]_o$, and GJC inhibition. The study described in Chapter 4 was designed to address confounding results due to changing $[K^+]_o$ in our previous work [11]. Therefore, the experiments were designed with three parameters in mind, 1) modulating $[K^+]_o$ from physiologic values up to hyperkalemia for each heart tested, 2) to vary $[Na^+]_o$ and $[Ca^{2+}]_o$ between two values each leading to a baseline of 4 base solutions, and 3) to repeat all experiments with 30 µM CBX to simulate GJ inhibition. Briefly the results of the study were,

1. The biphasic nature of the CV-$[K^+]_o$ relationship was maintained
    a. Independent of $[Na^+]_o$ or $[Ca^{2+}]_o$
2. With 155 mM $[Na^+]_o$, increasing $[Ca^{2+}]_o$ attenuated the effects of $[K^+]_o$ on CV
3. Increasing $[Ca^{2+}]_o$ from 1.25 to 2.0 mM decreased W_p with 155 mM $[Na^+]_o$
4. The inclusion of CBX abolished CV-$[K^+]_o$ sensitivity to $[Ca^{2+}]_o$
5. During hyperkalemia (10 mM $[K^+]_o$)
    a. Without CBX, CV is maintained with high $[Na^+]_o$, independent of $[Ca^{2+}]_o$
    b. With CBX, CV is maintained only with both high $[Na^+]_o$ and high $[Ca^{2+}]_o$

These results were the first extensive study to show the complex interactions between three of the main ionic modulators of cardiac conduction ($[Na^+]_o$, $[Ca^{2+}]_o$, and $[K^+]_o$).

While previous research has shown combinatory effects between $[Na^+]_o$ and $[Ca^{2+}]_o$ [12] as well as $[Na^+]_o$ and $[K^+]_o$ [11], these findings open the door for more intricate studies in the future to further understand the mechanism behind perfusate composition modification.

CONCLUSIONS

The findings described in this dissertation could have significant impact on therapeutic targets for cardiac disease while also impacting the reproducibility of cardiac research. Therapeutically, if the dynamics between the interplay in cardiac pefusate ions can be fully mapped out, then it may be possible to use specific ionic compositions in order to treat a plethora of cardiac disease states. However, problems arise in transitioning to clinical application for use in resuscitation fluids, as the body naturally modulates and buffers ions within specialized compartments of with dedicated organs such as the lungs and kidneys. As a research tool however, the knowledge of electrophysiological changes due to perfusate solution can lead to understanding in experimental reproducibility. Specifically in the cases when laboratories used perfusates which can lead to opposite results in the same experiment.

FUTURE DIRECTIONS

The use of artificial blood solutions during *ex vivo* cardiac experiments is not a new concept [13, 14]. However, the implications for changes in specific ion concentrations ($[Na^+]_o$, $[Ca^{2+}]_o$, and $[K^+]_o$) during disease states have not been fully explored. Changes to ionic concentration could be further understood through two distinct experiments.

1. Identify the effects of specialized cardiac perfusates on cardiac electrophysiology during ischemia. Specifically testing the effects of perfusate composition both on ischemia injury, as well as reperfusion injury, as this is a well-established injury model.
2. To develop a methodology to test the use of these cardiac perfusates during *in vivo* conditions in live animals. Complications regarding renal regulation of blood plasma levels could be explored, as this is will prove to be the main complication with ionic balance therapy *in vivo*. These experiments could then be transitioned into other species to determine if interactions are species dependent.

Current therapeutic targets often involve anti-arrhythmic drugs or implanted devices. However, through the development of specialized perfusate compositions to combat cardiac diseases, it would be possible to further understand the interactions between $[Na^+]_o$, $[Ca^{2+}]_o$, and $[K^+]_o$. However, the penultimate goal would be for these solutions to transition into clinical application. Through the study of an *in vivo* model, the first step into understanding the complicated nature between these perfusates and the body as a whole could be untangled.

REFERENCES

1. Olejnickova, V., M. Novakova, and I. Provaznik, *Isolated heart models: cardiovascular system studies and technological advances.* Med Biol Eng Comput, 2015. **53**(7): p. 669-78.
2. George, S.A., et al., *Extracellular sodium and potassium levels modulate cardiac conduction in mice heterozygous null for the Connexin43 gene.* Pflugers Arch, 2015.
3. George, S.A. and S. Poelzing, *Cardiac conduction in isolated hearts of genetically modified mice--Connexin43 and salts.* Prog Biophys Mol Biol, 2016. **120**(1-3): p. 189-98.
4. Veeraraghavan, R., R.G. Gourdie, and S. Poelzing, *Mechanisms of cardiac conduction: a history of revisions.* Am J Physiol Heart Circ Physiol, 2014. **306**(5): p. H619-27.
5. Veeraraghavan, R., et al., *Sodium channels in the Cx43 gap junction perinexus may constitute a cardiac ephapse: an experimental and modeling study.* Pflugers Arch, 2015.
6. Veeraraghavan, R., et al., *Potassium channels in the Cx43 gap junction perinexus modulate ephaptic coupling: an experimental and modeling study.* Pflugers Arch, 2016. **468**(10): p. 1651-61.
7. Greer-Short, A., et al., *Revealing the Concealed Nature of Long-QT Type 3 Syndrome.* Circ Arrhythm Electrophysiol, 2017. **10**(2): p. e004400.
8. Weidmann, S., *The effect of the cardiac membrane potential on the rapid availability of the sodium-carrying system.* J Physiol, 1955. **127**(1): p. 213-24.
9. Kagiyama, Y., J.L. Hill, and L.S. Gettes, *Interaction of acidosis and increased extracellular potassium on action potential characteristics and conduction in guinea pig ventricular muscle.* Circ Res, 1982. **51**(5): p. 614-23.
10. Buchanan, J.W., Jr., T. Saito, and L.S. Gettes, *The effects of antiarrhythmic drugs, stimulation frequency, and potassium-induced resting membrane potential changes on conduction velocity and dV/dtmax in guinea pig myocardium.* Circ Res, 1985. **56**(5): p. 696-703.

11. Entz, M., 2nd, et al., *Heart Rate and Extracellular Sodium and Potassium Modulation of Gap Junction Mediated Conduction in Guinea Pigs.* Front Physiol, 2016. **7**: p. 16.

12. George, S.A., et al., *Extracellular sodium dependence of the conduction velocity-calcium relationship: evidence of ephaptic self-attenuation.* Am J Physiol Heart Circ Physiol, 2016. **310**(9): p. H1129-39.

13. Ringer, S., *Concerning the Influence exerted by each of the Constituents of the Blood on the Contraction of the Ventricle.* J Physiol, 1882. **3**(5-6): p. 380-93.

14. Ringer, S., *A further Contribution regarding the influence of the different Constituents of the Blood on the Contraction of the Heart.* J Physiol, 1883. **4**(1): p. 29-42 3.

APPENDIX A

Copyrights and Licenses

Copyrights and Licenses